8-30-2019 3:00 PM

Effect of histatin- and statherin-derived engineered salivary peptides on Streptococcus mutans adhesion and on enamel demineralization provoked by cariogenic biofilms

Lina Maria Marin, *The University of Western Ontario*

Supervisor: Siqueira, Walter L., *The University of Western Ontario*
Joint Supervisor: Cury, Jaime A., *University of Campinas*
A thesis submitted in partial fulfillment of the requirements for the Doctor of Philosophy degree in Biomedical Engineering

Abstract

Dental biofilm is formed onto dental surfaces covered by a layer of specific salivary proteins and peptides named acquired enamel pellicle (AEP). It was previously demonstrated that the statherin- and histatin-derived engineered salivary peptides DR9-DR9 and DR9-RR14 were able to reduce enamel demineralization and displayed antimicrobial activity against *Streptococcus mutans*, respectively. However, these studies were carried under experimental conditions that did not mimic caries development induced by biofilm and sucrose exposure, the most cariogenic dietary sugar. In this thesis we assessed the effect of the engineered salivary peptides on 1) the adherence of *S. mutans* to hydroxyapatite (HAp), and 2) the reduction of enamel demineralization, using a validated *S. mutans* cariogenic biofilm model. We hypothesized that DR9-DR9 and DR9-RR14 would reduce *S. mutans* adherence and the cariogenicity of the biofilms, protecting enamel against demineralization. To test this hypothesis, we conducted two *in vitro* studies. In the first study, hydroxyapatite discs were treated with the peptides to induce AEP formation and then inoculated with *S. mutans* to quantify adhered bacteria, and to evaluate the total bacterial proteomes after adhesion periods of 2 h, 4 h, and 8 h. In the second study, a validated *in vitro* cariogenic *S. mutans* biofilm model was used to test the effect of DR9-DR9 and DR9-RR14 on enamel demineralization under two conditions 1) adsorbed onto the enamel surface forming the AEP, and 2) used to treat the biofilms 2x/day. Biofilms were grown for 144 h and the effect of the peptides on enamel demineralization, biomass, and total and extracellular matrix bacterial proteomes were evaluated. Results showed that DR9-DR9 reduced *S. mutans* adherence to HAp, but DR9-DR9 and DR9-RR14 did not have a significant effect on the development of the cariogenic biofilms formed. The engineered peptides did not modulate the bacterial proteome, neither when adhered to AEP nor when used to treat the biofilms during their formation. However, DR9-DR9 and DR9-RR14 significantly reduced enamel demineralization, suggesting that they control caries development by a physicochemical mechanism. The combinatory effect of reducing bacteria adhesion and limiting the mineral loss from the dental structure under high cariogenic challenge, suggests that the engineered peptides DR9-DR9 and DR9-RR14 represent a new translational approach for the prevention/treatment of dental caries.

Keywords

Acquired enamel pellicle, salivary proteins, statherin, histatin, *Streptococcus mutans*, bacterial adherence, dental biofilm, dental caries, demineralization, proteomics.

Summary for Lay Audience

Tooth decay continues to affect more than 2.5 billion people worldwide, calling to search for new therapeutic strategies to control this disease. Saliva has properties to modulate dental decay and we have recently found that small fragments (peptides) originated from the salivary proteins statherin and histatin are present on tooth surfaces where the oral bacteria stick before promoting tooth decay under dietary sugar consumption. Based on the differential biological properties that statherin and histatin display, we designed and engineered two peptides expecting to have a better effect on tooth decay prevention than their precursor salivary proteins. In the present study, we extended the promising results previously found because we showed that our engineered peptides were able to reduce the bacterial attachment and the dissolution of tooth enamel (tooth decay) provoked by biofilms formed from *Streptococcus mutans*, the most cariogenic oral bacteria, under sucrose exposure, the most cariogenic dietary sugar. The engineered peptides worked on enamel mineral balance without killing *S. mutans* bacteria, in agreement with the latest knowledge of the role of the oral microflora in health and disease. Our results may contribute to the creation of a novel and contemporary biotechnological strategy for the prevention/treatment of tooth decay.

Acknowledgments

First of all, I would like to thank my supervisors Dr. Jaime A. Cury and Dr. Walter L. Siqueira for the constant support and guidance during the development of my Ph.D. thesis. Thank you for the invaluable time you gave me to discuss the experimental design, the results and other relevant issues for the successful execution of this work. Your example has been fundamental during my training not only as a researcher but has also contributed to my formation as a person.

I would also like to thank the professors in the cariology area of the Graduate Program in Dentistry at the University of Campinas, Dr. Cínthia Pereira Machado Tabchoury, Dr. Antonio Pedro Ricomini-Filho, and Dr. Altair del Bel Cury. I am so grateful for the teachings and knowledge transmitted during my stay at the University of Campinas, and for advising me scientifically when necessary. I also would like to thank Dr. Amin Rizkalla, from Western University, for opening the doors of his laboratory and having allowed me to use the polisher to prepare some of the enamel slabs.

I am thankful to the members of my Advisory Committee at Western University for accompanying my progress and advising me during the realization of this thesis.

Thank you, Mr. Waldomiro Vieira Filho and Mr. José Alfredo da Silva, technicians of the Oral Biochemistry Laboratory at Piracicaba Dental School, for your support during my stay in Brazil.

I undoubtedly thank Yizhi Xiao (Cindy), manager of the Siqueira Lab, for being my friendly-hand in the laboratory and for always being ready to discuss and give me her valuable opinion when necessary. There are not words enough to thank you also for the time dedicated to the mass spectrometric analysis. Thanks also Cindy for facilitating the attainment of the necessary materials for the execution of the experiments.

I really appreciate the technical assistance provided by the co-op students Milena Petrica Mello, Yuxin Duan, and Alyssa Bruinink, during enamel slabs preparation and calcium analyzes.

Thanks to all the students and classmates who crossed my path during my stay in the laboratory of Oral Biochemistry of the Piracicaba Dental School, and in the laboratory of

Dr. Walter Siqueira at Western University. Your friendship and companionship were essential and made working days in the laboratory more enjoyable.

Table of Contents

List of Figures

List of Tables

List of Appendices

List of Abbreviations

AEP	Acquired Enamel Pellicle
BCA	Bicinchoninic Acid Assay
CFU	Colony Forming Units
ECM	Extracellular Matrix
HAp	Hydroxyapatite
Igs	Immunoglobulins
iEPS	Insoluble Extracellular Polysaccharides
Mr	Molecular Mass
MW	Molecular Weight
pIs	Isoelectric points
PRPs	Proline-rich Proteins
THB	Todd Hewitt Broth
TISAB II	Total Ionic Strength Adjustment Buffer
TYEB	Tryptone Yeast Extract Broth

Chapter 1

1 Introduction

Dental caries is considered as one of the most prevalent chronic diseases (Petersen et al. 2005), and the global burden of treating carious lesions is a matter of concern in terms of public health (Kassebaum et al. 2017). Carious lesions occur when the biofilms accumulated onto the dental surfaces are frequently exposed to fermentable dietary carbohydrates, provoking a progressive dissolution of the dental mineral structure by the acids produced from the metabolism of dietary sugars by biofilm-composing bacteria (Bowen et al. 2019). The formation of the dental biofilm is preceded by the adsorption of specific salivary biomolecules, mainly proteins and peptides, to the dental surfaces (Siqueira and Oppenheim 2009; Siqueira et al. 2007; Vitorino et al. 2007), forming an acellular film known as the Acquired Enamel Pellicle (AEP) (Dawes 1963). The formation of the AEP begins shortly after the exposure of dental surfaces to saliva, reaching a plateau state after 120 minutes (Lendenmann et al. 2000). The *in vivo* AEP is composed of approximately 130 different proteins, including alpha-amylase, albumin, immunoglobulins (Igs), agglutinin, proline-rich proteins (PRPs), statherin, histatins, mucin (MUC5B), carbonic anhydrases, lactoferrin, lysozyme, and cystatins (Siqueira et al. 2007). Approximately 50% of the AEP proteome corresponds to natural peptides (Siqueira and Oppenheim 2009; Siqueira et al. 2007) originated from the proteolysis of the salivary proteins by proteases of bacterial and human origin (Siqueira et al. 2012).

The composition of the AEP determines its properties, thus knowledge about the AEP may be useful to design strategies for caries control. Proteinaceous components of the AEP serve as receptors for bacterial ligands (adhesins), acting as a conditioning film that influences which bacteria will first adhere to dental surfaces (Li et al. 2004). This highly specific adhesin/receptor interaction regulates the adherence of oral microorganisms to dental surfaces, controlling the initial steps of biofilm formation (Li et al. 2004). As the AEP constituents play a key role in the bacterial colonization of the dental surfaces, modification of its proteinaceous components may control adhesion of certain pathogenic microorganisms to the teeth. In this regard, it has been demonstrated that the salivary proteins statherin and histatins can reduce the adhesion of *Streptococcus mutans* (Shimotoyodome et al. 2006), considered as the most cariogenic microorganism found in

dental biofilm (Hamada et al. 1984). Moreover, salivary proteins, known to exert antimicrobial functions like cystatins, lysozyme, myeloperoxidase, and histatins, were identified in the AEP (Siqueira et al. 2007), some of them conserving their biological activity when adsorbed onto dental surfaces (Hannig et al. 2005). Even though it is not known if histatins conserve antimicrobial function upon adsorption, antimicrobial activity against *S. mutans* was recently demonstrated by histatin 3 and its naturally derived 14-residue peptide known as RR14 (Basiri et al. 2017). *S. mutans* is considered the most cariogenic microorganism found in the dental biofilm due to its ability to ferment dietary carbohydrates, resist an acidic environment, and most importantly, to synthesize insoluble extracellular polysaccharides (iEPS) from sucrose metabolism. The synthesis of iEPS induces the formation of a more porous and thick biofilm, which facilitates carbohydrate diffusion through the biofilm (Cury et al. 2000) and acid retention at the interface between the biofilm and the dental surface (Koo et al. 2013).

Although the formation of the AEP constitutes the initial step for dental biofilm formation, it can help to control the development of carious lesions. This proteinaceous film has the ability to maintain the mineral composition of the teeth by forming a semipermeable barrier on the tooth surface, reducing its demineralization (Martins et al. 2013; Zahradnik et al. 1976; Zahradnik et al. 1977; 1978). Recently, it was demonstrated that both the salivary protein histatin 1, which naturally has a phosphoserine residue, and the synthetic phosphorylated form of histatin 3, firmly adsorb on hydroxyapatite (HAp), limiting the diffusion of acids throughout the AEP reducing the demineralization of HAp (Siqueira et al. 2010). Another well-known salivary protein that contributes to dental mineral homeostasis is statherin (Raj et al. 1992). This protein firmly adsorbs onto the enamel through its two phosphoserine residues located at the N-terminal region of the protein, inhibiting the spontaneous precipitation of calcium and phosphate ions on the dental surface (Nancollas and Mohan 1970; Raj et al. 1992). By doing so, statherin proteins keep the saturation state of saliva with relation to hydroxyapatite (HAp), promoting remineralization and protecting this mineral against demineralization (Kosoric et al. 2007; Shah et al. 2011). These functions are conserved in the naturally occurring 9-residue phosphopeptide derived from statherin, known as DR9 (Basiri et al. 2017; Valente et al. 2018; Xiao et al. 2015).

Salivary proteins respond to evolutionary pressure by the inclusion of functional domains into their primary structure, potentiating its activity (Oppenheim et al. 2012). Although

neither statherin nor histatins contain duplicated or multiplicated sequences of amino acids, this knowledge was used to synthetically duplicate DR9, obtaining DR9-DR9, which displayed enhanced ability to promote mineral homeostasis (Basiri et al. 2017; Valente et al. 2018; Xiao et al. 2015). Another evolutionary process leads to the formation of functional complexes by certain salivary proteins once secreted into the oral cavity, protecting them against proteolysis, modulating their biological functions, and allowing the distribution of the proteins throughout the oral cavity (Siqueira et al. 2012). The natural existence of proteinaceous complexes displaying multiple functions served as the basis for the development of the engineered hybrid peptide DR9-RR14 (Basiri et al. 2017; Valente et al. 2018; Xiao et al. 2015), which has an antibacterial effect against *S. mutans* (Basiri et al. 2017).

Since the global burden of treating carious lesions is a matter of concern in terms of public health, new therapeutic strategies should be developed to help control the incidence of cavitated and non-cavitated white spot carious lesions, and to promote the arrest or even the reversion of existing lesions. A promising therapeutic strategy for the control of dental caries development arose from the protective effect against demineralization and the antibacterial activity against *S. mutans* displayed by the statherin- and histatin-derived engineered salivary peptides DR9-DR9 and DR9-RR14 (Basiri et al. 2017). However, there is a gap in knowledge about the potential caries-protective effect of DR9-DR9 and DR9-RR14 peptides by reducing the adhesion of *S. mutans* to dental surfaces. Moreover, the anticaries effect of the engineered peptides was observed using a chemical caries model (Basiri et al. 2017), which does not fully mimic the process of carious lesions development. Hence, *in vitro* caries models to investigate the effects of novel therapeutic agents should consider the two main factors involved in the development of carious lesions: 1) biofilm accumulation on the dental surface, and 2) the frequent exposure to fermentable dietary carbohydrates (Cury and Tenuta 2009).

There is now significant interest in determining the microbiome of the human organism in order to know the microorganisms that make up the normal microbiota, which could be related to health-disease balance. However, regardless of the presence or absence of specific microorganisms in the human body, the proteins that are being expressed and/or secreted when the microorganisms adhere to the AEP must be known because they may further contribute to the architecture and development of the dental biofilm. Additionally, it is important to know the bacterial proteome when environmental conditions favor the

development of biofilm-mediated diseases, like dental caries (Bowen et al. 2019). Then, the studies designed to test the effect of DR9-DR9 and DR9-RR14 peptides on the control of cariogenic biofilm establishment and growth should focus on how these peptides can modulate the proteome of *S. mutans*, controlling its adhesion to the AEP and the subsequent cariogenic biofilm formation.

To fill the gaps in knowledge about the anticaries effect of the engineered peptides DR9-DR9 and DR9-RR14, the overall objective of this thesis was to evaluate their effect on the adherence of *S. mutans* to the AEP formed on hydroxyapatite and on enamel demineralization using an *S. mutans* cariogenic biofilm model. Our hypothesis was that the engineered peptides DR9-DR9 and DR9-RR14 in the AEP reduce *S. mutans* adherence and the cariogenicity of the biofilms, protecting enamel against demineralization.

Working towards this objective, we first assessed the effect of the salivary peptides DR9-DR9 and DR9-RR14 on the adhesion of *S. mutans* to hydroxyapatite (HAp) and to evaluate how they modulate the bacterial proteome upon binding to each single-component pellicle-coated surface (first manuscript). The results allowed us to decipher if the statherin- and histatin-derived salivary peptides reduce the bacterial colonization of the dental surfaces, which could lead to subsequent cariogenic biofilm development.

To further investigate the caries-protective effect of the engineered peptides, it was necessary to modify a cariogenic *S. mutans* biofilm model previously developed (Ccahuana-Vásquez and Cury 2010). The modified model was validated by assessing the effect of fluoride on enamel demineralization (second manuscript). This modified model allows the use of volumes up to 200 µL of any treatment solution, being useful as the micromodel of choice when the volume of test solutions is limited at the microliter scale, as in the case of the engineered peptides.

After having validated the cariogenic *S. mutans* biofilm model, it was used to evaluate the ability of the engineered peptides DR9-DR9 and DR9-RR14 to control enamel demineralization and to modulate crucial steps of cariogenic biofilm formation (third manuscript). The caries-protective effect was evaluated when the peptides were adsorbed onto the enamel surface forming the AEP, and when the biofilms were additionally treated 2x/day with the peptide solutions. These experiments also allowed us to identify and

characterize the bacterial intracellular and extracellular matrix proteome profiles used to determine if the peptides modulate the expression of bacterial proteins involved in biofilm cariogenicity.

1.1 References

Basiri T, Johnson ND, Moffa EB, Mulyar Y, Serra Nunes PL, Machado M, Siqueira WL. 2017. Duplicated or hybridized peptide functional domains promote oral homeostasis. J Dent Res. 96(10):1162-1167.

Bowen WH, Tenuta LMA, Koo H, Cury JA. 2019. Dental caries: Etiology and pathogenesis. In: Lamont RJ, Hajishengalis GM, Koo H, Jenkinson HF, editors. Oral microbiology and immunology. Third ed. Washington, DC: ASM Press. p. 251-265.

Ccahuana-Vásquez RA, Cury JA. 2010. S. Mutans biofilm model to evaluate antimicrobial substances and enamel demineralization. Braz Oral Res. 24(2):135-141.

Cury JA, Rebelo MA, Del Bel Cury AA, Derbyshire MT, Tabchoury CP. 2000. Biochemical composition and cariogenicity of dental plaque formed in the presence of sucrose or glucose and fructose. Caries Res. 34(6):491-497.

Cury JA, Tenuta LM. 2009. Enamel remineralization: Controlling the caries disease or treating early caries lesions? Braz Oral Res. 23 Suppl 1:23-30.

Dawes C. 1963. The nomenclature of the integuments of the enamel surface of tooth. Brit Dent J. 115:65-68.

Hamada S, Koga T, Ooshima T. 1984. Virulence factors of streptococcus mutans and dental caries prevention. J Dent Res. 63(3):407-411.

Hannig C, Hannig M, Attin T. 2005. Enzymes in the acquired enamel pellicle. Eur J Oral Sci. 113(1):2-13.

Kassebaum NJ, Smith AGC, Bernabe E, Fleming TD, Reynolds AE, Vos T, Murray CJL, Marcenes W. 2017. Global, regional, and national prevalence, incidence, and disability-adjusted life years for oral conditions for 195 countries, 1990-2015: A systematic analysis for the global burden of diseases, injuries, and risk factors. J Dent Res. 96(4):380-387.

Koo H, Falsetta ML, Klein MI. 2013. The exopolysaccharide matrix: A virulence determinant of cariogenic biofilm. J Dent Res. 92(12):1065-1073.

Kosoric J, Williams RAD, Hector MP, Anderson P. 2007. A synthetic peptide based on a natural salivary protein reduces demineralisation in model systems for dental caries and erosion. International Journal of Peptide Research and Therapeutics. 13(4):497-503.

Lendenmann U, Grogan J, Oppenheim FG. 2000. Saliva and dental pellicle--a review. Adv Dent Res. 14:22-28.

Li J, Helmerhorst EJ, Leone CW, Troxler RF, Yaskell T, Haffajee AD, Socransky SS, Oppenheim FG. 2004. Identification of early microbial colonizers in human dental biofilm. J Appl Microbiol. 97(6):1311-1318.

Martins C, Castro GF, Siqueira MF, Xiao Y, Yamaguti PM, Siqueira WL. 2013. Effect of dialyzed saliva on human enamel demineralization. Caries Res. 47(1):56-62.

Nancollas GH, Mohan MS. 1970. The growth of hydroxyapatite crystals. Arch Oral Biol. 15(8):731-745.

Oppenheim FG, Helmerhorst EJ, Lendenmann U, Offner GD. 2012. Anti-candidal activity of genetically engineered histatin variants with multiple functional domains. PLoS One. 7(12):e51479.

Petersen PE, Bourgeois D, Ogawa H, Estupinan-Day S, Ndiaye C. 2005. The global burden of oral diseases and risks to oral health. Bull World Health Organ. 83(9):661-669.

Raj PA, Johnsson M, Levine MJ, Nancollas GH. 1992. Salivary statherin. Dependence on sequence, charge, hydrogen bonding potency, and helical conformation for adsorption to hydroxyapatite and inhibition of mineralization. J Biol Chem. 267(9):5968-5976.

Shah S, Kosoric J, Hector MP, Anderson P. 2011. An in vitro scanning microradiography study of the reduction in hydroxyapatite demineralization rate by statherin-like peptides as a function of increasing n-terminal length. Eur J Oral Sci. 119 Suppl 1:13-18.

Shimotoyodome A, Kobayashi H, Tokimitsu I, Matsukubo T, Takaesu Y. 2006. Statherin and histatin 1 reduce parotid saliva-promoted streptococcus mutans strain mt8148 adhesion to hydroxyapatite surfaces. Caries Res. 40(5):403-411.

Siqueira WL, Custodio W, McDonald EE. 2012. New insights into the composition and functions of the acquired enamel pellicle. J Dent Res. 91(12):1110-1118.

Siqueira WL, Margolis HC, Helmerhorst EJ, Mendes FM, Oppenheim FG. 2010. Evidence of intact histatins in the in vivo acquired enamel pellicle. J Dent Res. 89(6):626-630.

Siqueira WL, Oppenheim FG. 2009. Small molecular weight proteins/peptides present in the in vivo formed human acquired enamel pellicle. Arch Oral Biol. 54(5):437-444.

Siqueira WL, Zhang W, Helmerhorst EJ, Gygi SP, Oppenheim FG. 2007. Identification of protein components in in vivo human acquired enamel pellicle using lc-esi-ms/ms. J Proteome Res. 6(6):2152-2160.

Valente MT, Moffa EB, Crosara KTB, Xiao Y, de Oliveira TM, Machado M, Siqueira WL. 2018. Acquired enamel pellicle engineered peptides: Effects on hydroxyapatite crystal growth. Sci Rep. 8(1):3766.

Vitorino R, Calheiros-Lobo MJ, Williams J, Ferrer-Correia AJ, Tomer KB, Duarte JA, Domingues PM, Amado FM. 2007. Peptidomic analysis of human acquired enamel pellicle. Biomed Chromatogr. 21(11):1107-1117.

Xiao Y, Karttunen M, Jalkanen J, Mussi MC, Liao Y, Grohe B, Lagugné-Labarthet F, Siqueira WL. 2015. Hydroxyapatite growth inhibition effect of pellicle statherin peptides. J Dent Res. 94(8):1106-1112.

Zahradnik RT, Moreno EC, Burke EJ. 1976. Effect of salivary pellicle on enamel subsurface demineralization in vitro. J Dent Res. 55(4):664-670.

Zahradnik RT, Propas D, Moreno EC. 1977. In vitro enamel demineralization by streptococcus mutans in the presence of salivary pellicles. J Dent Res. 56(9):1107-1110.

Zahradnik RT, Propas D, Moreno EC. 1978. Effect of salivary pellicle formation time on in vitro attachment and demineralization by streptococcus mutans. J Dent Res. 57(11-12):1036-1042.

Chapter 2

2 Effect of engineered salivary peptides on the adhesion of *Streptococcus mutans* to hydroxyapatite

2.1 Introduction

Once exposed to saliva, the dental surfaces get covered by an acellular film known as the AEP (Dawes 1963), formed by the adsorption of specific salivary proteins and peptides (Siqueira and Oppenheim 2009; Siqueira et al. 2007; Vitorino et al. 2007). The peptides found in the AEP originate from the proteolysis of different salivary proteins, once secreted in the oral cavity, by salivary proteases of bacterial and human origin (Siqueira et al. 2012). The AEP components act as receptors for bacterial ligands (adhesins), leading to a highly specific and irreversible attachment of bacterial cells to the dental surface. In this way, the AEP acts as a conditioning film that influence which bacteria will first adhere to the dental surfaces (Li et al. 2004), controlling the initial steps of biofilm formation.

Although dental biofilms help keep the physiological balance between health and disease, certain environmental conditions in the oral cavity can favour the transition from healthy to pathogenic dental biofilms (Marsh and Zaura 2017), contributing to the development of one of the most prevalent oral diseases worldwide, namely dental caries (Bratthall et al. 2006). Thus, dental carious lesions develop when organic acids, produced as the end product of biofilm-composing bacteria metabolism of dietary fermentable sugars, provoke the progressive dissolution of the mineral phase of the teeth (Bowen et al. 2019).

As the AEP constituents play a key role in the bacterial colonization of the dental surfaces (Li et al. 2004), the modification of its proteinaceous components may control the adhesion of certain pathogenic microorganisms to the teeth. In this regard, it has been demonstrated that the salivary proteins statherin and histatin can reduce the adhesion of *Streptococcus mutans* (Shimotoyodome et al. 2006), considered as the most cariogenic microorganism found in the dental biofilm (Hamada et al. 1984). Moreover, salivary proteins known to exert antimicrobial functions like cystatins, lysozyme, myeloperoxidase, and histatins, were identified in the AEP (Siqueira et al. 2007), some

of them conserving their biological activity when adsorbed onto dental surfaces (Hannig et al. 2005). Even though it is not known if histatins conserve their antimicrobial function upon adsorption, the antimicrobial activity against *S. mutans* was recently demonstrated by histatin 3 and its naturally derived 14-residue peptide known as RR14 (Basiri et al. 2017).

Adaptation of salivary proteins in response to evolutionary pressure is reflected in the formation of functional complexes by certain salivary proteins once secreted into the oral cavity, protecting them against proteolysis, modulating their biological functions and allowing their distribution throughout the oral cavity (Siqueira et al. 2012). The natural existence of proteinaceous complexes displaying multiple functions served as the basis for the development of the engineered hybrid peptide DR9-RR14 (Basiri et al. 2017; Valente et al. 2018; Xiao et al. 2015), which had an antibacterial effect against *S. mutans* (Basiri et al. 2017).

The knowledge of the functions exerted by these proteins, suggests the possibility of using the naturally-occurring peptides DR9 (Siqueira et al. 2010; Xiao et al. 2015) and RR14 (Helmerhorst et al. 2006), derived from statherin and histatin, respectively, and their engineered forms DR9-DR9 and DR9-RR14 (Basiri et al. 2017), to control the caries process by reducing the adhesion of *S. mutans* to dental surfaces. Thus, the aim of this study was to assess the effect of salivary peptides on the adhesion of *S. mutans* to HAp and to evaluate how they modulate the bacterial proteome upon binding to each single-component pellicle-coated surface.

2.2 Materials and Methods

2.2.1 Experimental design

An *in vitro S. mutans* adherence model was used to assess the effect of our engineered salivary peptides on 1) the adherence of *S. mutans* to HAp, and 2) the bacterial proteome upon binding to each single-component pellicle-coated surface. HAp discs were treated with one of the following: statherin (A), histatin 3 (B), DR9 (C), DR9-DR9 (D), DR9-RR14 (E), RR14 (F), parotid saliva (1 mg protein/mL) (positive control, G), and 50 mM NaCl pH 6.8 (negative control, H). Coated discs were incubated with *S. mutans* UA159 for 2 h, 4 h and 8 h (n = 12/treatment/time point). Adhered bacterial counts (Colony

Forming Units – CFU/disc*10^5) were determined at each time point in six discs. Proteome profiles were obtained after the mass spectrometry identification of the proteins extracted from adhered, planktonic and inoculum (baseline) bacteria. Two independent assays per experimental condition were performed. Our hypothesis was that the engineered salivary peptides reduce bacterial adherence, which was tested at a significant level α of 5% (two-way ANOVA and LDS test).

2.2.2 Collection of the parotid gland stimulated saliva

This study was approved by the Ethics Committee on Human Research at The University of Western Ontario (protocol number 16181E). Parotid gland saliva was collected with a Lashley cup between 9:00 and 11:00 a.m. from three volunteers with good general oral health who were not taking medications that could alter the salivary flow. The salivary secretion was stimulated by sugar-free acid candies, and the saliva was collected in a 50 mL polypropylene tube, which was submerged in a vessel containing ice. Immediately after collection, the saliva obtained from the different volunteers was pooled and the total protein concentration was determined by the bicinchoninic acid assay (BCA) using bovine serum albumin as the standard protein. Protein concentration in the saliva was adjusted to 1 mg/mL with 50 mM NaCl pH 6.8. The absence of contamination with microorganisms from the oral cavity was checked by inoculating 100 µL of this saliva in Brain and Heart Infusion Agar for 48 h at 37 °C and 10% CO_2. The remaining saliva solution was stored at -80 °C until use.

2.2.3 Proteins and peptides used

Synthetic statherin was purchased from Peptide Protein Research Ltd (Hampshire, UK), while synthetic histatin 3 and peptides derived from statherin or histatin 3 were purchased from Synpeptide (Shanghai, China). All proteins and peptides used in this study are listed in Table 1. Purity (> 95%) and molecular mass (Mr) from each protein and peptide were verified by high-performance liquid chromatography and mass spectrometry analysis. Isoelectric points (pIs) of statherin, histatin 3, and their peptides were determined using the calculator developed by Gauci et al. (Gauci et al. 2008). This approach calculates the pI of a protein and peptide at a given pH incorporating user-specified pKa values. The calculation is repeated until the pH corresponding to a net charge of zero is found (Gauci et al. 2008). The pI values quoted in Table 1 were calculated using the Scansite option

(Azzopardi et al. 2010). Protein and peptide solutions were prepared in 50 mM NaCl pH 6.8 at a final concentration of 198 μM, 24 h before starting the experiment. The final concentration was checked in a UV-light spectrophotometer at a wavelength of 215 nm.

2.2.4 Hydroxyapatite discs preparation

Dense ceramic HAp discs having 5-mm diameter and 2-mm thickness (Clarkson Chromatography Products Inc. PA USA), were vertically assembled in acrylic holders attached to the lid of a 24-well culture plate leaving exposed an area of approximately 70.7 mm^2 (Figure 1). Subsequently, the assembled lid with the HAp discs were sterilized by exposing them to ultraviolet light for 1 hour.

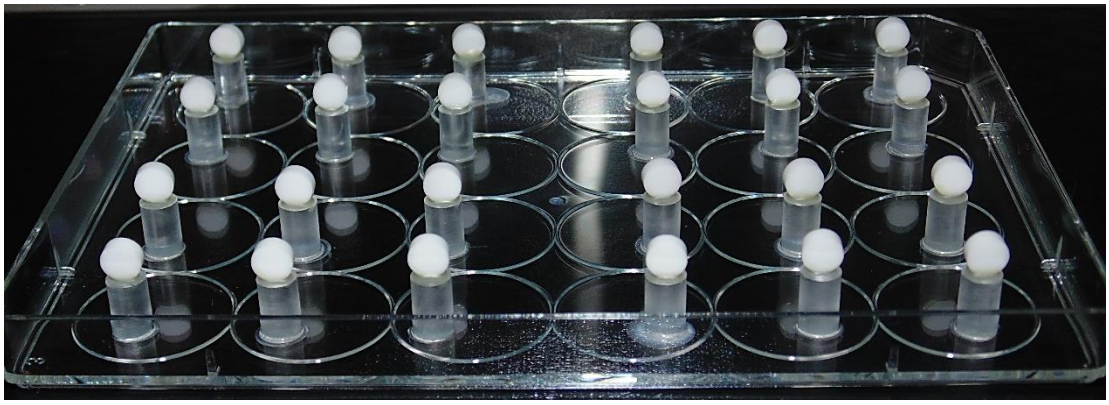

Figure 1. Photograph of hydroxyapatite discs assembled to a cell-culture plate lid.

2.2.5 Acquired pellicle formation

HAp discs were positioned in a 96-well culture plate and incubated for 24 h at 37 ºC under constant agitation at 60 rpm/min with 200 μL/well/slab of one of the following treatments: (A) statherin, (B) histatin 3, (C) DR9, (D) DR9-DR9, (E) DR9-RR14, (F) RR14, (G) stimulated parotid saliva as positive control, (H) 50 mM NaCl pH 6.8 as negative control.

2.2.6 *S. mutans* inoculation and adhesion to the AEP

After the AEP formation, HAp discs were washed three times with 50 mM NaCl pH 6.8 and then transferred to a 24-well culture plate containing 2 mL of Tryptone Yeast Extract Broth (TYEB) supplemented with 1% glucose and standard cell suspension (*S. mutans*

UA159, 1 x 10^8 CFU/mL), and incubated for 2 h, 4 h or 8 h at 37 ºC and 10% CO_2 to allow the bacteria to adhere to the HAp surface (n = 12/treatment/time point).

2.2.7 Quantitation of adhered *S. mutans*

To determine the number of bacteria adhered to the surface of the discs at each time point, a protocol previously reported (Sakuma et al. 2013) was here modified. For this, a calibration curve of fluorescence intensity versus the number of viable bacteria (CFU) was done by serially diluting the standard cell suspension (*S. mutans* UA159, 1 x 10^8 CFU/mL) from pure until 1:640 in 2 mL of 1% resazurin in KCl buffer (0.05 M KCl, 1 mM $CaCl_2$, and 0.1 mM $MgCl_2$) supplemented with 0.5% glucose. To determine the number of viable bacteria at each dilution, three 20-µL drops of each dilution were plated in Todd Hewitt Broth (THB) Agar and incubated for 48 h at 37 ºC and 10% CO_2. The remaining suspension from each dilution was incubated for 2 h at 37 ºC and the fluorescence intensity was measured with a fluorescence spectrophotometer (excitation wavelength, 560 nm; emission wavelength, 590 nm; model 650-40; Hitachi, Tokyo, Japan). At each adhesion time point, six out of twelve HAp discs per treatment group were washed three times with KCl buffer and then incubated for 2 h at 37 ºC with 2 mL of 1% resazurin in KCl buffer supplemented with 0.5% glucose. The number of viable adhered bacteria (CFU/disc) was determined after measuring the fluorescence intensity of the suspension in contact with each disc using a fluorescence spectrophotometer.

2.2.8 *S. mutans* proteins extraction

The remaining 6 discs per treatment were used to extract the bacterial proteins. At each time point, the corresponding HAp discs were washed three times with 0.9% NaCl, transferred to a microcentrifuge tube containing 1 mL of buffer (20 mM Tris-HCl pH 8.0, 10 mM $MgCl_2$, 1 mM PMSF), and then sonicated at 7 W for 30 s on ice to detach the bacteria adhered to the HAp discs. The discs were carefully removed, and the bacterial suspension was centrifuged at 4000 rpm for 5 min at 4 ºC. The planktonic cells in the culture medium from each of the six wells were pooled in a 15-mL tube and centrifuged at 4000 rpm for 5 min at 4 ºC. The pellet having the pooled adhered or the planktonic bacteria per treatment was resuspended in 150 µL of mutanolysin mix containing 20 mM Tris-HCl pH 8.0, 10 mM $MgCl_2$, 20% sucrose, 1 mM PMSF, 100 U/mL of mutanolysin (M9901, Sigma), and 1000 U/mL lysozyme (GTX65489, GeneTex). Protein extraction

was done by incubating the suspension for 2 h at 37 ºC, shaking the mixture every 20 min. The extracted cell wall proteins were dialyzed to clean them up from the buffer components using tubing with a molecular weight (MW) cutoff of 1,000 Da (Spectra/Por; Spectrum Laboratories Inc., Rancho Dominguez, Calif., USA). Dialysis was performed for 24 h at 4°C against 20 L of deionized water with 2 water volume changes. After dialysis, the protein concentration was determined by the BCA assay using a spectrophotometer at a wavelength of 562 nm. A protein equivalent of 5 μg was digested with trypsin (5% trypsin in 50 mM NH_4HCO_3, pH 7.8) for 16 h at 37 °C and purified with a C18 column for proteomic analysis. An aliquot of the bacterial suspension used to inoculate the HAp discs were processed to extract the bacterial proteins following the protocol previously described, and the obtained proteome profile was used as baseline (time point zero).

2.2.9 Proteomic analysis

The analysis of tandem mass spectrometry was performed according to the protocol described by Siqueira & Oppenheim (Siqueira and Oppenheim 2009) using a Velos LTQ (Thermo-Finnigan, San Jose, CA) which allows liquid chromatography to be performed in-line with a capillary column C18 connected to the mass spectrometer using electrospray ionization on a test scanner in the range of m/z values of 400-2000 and at the same time performing tandem MS/MS analysis. Subsequently the samples were diluted in a buffer containing 80% acetonitrile/19.9% H_2O/0.1% trifluoroacetic acid, dried and resuspended in 25 μL of 97.5% H_2O/2.4% acetonitrile/1% formic acid, and subsequently were subjected to reverse-phase LC-ESI-MS/MS. The 50 μm x 10 cm reverse phase HPLC capillary column was packed in the laboratory using a Magic C18 resin 5 μm diameter and 200 Å pore size (Michrom BioResources, Auburn, CA). The column was developed with a linear gradient of solvent B between 5% and 50% (acetonitrile 97.5%, formic acid 0.1%) at a flow rate of 110 nL/minute. The electrospray voltage and the ion transfer capillary temperature were 1.8 kV and 230 °C, respectively.

The obtained MS/MS spectra were searched against *Streptococcus mutans* protein databases (Swiss Prot and TrEMBL, Swiss Institute of Bioinformatics, Geneva, Switzerland, http://ca.expasy.org/sprot/) using SEQUEST algorithm in Proteome Discoverer 1.3 software (Thermo Scientific, San Jose, CA, USA). Search results were filtered for a False Discovery rate of 1% employing a decoy search strategy utilizing a

reverse database. An additional inclusion criterion for positive identification of proteins was that the same protein passed the filter score in at least three different MS analyses from the same group in a total of three mass spectrometry analyses per group. The proteins identified specifically during the adhesion phase at each time point (2 h, 4 h, 8 h) were determined by comparison with the proteome profiles obtained from the baseline and planktonic bacteria.

2.2.10 Statistical analysis

The normal distribution of the errors and the homogeneity of the variances were checked. Once these assumptions were checked, the number of viable bacteria adhered to HAp (CFU/disc*10^5) was analyzed by a two-way analysis of variance (ANOVA) followed by LSD test, considering the following factors: treatment at eight levels (A-H), and time at three levels (2 h, 4 h and 8 h). All statistical analyses were performed at a significance level α of 5%, using SPSS (IBM SPSS Statistics for Windows, Version 21.0. Armonk, NY: IBM Corp.).

2.3 Results

The pIs were calculated for each peptide and protein at pH 6.8. Histatin 3 and statherin, as positively and negatively charged proteins respectively, demonstrated pIs of 10.4 and 4.4. DR9-DR9 exhibited the lowest pI value (3.4) just below that of the natural statherin peptide DR9 whereas RR14 showed the highest value (11.0) and DR9-RR14 was intermediate (7.1). Values are provided in Table 1.

Table 1. Constructed peptides derived from statherin and histatin and their calculated pIs.

Peptide/ Protein Name	**Peptide Sequence**	**pI**
Statherin	DSpSpEEKFLRRIGRFGYGYGPYQPVPEQPLYPQPYQPQYQQYTF	4.4
Histatin 3	DSHAKRHHGYKRKFHEKHHSHRGYRSNYLYDN	10.4
DR9	DSpSpEEKFLR	3.6
DR9-DR9	DSpSpEEKFLRDSpSpEEKFLR	3.4
DR9-RR14	DSpSpEEKFLRRKFHEKHHSHRGYR	7.1
RR14	RKFHEKHHSHRGYR	11.0

Sp represents a phosphorylated serine.

2.3.1 Quantitation of adhered *S. mutans*

The statistical analysis showed that there was a statistically significant interaction between the effects of treatment and time on the number of viable bacteria adhered to HAp (CFU/disc*10^5) ($p<0.0001$) (Table 2). Therefore, pairwise comparisons were run for each factor under study.

Table 2. Viable bacteria adhered (CFU/disc*10^5) to HAp according to the treatments (A-H) and at each time point evaluated.

Treatment	Code	n	Time (h)		
			2	4	8
			Mean of CFU/disc*10^5 (± S.D.)		
Statherin	A	6	4.8 (± 0.7)	12.2 (± 2.7)	32.6 (± 10.6)
Histatin 3	B	6	1.2 (± 1.0)	5.8 (± 1.7)	17.0 (± 6.9)
DR9	C	6	4.3 (± 1.0)	8.3 (± 1.4)	18.8 (± 5.0)
DR9-DR9	D	6	4.3 (± 1.1)	8.3 (± 1.4)	25.3 (± 5.9)
DR9-RR14	E	6	3.2 (± 0.3)	8.1 (± 1.5)	38.1 (± 6.2)
RR14	F	6	1.3 (± 0.7)	7.5 (± 2.7)	25.5 (± 8.4)
Saliva	G	6	0.0 (± 0.2)	1.1 (± 1.0)	4.6 (± 1.1)
NaCl	H	6	1.8 (± 0.7)	5.1 (± 1.7)	17.3 (± 6.8)

Mean values of number of viable bacteria for each treatment at each time point are shown in Table 2. The pairwise comparison made within treatments at each time point (Figure 2) showed significant differences among groups ($p<0.0001$). As expected, the number of bacteria adhered increased over time, being the mean values obtained at 2 h statistically different from those obtained at 4 h and 8 h within the groups A, E, and F; while in the remaining groups only a significant difference was observed between 4 h and 8 h ($p<0.05$) (Figure 2).

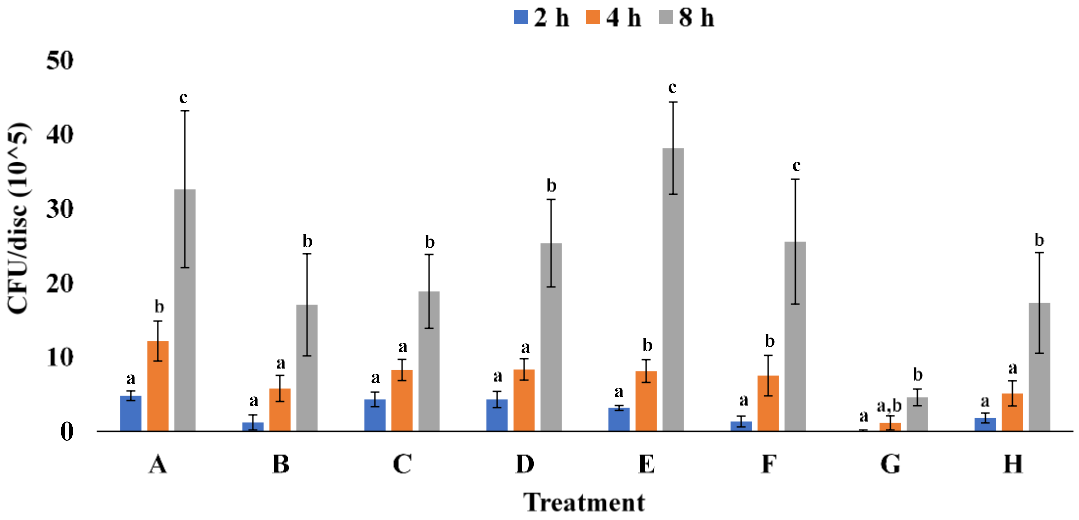

Figure 2. Colony-forming units (CFU/disc*10^5) of *S. mutans* adhered to HAp discs within treatment according to the adhesion time. Statherin (A), histatin 3 (B), DR9 (C), DR9-DR9 (D), DR9-RR14 (E), RR14 (F), Parotid saliva (G), 50 mM NaCl, pH 6.8 (H). Distinct lower-case letters show significant differences among time points within each treatment (ANOVA and LDS test, $p<0.05$) (Mean ± SD; n = 6).

Regarding the pairwise comparison made at each time point among treatments, a significant difference was also obtained ($p<0.0001$). The Figure 3 shows that after an incubation period of 2 h, the adhesion of *S. mutans* cells was higher on the HAp discs treated with the treatments A, C, and D, which values were significantly different from the positive control (G), where the lowest number of adhered bacteria was detected ($p<0.05$). When the adhesion time was prolonged to 4 h, only group A remained to show the highest number of adhered bacteria, being its value significantly higher than those found in the B, G and H treatment groups ($p<0.008$), and similar to the remaining groups (D, C, E, F; $p>0.05$). At 8 h, the positive control (G) was significantly different from all other treatment groups, being the group with less adhered bacteria at all the time points evaluated ($p<0.0001$). According to the statistical analysis, the mean values obtained at this time point in each group were, from highest to lowest, as follows: E>A>F=D>C=H=B>G ($p<0.022$).

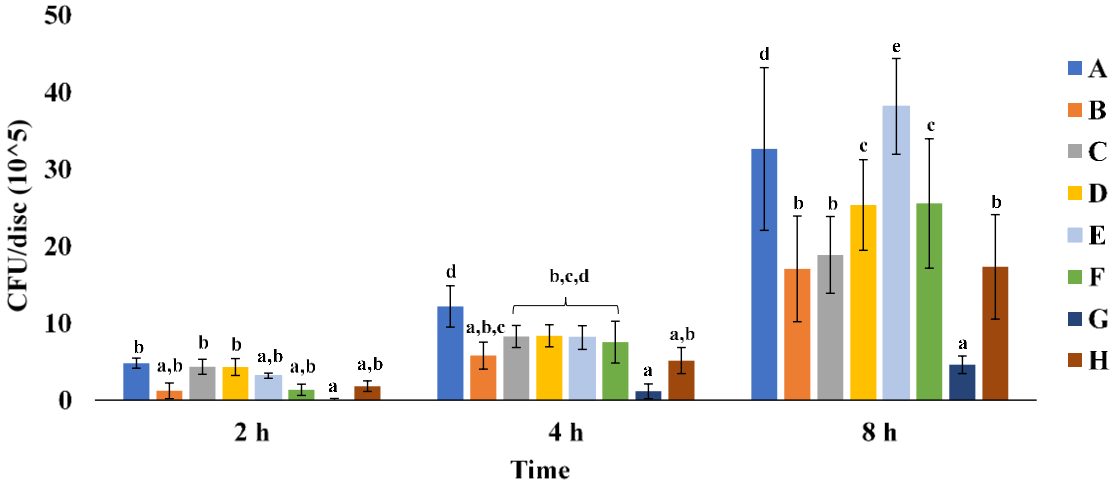

Figure 3. Colony-forming units (CFU/disc*10^5) of *S. mutans* adhered to HAp discs at each time point according to the treatments. Statherin (A), histatin 3 (B), DR9 (C), DR9-DR9 (D), DR9-RR14 (E), RR14 (F), Parotid saliva (G), 50 mM NaCl, pH 6.8 (H). Distinct lower-case letters show significant differences among groups at the same time point (2 h, 4 h, and 8 h) (ANOVA and LDS test, $p<0.05$) (Mean ± SD; n = 6).

2.3.2 Proteome profiles at baseline, and in the adhered and planktonic bacteria

The list of the proteins identified at baseline is shown in Table 3. Most of the proteins participate in translation and protein synthesis (63.2%), while the remaining proteins take part in carbohydrate metabolism and energy production (13.2%), and other biological processes (23.6%). The majority (79%) of the proteins identified at baseline were also found in the planktonic bacteria at the three time points evaluated (Table 3).

Table 3. *S. mutans* proteome profile at baseline (time point zero)

Gene name	Protein name	Protein function
adhE	Aldehyde-alcohol dehydrogenase	Alcohol metabolic process
ilvC *	Ketol-acid reductoisomerase (NADP(+))	Amino acid biosynthesis
gapC *	Glyceraldehyde-3-phosphate dehydrogenase	Carbohydrate metabolic process
spaP *	Cell surface antigen I/II	Cell wall antigen
hup *	DNA-binding protein HU	Chromosome condensation
eno	Enolase	Glycolytic process
pgk	Phosphoglycerate kinase	Glycolytic process
fbaA *	Fructose-1,6-biphosphate aldolase	Glycolytic process
gpmA *	2,3-bisphosphoglycerate-dependent phosphoglycerate mutase	Glycolytic process
lplA	Lipoate--protein ligase	Protein biosynthesis
groL *	60 kDa chaperonin	Protein folding
dnaK	Chaperone protein DnaK	Protein folding
clp *	Putative Clp-like ATP-dependent protease, ATP-binding subunit	Transcription
tuf	Elongation factor Tu	Translation
rplL *	50S ribosomal protein L7/L12	Translation
rplE *	50S ribosomal protein L5	Translation
rpsC *	30S ribosomal protein S3	Translation
rpsE *	30S ribosomal protein S5	Translation
rplK *	50S ribosomal protein L11	Translation
rpsB *	30S ribosomal protein S2	Translation
rpsJ *	30S ribosomal protein S10	Translation
rplU *	50S ribosomal protein L21	Translation
rplA *	50S ribosomal protein L1	Translation
rpsD *	30S ribosomal protein S4	Translation
rpsG	30S ribosomal protein S7	Translation
rplO *	50S ribosomal protein L15	Translation

rs1 *	Putative ribosomal protein S1 sequence specific DNA-binding protein	Translation
rpsH *	30S ribosomal protein S8	Translation
rplJ *	50S ribosomal protein L10	Translation
fusA *	Elongation factor G	Translation
rplF *	50S ribosomal protein L6	Translation
rplX *	50S ribosomal protein L24	Translation
rpsS	30S ribosomal protein S19	Translation
tsf	Elongation factor Ts	Translation
oppA *	Putative oligopeptide ABC transporter, substrate-binding protein OppA	Transport
livK	Putative ABC transporter, branched chain amino acid-binding protein	Transport
SMU_1641c	Uncharacterized protein	Uncharacterized
SMU_63c	Uncharacterized protein	Uncharacterized

** Represents the proteins that were commonly identified at baseline and in the planktonic bacteria*

Table 4 shows the proteins identified in the adhered bacteria. The proteins exclusively expressed in the adhered bacteria were determined after the comparison between the proteome profiles obtained from the adhered *S. mutans* with the baseline and planktonic bacteria. The data revealed that the uncharacterized protein *SMU_1979c* was expressed exclusively in the adhered bacteria from almost all the treatment groups and at the three time points evaluated. Other proteins were found to be expressed only during the adhesion phase in specific treatment groups. At 2 h, *carB* was identified in the group E. The proteins *SMU_488*, *gatA* and *clpE* were identified at 4 h in the groups B, E and F, respectively. At 8 h, *SMU_109* was identified in group B; *SMU_515* and *murE* were identified in group C; and *carB* in the group D. During the first four hours, the proteins identified in all groups were found solely in the adhered bacteria, while most of the proteins expressed by adhered bacteria at 8 h were also found expressed by the planktonic bacteria at the same time point and at baseline. Overall, no proteins were identified in the adhered bacteria at 2 h in the groups A, D, and F; and at 8 h in the group G.

The list of the proteins identified in the planktonic bacteria is included as an appendix (Appendix 1).

Table 4. Proteins identified in the adhered bacteria according to the treatments and time point evaluated.

	Treatment																							
	A			B			C			D			E			F			G			H		
Time (h) / Gene Name	2	4	8	2	4	8	2	4	8	2	4	8	2	4	8	2	4	8	2	4	8	2	4	8
carB *												x	x											
clpE *																	x							
dnaK			x									x												
eno			x												x									
gatA *														x										
groL			x									x												
murE *									x															
pgk			x									x			x									x
rplL															x									
rpoC									x															
SMU_109 *						x																		
SMU_1641c			x									x												
SMU_1979c *		x	x	x	x	x	x	x			x		x	x			x	x	x	x		x	x	
SMU_488 *					x																			
SMU_515 *									x															
tuf			x																					

** Represents the proteins that were exclusively identified in the adhered bacteria*

2.4 Discussion

The AEP can modulate the adhesion of the cariogenic bacterium *S. mutans* onto dental surfaces, either by promoting (Brady et al. 1992; Gibbons and Hay 1989) or inhibiting (Shimotoyodome et al. 2006) its attachment to the proteinaceous components of the salivary pellicle. Therefore, the modification of the composition of the AEP could represent a novel strategy to reduce the adhesion of pathogenic microbes and further control the development of pathogenic dental biofilms. In this study, we assessed the potential inhibitory effect of our engineered salivary peptides DR9-DR9 and DR9-RR14 (Basiri et al. 2017), adsorbed onto HAp, on *S. mutans* adhesion. Additionally, a bottom-up proteomic approach was used to determine if the peptides modulate the bacterial proteome profiles upon adhesion to the HAp surface.

The results of this study showed that the number of bacterial cells adhered increased over time, independently of the composition of the AEP (Table 2 and Figure 2). As expected, bacterial counts at 8 h were significantly higher, in all treatment groups, than the numbers obtained at 2 h and 4 h (Figure 2), explained by the fact that bacteria growth occurs in an exponential rate, and event successfully reproduced in the model used to perform these experiments. During the eight hours of bacterial adherence, unspecific and specific mechanisms of HAp colonization may have taken place, allowing *S. mutans* cells to come in close contact with the proteins/peptides used to form the AEP (Busscher and van der Mei 1997; Whittaker et al. 1996). In the case of the negative control group (H), which lacks AEP, the unspecific mechanism of bacterial adhesion may explain the results. Previous studies have shown that streptococci adhere to bare HAp through physicochemical interactions, since this substratum exhibits both anionic and cationic regions, being the anionic regions the ones that predominate (Gorbunoff and Timasheff 1984). If the anionic cell-wall components of *S. mutans* interact directly with HAp, this attachment must be mediated by the cationic regions of the mineral. But as negatively charged regions predominate in the HAp surface, this phenomenon is unlikely to happen due to the electrostatic repulsion between the bacteria and the mineral surface. Then, neutralization of the net HAp surface charge mediated by the adsorption of the calcium from the culture medium onto the HAp, increased the electrostatic forces between both anionic bacterial and mineral surfaces (Rölla et al. 1977).

The comparison made among treatments at each time point showed that the composition of the AEP did affect the number of bacteria adhered to HAp, with the most significant differences found at 8 h (Figure 3). At this time point, bacteria attached to the surface treated with statherin (A) was significantly higher than that obtained with almost all the other groups, while similar to the engineered peptide DR9-RR14 (E). The great number of bacteria adhered observed in the group treated with statherin, suggests that this protein exposes receptor sites (cryptitopes), at the C-terminal region, for oral bacteria ligands upon adsorbed to the dental surfaces, facilitating the bacterial adhesion and subsequent proliferation on the dental surface, as previously observed with other oral microorganisms (Goobes et al. 2006). In fact, as the statherin-derived peptide DR9 belongs to the N-terminal region of the protein (Basiri et al. 2017; Xiao et al. 2015), the absence of receptors at the C-terminal region may be the first explanation to the lower number of bacteria found adhered to the AEP formed from the salivary peptides DR9 (C) and DR9-DR9 (D) (Figure 3). The second reason why fewer bacteria were found adhered to HAp discs treated with the statherin-derived peptides DR9 (C) and DR9-DR9 (D) is because of the acidic nature of these peptides at pH 7.0. Previous studies have shown that adsorbed acidic proteins reduce bacterial attachment by increasing the repulsive electrostatic forces between the anionic protein and the bacterial cell wall (Reynolds and Wong 1983; Simonson and Reiher 1981), or by competing with bacteria for HAp-binding sites (Rolla 1977).

Another mechanism used by the proteins/peptides to inhibit the bacterial adhesion maybe by exerting an antimicrobial activity against *S. mutans*, reducing its viability once entering in contact with the dental surface. Recently, it was demonstrated that histatin 3 as well as the hybrid peptide DR9-RR14 display antibacterial activity against *S. mutans*, which killing activity of the former was similar to the RR14 peptide (Basiri et al. 2017). However, DR9-RR14 was the one that promoted the highest bacterial adherence at 8 h in comparison with the other groups (Figure 3), suggesting that this peptide cannot exert antimicrobial activity against *S. mutans* once adsorbed onto HAp. Contrary to the reduction of bacterial attachment induced by acidic proteins previously discussed, basic proteins promote bacterial adherence (Reynolds and Wong 1983; Simonson and Reiher 1981), explaining why more bacteria was found attached to the HAp treated with RR14 than with histatin 3, since it was the molecule that exhibited the highest pI, and therefore, the highest cationic charge at the pH used during bacterial adherence (7.0) (Table 1). As

the hybrid peptide has a pI of 7.1, its charge must be close to neutral during the adherence experiments, and no electrostatic forces mediated the attachment of *S. mutans* to HAp. Besides, the secondary structure prediction of the DR9-RR14 peptide suggests an α-helix formation from the amino acids in the 3rd to the 15th positions (Heffernan et al. 2016), considered a fundamental structure for the protein/mineral interaction (Long et al. 2001; Makrodimitris et al. 2007; Raj et al. 1992). Thus, we speculate that the remaining 8 amino acids in the C-terminal region of the hybrid peptide may be forming a cryptitope that promotes specific bacterial adherence, however, the mechanism employed by DR9-RR14 to promote bacterial adherence remains to be further elucidated.

Our findings indicate that the number of bacteria adhered to the AEP formed from parotid saliva (G) was significantly lower than all other treatment groups over time (Figure 3). In this study, the group treated with histatin 3 (B) showed lesser bacterial adherence over time, similar to that observed with the negative control (H) (Figure 2). This finding suggests that the inhibitory effect observed in the group G may be due to the greater amount of this protein (and others from the histatin family) in the parotid saliva, from which the protein concentration was adjusted to 1 mg/mL. Then, the saliva used may contain a number of histatins four times higher than the used to form the single-component AEP formed from histatin 3 (B) (198 μM) (Jensen et al. 1994), inhibiting the growth of *S. mutans* (MacKay et al. 1984; Payne et al. 1991). Besides, glycoproteins found in parotid saliva promote bacterial adhesion to HAp, but its adsorption onto HAp may be inhibited by the anionic phosphoproteins histatin 1 and statherin, which compete with larger salivary glycoproteins for a similar binding site upon HA surfaces (Gibbons and Hay 1989; Shimotoyodome et al. 2006). As the treatment of *S. mutans* with AEP-forming salivary proteins in suspension before attaching to the dental surfaces reduce bacterial colonization (Roger et al. 1994), further studies may be done to test if the same phenomenon occurs when our engineered salivary peptides DR9- DR9 and DR9-RR14 are used.

Concerning the bacterial proteome analyses, data suggest that the treatments done to form the single-component AEP onto HAp did not modulate the bacterial proteome upon adherence. It is noteworthy that the protein *SMU_1979c* was the only protein that was found expressed in all groups at the three time points evaluated (Table 4). *SMU_1979c* is an hypothetical protein having a conserved protein domain with adenine-specific DNA

methylase activity (Ajdic et al. 2002), regulating cellular processes like the initiation of replication, recombination, and repair. To the best of our knowledge, this is the first study in which this protein was found expressed exclusively by the adhered *S. mutans*, suggesting that it may play a critical role in the regulation of gene expression during the growth of adhered bacteria. Based on the functions exerted by other DNA methylases expressed by *S. mutans* (*SMU_504*), it can be suggested that *SMU_1979c* may also regulate the expression of virulence factors associated with the cariogenic potential of this bacterium (Banas et al. 2011). Then, further studies should be done to decipher the role of *SMU_1979c* on bacterial adherence and the cariogenicity of *S. mutans* biofilms.

Regarding the methodological aspects of this study, the proposed resazurin-based method to quantify bacteria adhered to the dental surfaces is suitable to differentiate the number of adhered bacteria at different time points when the HAp surface is treated with a specific protein/peptide (Table 2). Moreover, these experiments allowed us to successfully assess the effect of different salivary peptides, adsorbed onto HAp forming the AEP, on the adhesion of *S. mutans*, as a function of time. Based on the data obtained from the positive control group (G) (Figure 3), further studies should evaluate the inhibitory effect of concentrations higher than 198 µM of our engineered peptides on the adhesion of *S. mutans* to HAp. The observed effect on the adhesion of our engineered salivary peptides used as a single peptide solution may differ if combined with saliva due to the possible interaction between the salivary components and our engineered peptides during the formation of the AEP, which was not simulated (Yin et al. 2006). However, this investigation using a single component AEP approach and an *S. mutans* adhesion model, suggested, for the first time, the potential use of the engineered salivary peptide DR9-DR9 to control *S. mutans* colonization of the dental surfaces.

2.5 References

Ajdic D, McShan WM, McLaughlin RE, Savic G, Chang J, Carson MB, Primeaux C, Tian R, Kenton S, Jia H et al. 2002. Genome sequence of streptococcus mutans ua159, a cariogenic dental pathogen. Proc Natl Acad Sci U S A. 99(22):14434-14439.

Azzopardi PV, O'Young J, Lajoie G, Karttunen M, Goldberg HA, Hunter GK. 2010. Roles of electrostatics and conformation in protein-crystal interactions. PLoS One. 5(2):e9330.

Banas JA, Biswas S, Zhu M. 2011. Effects of dna methylation on expression of virulence genes in streptococcus mutans. Appl Environ Microbiol. 77(20):7236-7242.

Basiri T, Johnson ND, Moffa EB, Mulyar Y, Serra Nunes PL, Machado M, Siqueira WL. 2017. Duplicated or hybridized peptide functional domains promote oral homeostasis. J Dent Res. 96(10):1162-1167.

Bowen WH, Tenuta LMA, Koo H, Cury JA. 2019. Dental caries: Etiology and pathogenesis. In: Lamont RJ, Hajishengalis GM, Koo H, Jenkinson HF, editors. Oral microbiology and immunology. Third ed. Washington, DC: ASM Press. p. 251-265.

Brady LJ, Piacentini DA, Crowley PJ, Oyston PC, Bleiweis AS. 1992. Differentiation of salivary agglutinin-mediated adherence and aggregation of mutans streptococci by use of monoclonal antibodies against the major surface adhesin p1. Infect Immun. 60(3):1008-1017.

Bratthall D, Petersen PE, Stjernsward JR, Brown LJ. 2006. Oral and craniofacial diseases and disorders. In: nd, Jamison DT, Breman JG, Measham AR, Alleyne G, Claeson M, Evans DB, Jha P, Mills A, Musgrove P, editors. Disease control priorities in developing countries. Washington (DC): World BankThe International Bank for Reconstruction and Development/The World Bank Group.

Busscher HJ, van der Mei HC. 1997. Physico-chemical interactions in initial microbial adhesion and relevance for biofilm formation. Adv Dent Res. 11(1):24-32.

Dawes C. 1963. The nomenclature of the integuments of the enamel surface of tooth. Brit Dent J. 115:65-68.

Gauci S, van Breukelen B, Lemeer SM, Krijgsveld J, Heck AJ. 2008. A versatile peptide pi calculator for phosphorylated and n-terminal acetylated peptides experimentally tested using peptide isoelectric focusing. Proteomics. 8(23-24):4898-4906.

Gibbons RJ, Hay DI. 1989. Adsorbed salivary acidic proline-rich proteins contribute to the adhesion of streptococcus mutans jbp to apatitic surfaces. J Dent Res. 68(9):1303-1307.

Goobes G, Goobes R, Schueler-Furman O, Baker D, Stayton PS, Drobny GP. 2006. Folding of the c-terminal bacterial binding domain in statherin upon adsorption onto hydroxyapatite crystals. Proc Natl Acad Sci U S A. 103(44):16083-16088.

Gorbunoff MJ, Timasheff SN. 1984. The interaction of proteins with hydroxyapatite. Iii. Mechanism. Anal Biochem. 136(2):440-445.

Hamada S, Koga T, Ooshima T. 1984. Virulence factors of streptococcus mutans and dental caries prevention. J Dent Res. 63(3):407-411.

Hannig C, Hannig M, Attin T. 2005. Enzymes in the acquired enamel pellicle. Eur J Oral Sci. 113(1):2-13.

Heffernan R, Dehzangi A, Lyons J, Paliwal K, Sharma A, Wang J, Sattar A, Zhou Y, Yang Y. 2016. Highly accurate sequence-based prediction of half-sphere exposures of amino acid residues in proteins. Bioinformatics. 32(6):843-849.

Helmerhorst EJ, Alagl AS, Siqueira WL, Oppenheim FG. 2006. Oral fluid proteolytic effects on histatin 5 structure and function. Arch Oral Biol. 51(12):1061-1070.

Jensen JL, Xu T, Lamkin MS, Brodin P, Aars H, Berg T, Oppenheim FG. 1994. Physiological regulation of the secretion of histatins and statherins in human parotid saliva. J Dent Res. 73(12):1811-1817.

Li J, Helmerhorst EJ, Leone CW, Troxler RF, Yaskell T, Haffajee AD, Socransky SS, Oppenheim FG. 2004. Identification of early microbial colonizers in human dental biofilm. J Appl Microbiol. 97(6):1311-1318.

Long JR, Shaw WJ, Stayton PS, Drobny GP. 2001. Structure and dynamics of hydrated statherin on hydroxyapatite as determined by solid-state nmr. Biochemistry. 40(51):15451-15455.

MacKay BJ, Denepitiya L, Iacono VJ, Krost SB, Pollock JJ. 1984. Growth-inhibitory and bactericidal effects of human parotid salivary histidine-rich polypeptides on streptococcus mutans. Infect Immun. 44(3):695-701.

Makrodimitris K, Masica DL, Kim ET, Gray JJ. 2007. Structure prediction of protein-solid surface interactions reveals a molecular recognition motif of statherin for hydroxyapatite. J Am Chem Soc. 129(44):13713-13722.

Marsh PD, Zaura E. 2017. Dental biofilm: Ecological interactions in health and disease. J Clin Periodontol. 44 Suppl 18:S12-S22.

Payne JB, Iacono VJ, Crawford IT, Lepre BM, Bernzweig E, Grossbard BL. 1991. Selective effects of histidine-rich polypeptides on the aggregation and viability of streptococcus mutans and streptococcus sanguis. Oral Microbiol Immunol. 6(3):169-176.

Raj PA, Johnsson M, Levine MJ, Nancollas GH. 1992. Salivary statherin. Dependence on sequence, charge, hydrogen bonding potency, and helical conformation for adsorption to hydroxyapatite and inhibition of mineralization. J Biol Chem. 267(9):5968-5976.

Reynolds EC, Wong A. 1983. Effect of adsorbed protein on hydroxyapatite zeta potential and streptococcus mutans adherence. Infect Immun. 39(3):1285-1290.

Roger V, Tenovuo J, Lenander-Lumikari M, Soderling E, Vilja P. 1994. Lysozyme and lactoperoxidase inhibit the adherence of streptococcus mutans nctc 10449 (serotype c) to saliva-treated hydroxyapatite in vitro. Caries Res. 28(6):421-428.

Rolla G. 1977. Formation of dental integuments--some basic chemical considerations. Swed Dent J. 1(6):241-251.

Rölla G, Robrish SA, Bowen WH. 1977. Interaction of hydroxyapatite and protein-coated hydroxyapatite with streptococcus mutans and streptococcus sanguis. Acta Pathol Microbiol Scand B. 85B(5):341-346.

Sakuma Y, Washio J, Sasaki K, Takahashi N. 2013. A high-sensitive and non-radioisotopic fluorescence dye method for evaluating bacterial adhesion to denture materials. Dent Mater J. 32(4):585-591.

Shimotoyodome A, Kobayashi H, Tokimitsu I, Matsukubo T, Takaesu Y. 2006. Statherin and histatin 1 reduce parotid saliva-promoted streptococcus mutans strain mt8148 adhesion to hydroxyapatite surfaces. Caries Res. 40(5):403-411.

Simonson LG, Reiher DA. 1981. Effect of human saliva and various compounds on the adsorption of the bacterium streptococcus mutans to hydroxyapatite. Arch Oral Biol. 26(2):143-146.

Siqueira WL, Custodio W, McDonald EE. 2012. New insights into the composition and functions of the acquired enamel pellicle. J Dent Res. 91(12):1110-1118.

Siqueira WL, Margolis HC, Helmerhorst EJ, Mendes FM, Oppenheim FG. 2010. Evidence of intact histatins in the in vivo acquired enamel pellicle. J Dent Res. 89(6):626-630.

Siqueira WL, Oppenheim FG. 2009. Small molecular weight proteins/peptides present in the in vivo formed human acquired enamel pellicle. Arch Oral Biol. 54(5):437-444.

Siqueira WL, Zhang W, Helmerhorst EJ, Gygi SP, Oppenheim FG. 2007. Identification of protein components in in vivo human acquired enamel pellicle using lc-esi-ms/ms. J Proteome Res. 6(6):2152-2160.

Valente MT, Moffa EB, Crosara KTB, Xiao Y, de Oliveira TM, Machado M, Siqueira WL. 2018. Acquired enamel pellicle engineered peptides: Effects on hydroxyapatite crystal growth. Sci Rep. 8(1):3766.

Vitorino R, Calheiros-Lobo MJ, Williams J, Ferrer-Correia AJ, Tomer KB, Duarte JA, Domingues PM, Amado FM. 2007. Peptidomic analysis of human acquired enamel pellicle. Biomed Chromatogr. 21(11):1107-1117.

Whittaker CJ, Klier CM, Kolenbrander PE. 1996. Mechanisms of adhesion by oral bacteria. Annu Rev Microbiol. 50:513-552.

Xiao Y, Karttunen M, Jalkanen J, Mussi MC, Liao Y, Grohe B, Lagugné-Labarthet F, Siqueira WL. 2015. Hydroxyapatite growth inhibition effect of pellicle statherin peptides. J Dent Res. 94(8):1106-1112.

Yin A, Margolis HC, Yao Y, Grogan J, Oppenheim FG. 2006. Multi-component adsorption model for pellicle formation: The influence of salivary proteins and non-salivary phospho proteins on the binding of histatin 5 onto hydroxyapatite. Arch Oral Biol. 51(2):102-110.

Chapter 3

3 Validation of a cariogenic biofilm model by evaluating the effect fluoride on enamel demineralization

3.1 Introduction

Dental biofilm is a complex microbial community developed on dental surfaces and embedded in an array of biopolymers of bacterial and host origin (Marsh 2004). Under physiological conditions, different microorganism species live in the same habitat forming a stable community, keeping the balance between health and disease (Marsh 1994). This microbial homeostasis can be disrupted by environmental changes, like the acidification within the biofilm induced by the frequent consumption of dietary sugars. Low-pH microenvironments promote the dominance of *Streptococcus mutans*, an acidogenic and aciduric microbial species, favoring the development of virulent biofilms (Marsh 1994). The constant production of acids close to the tooth surface leads to a progressive dissolution of the mineral phase of the teeth, favoring the development of dental carious lesions (Koo et al. 2013). Thus, dental caries is a biofilm/sugar-dependent disease (Bowen et al. 2019), and these two factors had been considered to simulate the process of carious lesion formation in a laboratory setting (Amaechi et al. 2019).

Diverse *in vitro* biofilm models have been reported in the literature, differing from each other in specific parameters related to the cariogenicity of the biofilms (Amaechi et al. 2019). Each cariogenic biofilm model allows the study of the biofilms virulence and the effect of anticaries/antimicrobial treatments on the biofilms and the de/remineralization process (Bowen et al. 2019). However, only few of the models available to date have been validated by testing the dose-response effect of caries-preventive strategies (Maske et al. 2017). From the validated models, the one proposed by (Ccahuana-Vásquez and Cury 2010) is a batch *S. mutans* biofilm model with dose-response effect of chlorhexidine on the biofilms (Ccahuana-Vásquez and Cury 2010) and of fluoride on enamel and dentine demineralization (Fernández et al. 2016). However, this is a model that does not allow the use of volumes lower than 2 mL of the treatment solutions, limiting its use in a microliter scale. In the present study, we modified a cariogenic biofilm model previously

developed (Ccahuana-Vásquez and Cury 2010) and tested the dose-response effect of fluoride on enamel demineralization. Our model may be useful in the assessment of the anticaries effect of substances when their volumes are limited to 200 μL, as would be the case for novel biotechnological approaches for the control of enamel demineralization (Basiri et al. 2017).

3.2 Materials and Methods

3.2.1 Experimental design

A modified *in vitro* cariogenic *S. mutans* biofilm model was validated by assessing the dose-response effect of fluoride on enamel demineralization. For this, *S. mutans* biofilms were developed for 144 h on saliva-coated bovine enamel slabs which were randomly allocated to each of the treatment groups (n = 10/group). To simulate daily toothbrushing with fluoride toothpaste, biofilms were treated 2x/day with solutions containing 125, 275 and 1250 μg F/mL, or with purified water as a negative control. Aliquots from the exchanged culture medium were stored and analyzed to determine: 1) pH, as an indicator of the acidogenicity of developing biofilms; 2) calcium released daily from enamel to the culture medium (mM Ca), used to calculate the cumulative calcium released from the sum of the concentration found in the last three days of exposure to sucrose (time point: 80 h, 104 h and 128 h), and expressed as μg Ca/cm^2 of enamel; 3) fluoride (mM F). At 144 h, biofilms were collected and processed to calculate the biofilm bound and water-soluble fluoride concentrations, expressed as nmol F/g biofilm. Enamel slabs were also collected to analyze the firmly-bound fluoride concentration (μg F/g enamel). Statistical analysis of the data was performed at a significance level α of 5% (ANOVA and Tukey test; exponential regression).

3.2.2 Collection of stimulated parotid gland saliva

This study was approved by the Human Research Ethics Committee at The University of Western Ontario (protocol number 16181E). Parotid gland saliva was collected with a Lashley cup between 9:00 and 11:00 a.m. from three volunteers with good general oral health who were not taking medications that could alter the salivary flow. Salivary secretion was stimulated by sugar-free acid candies, and the saliva was collected in a 50 ml polypropylene tube, which was submerged in a vessel containing ice. Immediately

after collection, the secretion obtained from the different volunteers was pooled and the total protein concentration was determined by the bicinchoninic acid assay (BCA) using bovine serum albumin as the standard protein. Protein concentration in the saliva was adjusted to 1 mg/mL with 50 mM NaCl pH 6.8. The absence of contamination with microorganisms from the oral cavity was checked by inoculating 100 µL of this secretion in Brain and Heart Infusion Agar for 48 h at 37 °C and 10% CO_2. The remaining secretion solution was stored at -80 °C until use.

3.2.3 Enamel slabs preparation and description of the model

Bovine enamel slabs having 7-mm length, 4-mm width, and 1-mm depth, were obtained from the central region of bovine incisor teeth crowns, where the surface is flatter. The dentin of each slab was completely abraded using a polisher and sand paper with grain size of 400. Subsequently, the enamel surface of each slab was flattened, worn and polished with 0.1 µm diamond paste to obtain slabs of enamel with homogeneous surfaces. The enamel slabs were randomly distributed to each of the treatment groups and vertically assembled in acrylic holders having a 2-mm-depth slot in the middle, which were previously bonded to the lid of a 24-well culture plate. Thus, two surfaces of the enamel slabs were exposed, with an area of 40 mm^2. The disposition of the enamel slabs in the lid allowed them to fit both a 96- and a 24-well culture plate (Figure 4). Subsequently, the assembled lid with the enamel slabs together with the culture plate were sterilized by exposing them to ultraviolet light for 1 h (Kummer et al. 2013).

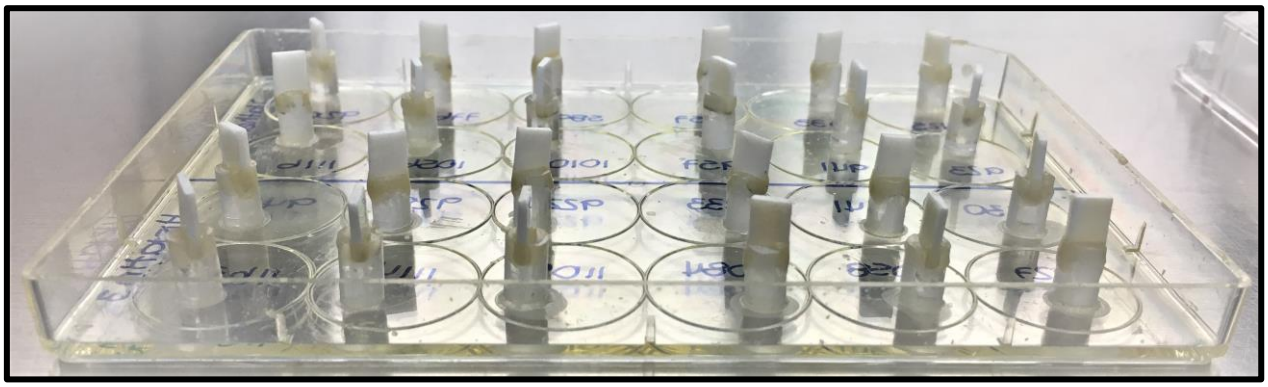

Figure 4. Photograph of enamel slabs assembled to a cell-culture plate lid.

3.2.4 *S. mutans* cariogenic biofilm development

Before starting the biofilm formation, the acquired enamel pellicle (AEP) was allowed to form onto enamel slabs using a 96-well plate. For this, each slab was incubated with 200 μL of parotid secretion/well for 2 h at 37 °C under constant stirring at 60 rpm/min. After two hours of AEP formation, the enamel slabs were washed three times with 0.9% NaCl and transferred to a 24-well plate containing 2 mL of TYEB supplemented with 1% glucose and bacterial inoculum (*S. mutans* UA159, 1 x 10^8 CFU/mL). The enamel slabs were incubated for 8 h at 37 °C and 10% CO_2 to allow bacterial adhesion to the AEP (Ccahuana-Vásquez and Cury 2010), but the concentration of the phosphate buffer was increased by 10x to avoid sudden drop in pH due to the glucose fermentation that occurs during these first 8 hours.

After the adhesion period, the enamel slabs were transferred to fresh TYEB medium containing 0.1 mM glucose and incubated for 16 h at 37 °C and 10% CO_2. From the following day, the biofilms were submitted to periods of "feast" and "famine", in which the biofilms were kept for 8 h/day at 37 ºC and 10% CO_2 in TYEB containing 1% sucrose, simulating cariogenic challenges with carbohydrate exposure. After the cariogenic challenge, the biofilms were washed three times with 0.9% NaCl and rested at 37 °C and 10% CO_2 in TYEB medium containing 0.1 mM glucose. The substituted culture medium was stored for further analyses. Fluoride treatments were performed after 8 h of the cariogenic challenge with 1% sucrose and in the following morning, after the overnight incubation. To perform the treatments, enamel slabs were removed daily from the culture medium, washed three times with 0.9% NaCl, transferred to a 24-well plate containing 2 mL of the corresponding treatment solutions (0, 125, 275, or 1250 μg F/mL) and incubated for 1 minute at room temperature. After the treatment time was completed, the slabs were washed three times with 0.9% NaCl, and finally transferred to the corresponding culture medium. These procedures were repeated over the following days until the biofilms completed 144 hours of formation (Figure 5).

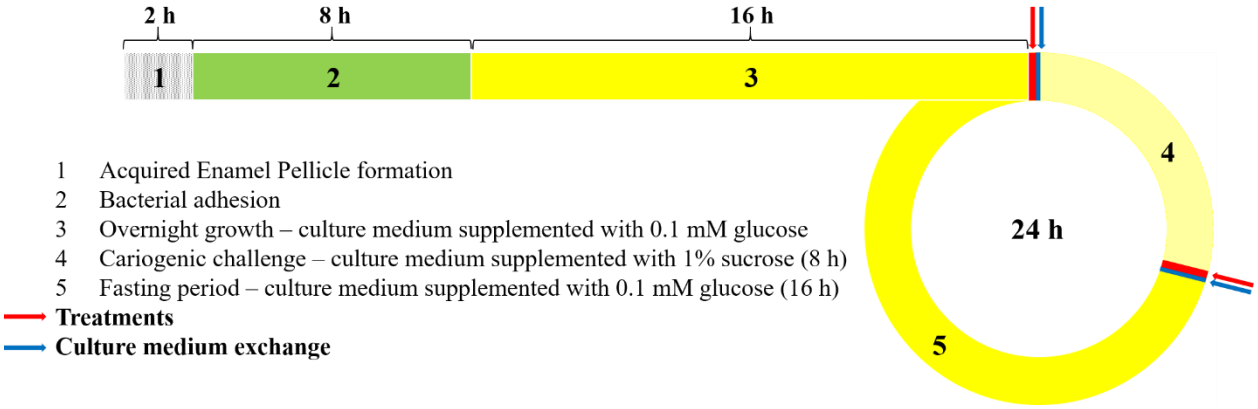

Figure 5. Outline of the experiment. 1) Enamel slabs were incubated with parotid saliva for 2 h to form the AEP. 2) Saliva-coated enamel slabs were inoculated with *S. mutans* in culture medium supplemented with 1% glucose and the bacteria were let to adhere for 8 h. 3) Enamel slabs were let to rest overnight in culture medium supplemented with 0.1 mM glucose. Cariogenic biofilms were formed by repeating the daily pH-cycling regime depicted in the diagram (steps 4 and 5), to which the culture medium was changed twice per day (blue lines): 4) Cariogenic challenge was done by feeding the bacteria with 1% sucrose for 8 h/day. 5) Bacteria fasted overnight in culture medium having 0.1 mM glucose. The corresponding fluoride treatments (red line) were done twice per day before and after the cariogenic challenges.

3.2.5 Culture medium analyses

The acid production by the bacteria in the biofilm was analyzed 2x/day by determining the pH of the culture medium (after each cariogenic challenge and in the following morning, after 16 h of incubation). For this, a pH electrode connected to a pH meter with a pH measurement resolution of ± 0.01, previously calibrated with pH 4.0 and 7.0 standards, was used. After the pH measurement, calcium and fluoride ion concentrations in the culture medium were assessed. For the calcium analyses, 25 µL of the culture medium from each well were used to quantify the calcium concentration (mM), using the Arzenazo III colorimetric method (Vogel et al. 1983) and an spectrophotometer reader at 650 nm, and solutions with known concentrations of calcium as standards (0 – 1.2 mM). Absorbance readings were performed at 650 nm on a 96-well plate spectrophotometer reader. The cumulative calcium concentration in the culture medium (µg Ca/cm²) was determined by the sum of the concentrations found in the last three days of exposure to sucrose (time points: 80 h, 104 h and 128 h). Fluoride analyses were performed after buffering and neutralizing 500 µL of the culture medium with 500 µL of TISAB II (1:1) using a fluoride ion-selective electrode (Orion 9609, ThermoScientific, USA) coupled to an ion analyzer (Fisherbrand accumet AB250, FisherScientific, USA), which was

previously calibrated with standards containing 0.062 – 32 µg F/mL, prepared similarly to the samples.

3.2.6 Biofilm harvesting and analyses

At 144 h, in the morning of the last day of experiment, biofilms were washed three times with 0.9% NaCl, transferred to pre-weighed 1.5-mL microcentrifuge tubes containing 1 mL of 0.9% NaCl, and then sonicated at an amplitude of 10% (Sonic dismembrator, model 500, Fisher Scientific) for 30 s on ice to detach the biofilms from the enamel slabs. The slabs were carefully removed and stored for further analyses. The biofilm suspension was centrifuged at 16,000 × *g* for 5 min at 4 °C and the supernatant was recovered, neutralized and buffered with TISAB II (1:1), and analyzed with a fluoride ion-specific electrode to quantify the water-soluble fluoride concentration in the biofilm (nmol F/g biofilm). The pellet was weighed to determine the biofilm wet mass (g) and then processed to extract the biofilm-bound fluoride. For this, each biofilm pellet was treated with 0.5 M HCl for 3 h under constant agitation at room temperature (Fernández et al. 2016) and then centrifuged at 16,000 × *g* for 3 min at 4 °C. Biofilm-bound fluoride concentration (nmol F/g biofilm) was determined in the supernatant after mixing it with an equal volume of TISAB II containing 0.5 M NaOH. The fluoride analyses were done as described above, using standard solutions containing 0.062 – 1.0 µg F/mL, prepared similarly to the samples, to calibrate the electrode.

3.2.7 Determination of firmly-bound fluoride in enamel

Enamel slabs were washed, dried, and all surfaces were isolated with wax, leaving exposed only the external enamel surface, with an area of ~28 mm². Each slab was immersed in 0.5 M HCl for 30 s under agitation at 150 rpm. Slabs from the negative control group were immersed in 250 µL, while 500 µL were used for fluoride-treated slabs. Each acid extract was buffered and neutralized with the same volume of TISAB II containing 0.5 M NaOH, and the calcium and fluoride concentrations were determined following the same protocol described for the culture medium and biofilm-bound fluoride analyses, respectively. The amount of enamel dissolved was calculated based on the calcium concentration (38%) and density (2.92 g/cm³) (Koo and Cury 1998) of enamel, allowing the calculation of the fluoride concentration in the removed layer of enamel (µg F/g enamel).

3.2.8 Statistical analysis

The normal distribution of errors and the homoscedasticity of variances were checked for all response variables tested, transforming those that did not satisfy these assumptions. As soon as these assumptions were fulfilled, the analysis of variance (ANOVA) was performed, followed by the Tukey test. In addition, a exponential regression of the calcium concentration (µg Ca/cm²) in the culture medium was performed according to the fluoride concentration (µg F/mL) in the treatment solutions. All analyses were performed at a significance level α of 5%, using SPSS software (IBM SPSS Statistics for Windows, Version 21.0, Armonk, NY: IBM Corp.).

3.3 Results

The pH values of the culture medium determined throughout the experiment showed a remarkable drop from the third day of the experiment (56 h). Although pH profiles as a function of time were similar among treatment groups (Figure 6), there was a lower pH decrease in the group treated with 1250 µg F/mL at 104 h and 128 h, being statistically different from the pH obtained at these time points in the other groups (ANOVA and Tukey test, $p < 0.05$).

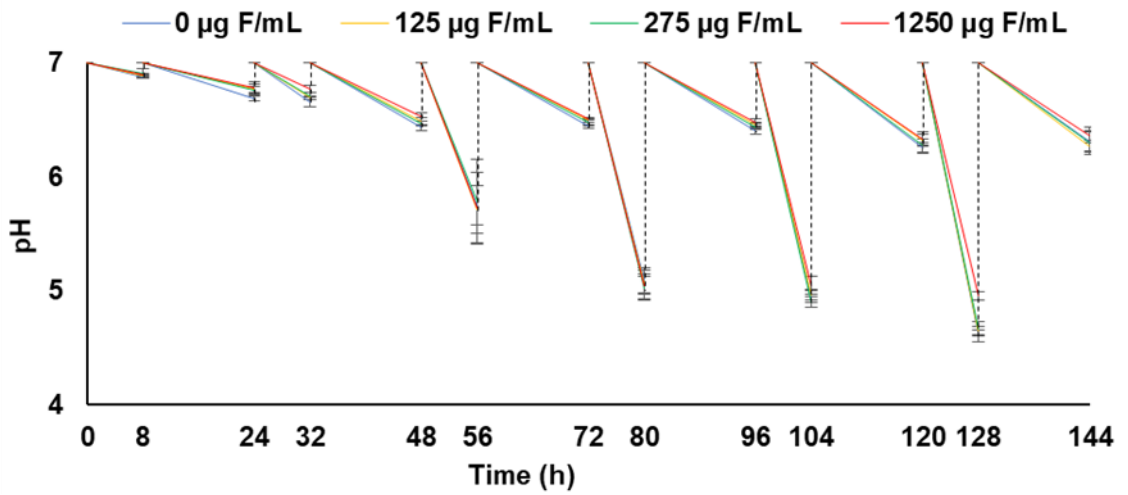

Figure 6. pH of the culture medium according to the treatments as a function of time. Each time the culture medium is changed, the pH returns to the basal pH (pH = 7.0, dashed lines). Mean ± S.D. (n = 10).

The profile of calcium concentration in the culture medium as a function of time showed, for all treatment groups, an inverse relationship with the pH values, since the lower the pH, the highest the calcium concentration (Figure 7A). Conversely, the fluoride concentration was lower when the pH dropped (Figure 7B.

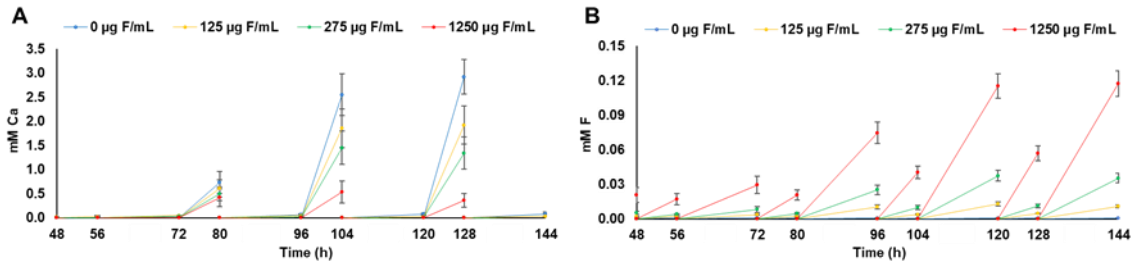

Figure 7. Calcium (A) and fluoride (B) concentration in the culture medium, according to the treatments. Ions concentration was measured before (time points 48 h, 72 h, 96 h, 120 h, 144 h) and after (time points 56 h, 80 h, 104 h, 128 h) sucrose exposure. Mean ± S.D. (n = 10)

As the calcium released from enamel was detected only from the third day of experiment (at 80 h), its concentration found after sucrose exposure during the last three days of biofilm formation (time points 80 h, 104 h and 128 h) was used to determine the cumulative calcium concentration (Figure 8). The *S. mutans* cariogenic biofilm model used in this study was shown to have a dose-response effect with an exponential relationship (R^2 = 0.9607) between the cumulative calcium concentration in the culture medium and the fluoride concentration of the treatments, being higher the demineralization in the absence of fluoride ($p < 0.0001$) (Figure 8).

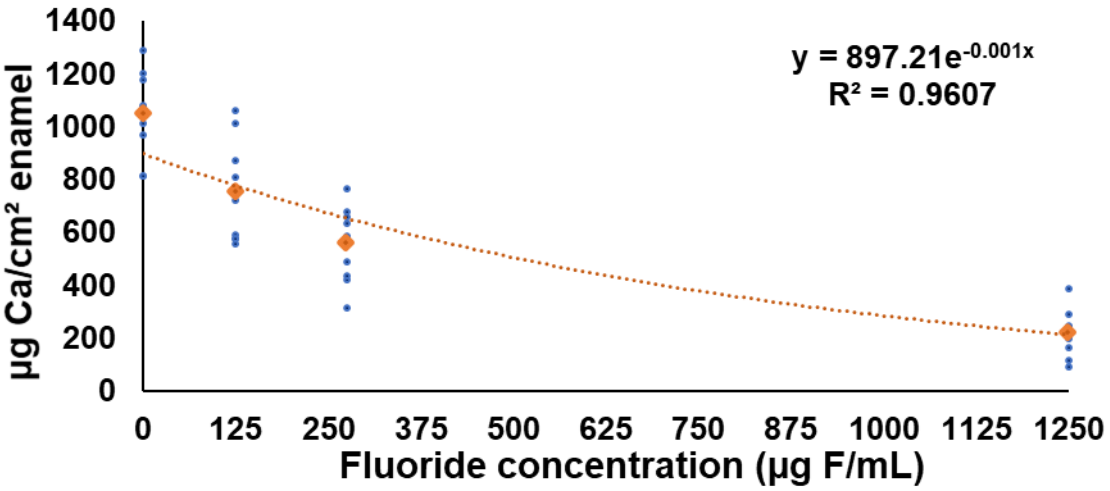

Figure 8. Exponential regression of the cumulative calcium concentration in the culture medium according to the treatments. Exponential regression between the fluoride concentration (µg F/mL) in the treatment solutions and the cumulative calcium concentration (µg F/cm²) in the culture medium. The fit was statistically significant ($p < 0.001$, $R^2 = 0.9607$). Averages (♦) followed by different lower-case letters indicate statistically significant differences among the treatment groups (ANOVA and Tukey test, $p < 0.001$; $n = 10$).

The findings from the fluoride firmly-bound to the enamel confirmed the dose-response effect found and showed no statistical differences between the groups treated with 275 and 1250 µg F/mL, while these groups did differ from the other two groups (Figure 9).

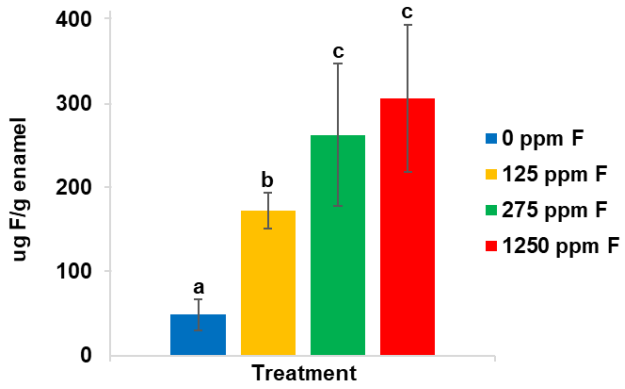

Figure 9. Firmly-bound fluoride concentration (µg F/g) on enamel according to the treatments. Means followed by different lower-case letters indicate statistically significant differences among the treatment groups (ANOVA and Tukey test, $p < 0.0001$). For statistical analysis, data were Log_{10}-tranformed. One datum from the 275 µg F/mL group was considered as outlier: 333.02.

.

Regarding the biofilm analyses, the soluble fluoride concentration was dose-dependent and significantly different among groups (Figure 10A), while the biofilm-bound fluoride concentration differed only between the negative control and the group treated with a solution having 1250 µg F/mL (Figure 10B).

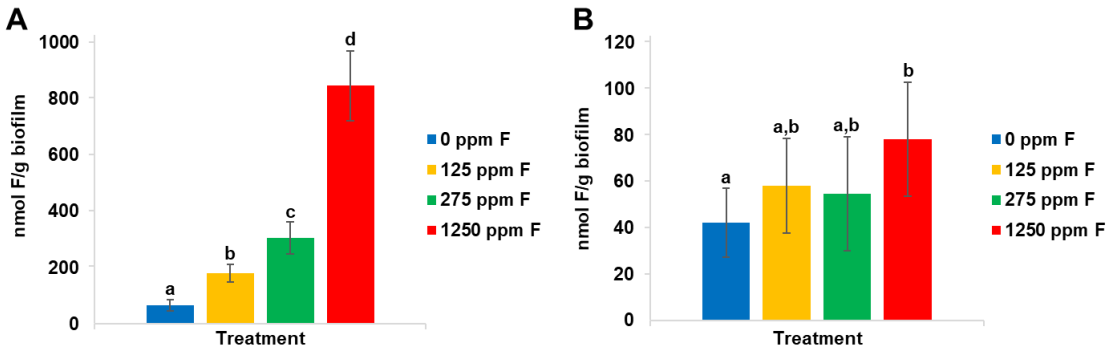

Figure 10. Biofilm soluble (A) and bound (B) fluoride concentration (nmol F/g) according to the treatments. Means followed by different lower-case letters indicate statistically significant differences among the treatment groups (ANOVA and Tukey test, $p < 0.007$). For statistical analysis, soluble-fluoride concentration was Log_{10}-tranformed. The following data from the 275 µg F/mL group were considered as outliers: A) one (432.3 nmol F/g biofilm); B) two (234.2 and 532.3 nmol F/g biofilm).

3.4 Discussion

In vitro biofilm models have been extensively used to study the pathogenicity of biofilms, the process of carious lesion development, and the caries-preventive effect of different therapeutic approaches (Bowen et al. 2019). However, only few of the models available to date had been validated in terms of the dose-response effect of anti-caries and/or antimicrobial substances (Maske et al. 2017). In this study, a validated cariogenic *S. mutans* biofilm model developed by Ccahuana-Vasquez and Cury (Ccahuana-Vásquez and Cury 2010), the advantages, limitations, and applications of which were recently described (Amaechi et al. 2019), was modified allowing the use of microliter volumes of any test solution.

The modified *S. mutans* biofilm model was validated in terms of the dose-response effect of fluoride on enamel demineralization (Figure 8) when the use 2x/day of a toothpaste having low, regular and high fluoride concentration was simulated. During the validation

of the model, fluoridated solutions containing 125, 275, 1250 µg F/mL were used, which reflect the dilution 1:3 that occurs in the oral cavity by saliva while toothbrushing with toothpastes containing 500, 1100 and 5000 µg F/g, respectively (Duke and Forward 1982). Fluoride was selected because it is considered as the agent responsible for the reduction of caries prevalence observed worldwide during the last half century (Petersen et al. 2005), and there is strong evidence to recommend its use throughout the population, regardless of age (dos Santos et al. 2013; Marinho et al. 2003; Walsh et al. 2010). The results showed that this model is sensitive enough to detect the effect of low concentrations of fluoride on the reduction of enamel demineralization (i.e. 125 µg F/mL). The sensitivity and dose-response of the model was observed both in the daily calcium concentration found in the culture medium (Figure 7A), as a chemical indicator of enamel demineralization, and in the cumulative calcium concentration determined by the sum of the concentrations found during the last three days of sucrose exposure (Figure 8), when an increase in the calcium concentration was detected.

Our model can be classified as a cycling model, which better mimics the *in vivo* caries process (Maske et al. 2017). pH shifts during biofilm growth were observed, firstly, when biofilms were subjected to cariogenic challenges for 8 consecutive hours (time points 80 h, 104 h, 128 h) and the pH dropped due to the acids produced as end products of sucrose metabolism by the bacteria in the biofilm (Figure 6) (Bowen et al. 1966). As a result, the mineral phase of enamel was dissolved (Bowen et al. 2019), leading to an increase in calcium concentration in the culture medium (Figure 7A). Secondly, in the absence of sucrose, when the biofilms were let to rest overnight in a culture medium supplemented with the physiological glucose concentration found in saliva (0.1 mM), no demineralization occurred (time points 96 h, 120 h, 144 h), and remineralization took place.

The caries-protective effect of the different concentrations of fluoride tested was mainly physicochemical and directly proportional to the concentration of fluoride used. As the fluoride found in the culture medium corresponds to the one retained and released from the biofilms after the treatments, the fact that less fluoride was detected after the cariogenic challenges (time points 56 h, 80 h, 104 h, 128 h) (Figure 7B) indicates that it interfered with the caries process by reducing enamel demineralization. The higher the fluoride concentration in the treatment solutions, the less the enamel got dissolved (Figure 7A and Figure 8), and the higher the fluoride concentration in the culture medium (Figure

7B). As a consequence of this mechanism, fluoride uptake by enamel increased also in a dose-response manner (Figure 9) (Bowen et al. 2019). The remineralization process also happened in a dose-dependent manner and was facilitated by the calcium in the culture medium and the fluoride available in the biofilms during the overnight period (Fernández et al. 2016), as observed by the concentration of water-soluble fluoride found at 144 h (Figure 10), when the biofilms were collected.

Another mechanism that may have taken place on the reduction of enamel demineralization was the bacteriostatic effect observed only when a solution containing the highest fluoride concentration (1250 µg F/mL) was used. This phenomenon was evident in the acidogenesis profile obtained, were a significant reduction in the acids produced by the biofilms treated with 1250 µg F/mL at 104 h and 128 h was observed (Figure 6). Fluoride inhibits specific enzymes involved in the bacterial acidogenesis pathways when 0.526 mM F is kept constantly in the medium surrounding the biofilms (Bradshaw et al. 2002). However, the concentration of fluoride found in the culture medium, which reflects its concentration within the biofilm, was 5x lower (Figure 7B), nullifying the hypothesis of enolase inhibition. Then, this finding may be explained by the fact that in highly acidic environments, like the one created in the biofilm/enamel interface during the cariogenic challenges, 0.1 mM F may be enough for glycolytic arrest (Marquis 1995), a crucial metabolic pathway needed for acid production. Besides, this finding cannot be attributed to a bactericidal effect because no differences were found in the biofilm wet mass among the treatment groups (Appendix 2).

Regarding the methodological aspects, the use of a single bacterium species may be considered as a limitation of the model. However, a monospecies biofilm model was selected because *S. mutans* displays unique properties (Klein et al. 2015; Koo et al. 2013; Paes Leme et al. 2006; Quivey et al. 2000) that allow it to be considered the most cariogenic microorganism of the dental biofilm (Hamada et al. 1984). For the same reason sucrose was selected, because it is the most cariogenic dietary fermentable sugar (Paes Leme et al. 2006). Another limitation of the study could be the continuous exposure to sucrose during 8h/day, compared to the original model in which the cariogenic challenges are done 8x/day with 10% sucrose for three minutes each (Ccahuana-Vásquez and Cury 2010). Nevertheless, the cariogenicity of the biofilms developed using each model was similar (data not shown) and, in both models, bacteria were submitted to a feast period (cariogenic challenge), followed by an overnight famine period, simulating the pH-

cycling that occurs at the interface between the dental surface and the biofilm fluid, which leads to the de/remineralization process (Bowen et al. 2019). Besides, this modified model has the advantage of reducing biofilm manipulation during its development, compared to the original model (Ccahuana-Vásquez and Cury 2010), and allows the use of volumes at least 200 µL of any treatment solution, as in our case, the saliva used to form the AEP.

In summary, our *S. mutans* cariogenic biofilm model can be used to test the caries-protective effect of fluoridated solutions and other compounds, the amount of which is limited to the microliter scale. Thus, this model is suitable to be used both as a macro- and a micromodel. As the model was validated and shown to be sensitive enough to detect dose-dependent effect of fluoride on enamel demineralization, further studies can be conducted to compare the anticaries efficacy of novel therapeutic approaches versus any of the fluoridated solutions tested in this study, as a positive control.

3.5 References

Amaechi BT, Tenuta LMA, Ricomini Filho AP, Cury JA. 2019. Protocols to study dental caries in vitro: Microbial caries models. Methods Mol Biol. 1922:357-368.

Basiri T, Johnson ND, Moffa EB, Mulyar Y, Serra Nunes PL, Machado M, Siqueira WL. 2017. Duplicated or hybridized peptide functional domains promote oral homeostasis. J Dent Res. 96(10):1162-1167.

Bowen WH, Eastoe JE, Cock DJ. 1966. The effect of sugar solutions on the ph of plaque in caries-active monkeys (macaca irus). Arch Oral Biol. 11(8):833-838.

Bowen WH, Tenuta LMA, Koo H, Cury JA. 2019. Dental caries: Etiology and pathogenesis. In: Lamont RJ, Hajishengalis GM, Koo H, Jenkinson HF, editors. Oral microbiology and immunology. Third ed. Washington, DC: ASM Press. p. 251-265.

Bradshaw DJ, Marsh PD, Hodgson RJ, Visser JM. 2002. Effects of glucose and fluoride on competition and metabolism within in vitro dental bacterial communities and biofilms. Caries Res. 36(2):81-86.

Ccahuana-Vásquez RA, Cury JA. 2010. S. Mutans biofilm model to evaluate antimicrobial substances and enamel demineralization. Braz Oral Res. 24(2):135-141.

dos Santos AP, Nadanovsky P, de Oliveira BH. 2013. A systematic review and meta-analysis of the effects of fluoride toothpastes on the prevention of dental caries in the primary dentition of preschool children. Community Dent Oral Epidemiol. 41(1):1-12.

Duke SA, Forward GC. 1982. The conditions occurring in vivo when brushing with toothpastes. Br Dent J. 152(2):52-54.

Fernández CE, Tenuta LM, Cury JA. 2016. Validation of a cariogenic biofilm model to evaluate the effect of fluoride on enamel and root dentine demineralization. PLoS One. 11(1):e0146478.

Hamada S, Koga T, Ooshima T. 1984. Virulence factors of streptococcus mutans and dental caries prevention. J Dent Res. 63(3):407-411.

Klein MI, Hwang G, Santos PH, Campanella OH, Koo H. 2015. Streptococcus mutans-derived extracellular matrix in cariogenic oral biofilms. Front Cell Infect Microbiol. 5:10.

Koo H, Falsetta ML, Klein MI. 2013. The exopolysaccharide matrix: A virulence determinant of cariogenic biofilm. J Dent Res. 92(12):1065-1073.

Koo RH, Cury JA. 1998. Soluble calcium/smfp dentifrice: Effect on enamel fluoride uptake and remineralization. Am J Dent. 11(4):173-176.

Kummer KM, Taylor EN, Durmas NG, Tarquinio KM, Ercan B, Webster TJ. 2013. Effects of different sterilization techniques and varying anodized tio(2) nanotube dimensions on bacteria growth. J Biomed Mater Res B Appl Biomater. 101(5):677-688.

Marinho VC, Higgins JP, Sheiham A, Logan S. 2003. Fluoride toothpastes for preventing dental caries in children and adolescents. Cochrane Database Syst Rev. (1):CD002278.

Marquis RE. 1995. Antimicrobial actions of fluoride for oral bacteria. Can J Microbiol. 41(11):955-964.

Marsh PD. 1994. Microbial ecology of dental plaque and its significance in health and disease. Adv Dent Res. 8(2):263-271.

Marsh PD. 2004. Dental plaque as a microbial biofilm. Caries Res. 38(3):204-211.

Maske TT, van de Sande FH, Arthur RA, Huysmans M, Cenci MS. 2017. In vitro biofilm models to study dental caries: A systematic review. Biofouling. 33(8):661-675.

Paes Leme AF, Koo H, Bellato CM, Bedi G, Cury JA. 2006. The role of sucrose in cariogenic dental biofilm formation--new insight. J Dent Res. 85(10):878-887.

Petersen PE, Bourgeois D, Ogawa H, Estupinan-Day S, Ndiaye C. 2005. The global burden of oral diseases and risks to oral health. Bull World Health Organ. 83(9):661-669.

Quivey RG, Jr., Kuhnert WL, Hahn K. 2000. Adaptation of oral streptococci to low ph. Adv Microb Physiol. 42:239-274.

Vogel GL, Chow LC, Brown WE. 1983. A microanalytical procedure for the determination of calcium, phosphate and fluoride in enamel biopsy samples. Caries Res. 17(1):23-31.

Walsh T, Worthington HV, Glenny AM, Appelbe P, Marinho VC, Shi X. 2010. Fluoride toothpastes of different concentrations for preventing dental caries in children and adolescents. Cochrane Database Syst Rev. (1):CD007868.

Chapter 4

4 Engineered salivary peptides reduce enamel demineralization provoked by cariogenic *S. mutans* biofilm

4.1 Introduction

Dental caries is a biofilm- and diet-dependent disease (Bowen et al. 2019) that provokes a gradual dissolution of the dental mineral structure by the acids produced from dietary sugars by bacterial fermentation. The adsorption of selective salivary proteins and peptides to the dental surfaces precedes dental biofilm formation (Siqueira and Oppenheim 2009; Siqueira et al. 2007b; Vitorino et al. 2007), forming an acellular film known as acquired enamel pellicle (AEP) (Dawes 1963). The in vivo AEP is composed by around 130 different proteins (Siqueira et al. 2007b), and approximately 50% are natural peptides (Siqueira and Oppenheim 2009; Siqueira et al. 2007b; Vitorino et al. 2007). These natural peptides are produced in the oral cavity from secreted salivary proteins by the action of salivary proteases of bacterial and human origin (Siqueira et al. 2012). Amongst the natural peptides identified in the AEP, those originating from PRPs, histatin and statherin, considered as the major pellicle precursor proteins (Yao et al. 1999), are the most abundant natural peptides composing the AEP (Siqueira and Oppenheim 2009).

The composition of the AEP determines its properties and thus its components may be useful to design strategies for caries control. Proteinaceous components of the AEP have the ability to promote the homeostasis of teeth mineral composition by forming a semipermeable barrier on the tooth surface, reducing its demineralization (Martins et al. 2013; Zahradnik et al. 1976; Zahradnik et al. 1977; 1978b). Recently, it was demonstrated that both the salivary protein histatin 1, which naturally has a phosphoserine residue, and the synthetic phosphorylated form of histatin 3, firmly adsorb on hydroxyapatite, limiting the diffusion of acids throughout the AEP and reducing its demineralization (Siqueira et al. 2010). Another well-known salivary protein that contributes to dental mineral homeostasis is statherin. This protein firmly adsorbs on dental surfaces through its two

phosphoserine residues located at the N-terminal region of the protein, inhibiting the spontaneous precipitation of calcium and phosphate ions on the dental surface (Nancollas and Mohan 1970; Raj et al. 1992). By doing so, statherin proteins keep the saturation state of saliva with relation to HAp, promoting the remineralization and protecting this mineral against demineralization (Kosoric et al. 2007; Shah et al. 2011). These functions are conserved in the naturally occurring 9-residue phosphopeptide derived from statherin, known as DR9, as well as in its engineered duplicated form known as DR9-DR9 (Basiri et al. 2017; Valente et al. 2018; Xiao et al. 2015).

Regarding the antimicrobial activity of the AEP components, it was suggested that the presence of histatin 1 and statherin proteins in the AEP leads to inhibition of *Streptococcus mutans* adherence, the most cariogenic microorganism in the dental biofilm (Hamada et al. 1984), to dental surfaces (Shimotoyodome et al. 2006). Moreover, the antimicrobial activity against *S. mutans* was recently demonstrated for histatin 3, its naturally derived 14-residue peptide known as RR14, and the engineered hybrid peptide DR9-RR14 (Basiri et al. 2017).

The knowledge of the functions exerted by histatin and statherin, and their derived natural peptides RR14 and DR9, respectively, suggests using engineered DR9-DR9 and DR9-RR14 peptides to control caries by interfering simultaneously with dental biofilm formation and the physicochemical process of dental caries development, as previously suggested (Basiri et al. 2017). However, the potential caries-protective effect of DR9-DR9 and DR9-RR14 peptides was observed using a chemical caries model (Basiri et al. 2017), which does not mimic the process of carious lesion development. The *in vitro* caries models used to investigate the caries-protective effect of novel therapeutic agents should consider the two main factors involved in the carious lesion development: biofilm accumulation on the dental surface and the frequent exposure to sucrose, whose cariogenicity is superior to glucose, being only fermented to acids (Cury and Tenuta 2009). Thus, this study aimed to assess a new biotechnological strategy for controlling dental caries by using AEP engineered peptides DR9-DR9 and DR-RR14 in an *S. mutans* cariogenic biofilm model. More specifically, the ability of those peptides to control enamel demineralization and to modulate crucial steps of cariogenic biofilm formation was analyzed. Additionally, for the first time, the bacterial intracellular and ECM proteome profiles were identified and characterized.

4.2 Materials and Methods

4.2.1 Experimental Design

A validated *in vitro* cariogenic *S. mutans* biofilm model was used to test the effect of DR9-DR9 and DR9-RR14 on enamel demineralization when 1) adsorbed onto the enamel surface forming the AEP, and 2) used to treat the biofilms 2x/day. For this, enamel slabs (n = 12/group) were randomly allocated to one of the following treatments: statherin (A), histatin 3 (B), DR9 (C), DR9-DR9 (D), DR9-RR14 (E), RR14 (F), 12,300 µg F/mL (G, positive control), or 50 mM NaCl pH 6.8 (H, negative control). The response variables were: 1) pH of the culture medium, determined 2x/day as an indicator of the acidogenicity of developing biofilms; 2) cumulative calcium released from the enamel slabs, calculated from the concentration found in the culture medium, as a chemical indicator of enamel demineralization (Amaechi et al. 2019) and expressed in µg Ca/cm² of enamel; 3) biofilm biomass (CFU/biofilm and mg protein/biofilm), evaluated in eight of the biofilms collected on the sixth day of the experiment. Also, intracellular and extracellular proteome profiles were obtained after the mass spectrometry identification of the proteins extracted from four biofilms/group. Two independent assays per experimental condition were performed. Our working hypothesis was that our engineered peptides reduce enamel demineralization under highly cariogenic conditions, and it was tested at a significance level α of 5% (ANOVA and Tukey test).

4.2.2 Proteins and peptides used

Synthetic statherin was purchased from Peptide Protein Research Ltd (Hampshire, UK), while synthetic histatin 3 and peptides derived from statherin or histatin 3 were purchased from Synpeptide (Shanghai, China). All the proteins and peptides used in this study are described in Table 5. High-Performance Liquid Chromatography and Mass Spectrometry were used to verify the purity (> 95%) and relative Mr of each protein and peptide. The isoelectric points (pI) of the proteins, as well as the peptides, were determined by the calculator developed by Gauci et al. (Gauci et al. 2008), which calculates the pI of each protein and peptide at a specific pH and various pKa values specified by the user. Thus, the calculation was carried out until the pH at which the net charge is zero was found. The pI values listed in Table 5 were calculated using the Scansite option (Azzopardi et al. 2010). Protein and peptide solutions were prepared in 50 mM NaCl pH 6.8 at a final

concentration of 198 μM, 24 h before starting the experiment. The final concentration was checked in a UV-light spectrophotometer at a wavelength of 215 nm.

4.2.3 Enamel slabs preparation and assembly in the culture plate

Bovine enamel slabs measuring 7-mm length, 4-mm width, and 1-mm depth, were obtained from the central region of bovine incisor teeth crowns, where the surface is flatter. The dentin of each slab was thoroughly abraded using a polisher and sandpaper with a grain size of 400. Subsequently, the enamel surface of each slab was flattened and polished with 0.1 μm diamond paste to obtain enamel slabs having homogeneous surfaces. In the model employed, enamel slabs were randomly distributed to each of the treatment groups and assembled vertically in acrylic holders having a 2-mm-depth slot in the middle, which were previously bonded to the lid of a 24-well culture plate. Thus, two surfaces of the enamel slabs were exposed, with an area of 40 mm^2 (Figure 11). The specimens were assembled to allow us to treat them individually with small volumes of peptide/protein solutions (200 μL/well) using a 96-well plate, and to develop the cariogenic biofilms in a 24-well plate with the standard volume of culture medium (2 mL/well). Subsequently, the assembled lid with the enamel slabs together with the culture plate were sterilized by exposing them to ultraviolet light for 1 h (Kummer et al. 2013).

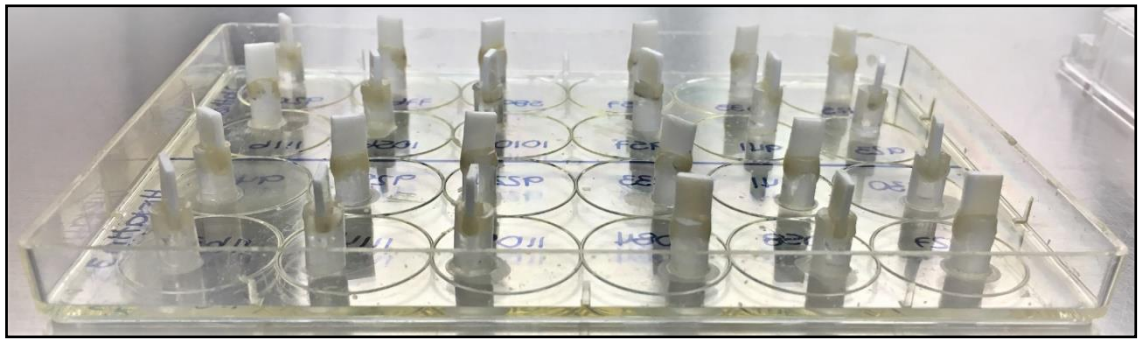

Figure 11. Photograph of enamel slabs assembled to a cell-culture plate lid.

4.2.4 Acquired Enamel Pellicle Formation

Enamel slabs were positioned in a 96-well culture plate and incubated for 24 h at 37 ºC under constant agitation at 60 rpm/min with 200 μL/well/slab of one of the following treatments: (A) statherin, (B) histatin 3, (C) DR9, (D) DR9-DR9, (E) DR9-RR14, (F)

RR14, (G) 12,300 µg F/mL as positive control, (H) 50 mM NaCl pH 6.8 as negative control.

4.2.5 *S. mutans* cariogenic biofilm development

The biofilm model was based on a validated cariogenic *S. mutans* biofilm model developed by Ccahuana-Vasquez and Cury (Ccahuana-Vásquez and Cury 2010). The advantages, limitations, and applications of this model were recently described in detail (Amaechi et al. 2019). The original macromodel was modified enabling us to evaluate the effect of treatments on enamel demineralization when the volume (micromodel) of the test solution is limited, as in the case of our engineered peptides. This modified model was also revalidated, demonstrating a dose-dependent effect of fluoride (0, 125, 275 and 1250 µg F/mL) on enamel demineralization (data not shown). After the AEP formation, enamel slabs were washed three times with 50 mM NaCl pH 6.8 and then transferred to a 24-well culture plate having the standard cell suspension (*S. mutans* UA159, 1 x 10^8 CFU/mL) in 2 mL of TYEB buffered 10x (to avoid pH dropping and enamel demineralization during the adhesion period) and supplemented with 1% glucose. The slabs were incubated for 8 h at 37 ºC and 10% CO_2 to allow bacterial adhesion, then washed three times with 0.9% NaCl, transferred to fresh TYEB supplemented with 0.1 mM glucose and incubated for 16 h at 37 ºC and 10% CO_2. From the next day, at 24 h time point, slabs were exposed to 1% sucrose in TYEB for 8 h at 37 ºC and 10% CO_2, as a daily constant cariogenic challenge. After 8 h, the culture medium was replaced by fresh TYEB supplemented with 0.1 mM glucose and biofilms were let rest overnight at 37 ºC and 10% CO_2. These procedures were repeated during the following days until the biofilms completed 144 h of formation (Figure 12). The replaced culture medium was stored to assess its pH, as an indicator of acidogenesis by the developing biofilms, and to determine the calcium concentration in the culture medium, as a chemical indicator of enamel demineralization.

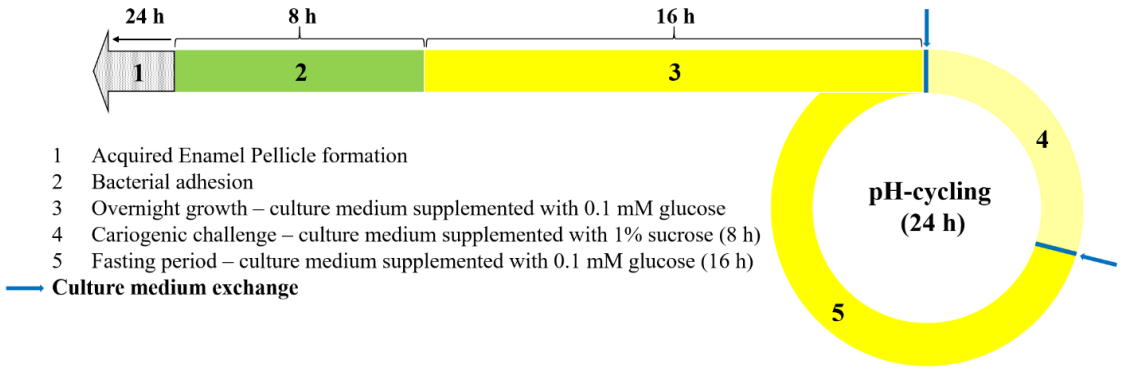

Figure 12. Outline of the experiment. 1) Enamel slabs were incubated with parotid saliva for 2 h to form the AEP. 2) Saliva-coated enamel slabs were inoculated with *S. mutans* in culture medium supplemented with 1% glucose and the bacteria were let to adhere for 8 h. 3) Enamel slabs were let to rest overnight in culture medium supplemented with 0.1 mM glucose. Cariogenic biofilms were formed by repeating the daily pH-cycling regime depicted in the diagram (steps 4 and 5), to which the culture medium was changed twice per day (blue lines and arrows): 4) Cariogenic challenge was done by feeding the bacteria with 1% sucrose for 8 h/day. 5) Bacteria fasted overnight in culture medium having 0.1 mM glucose.

In the experiments in which the biofilms were treated daily, treatments were done with the same solutions used to form the AEP (except for group G, which was treated with a solution containing 275 µg F/mL, simulating the dilution that occurs in the saliva while toothbrushing with a toothpaste containing 1100 µg F/g (Duke and Forward 1982). Treatment solutions were prepared fresh daily. The treatments were performed 2x/day, in the morning, after 16 h of incubation in TYEB supplemented with 0.1 mM glucose, and after 8 h of the cariogenic challenge with 1% sucrose. For this, the biofilms were removed from the culture medium, washed three times with 0.9% NaCl, transferred to a 96-well plate containing 200 µL of the corresponding treatment solution and incubated for 10 minutes at room temperature. After the treatment period, the slabs were washed three times with 0.9% NaCl and finally transferred to the corresponding culture medium (Figure 13).

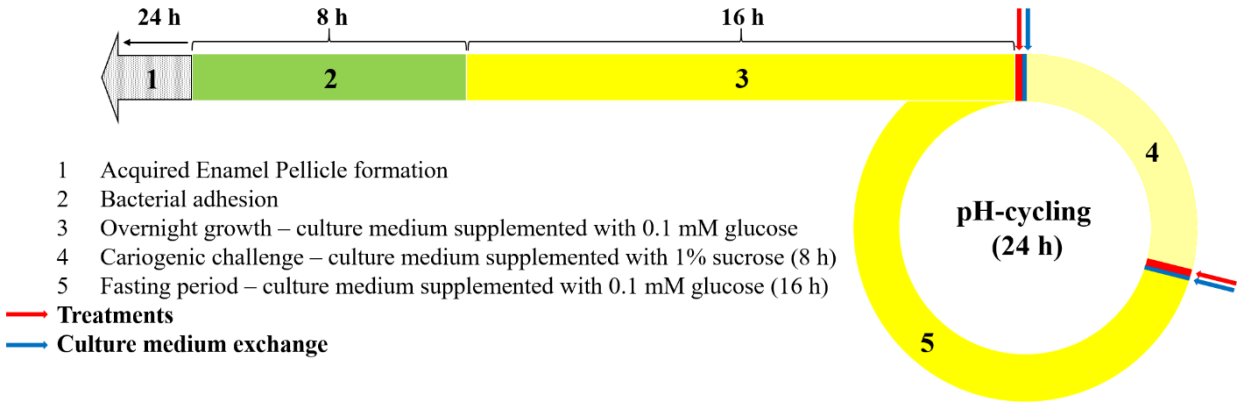

Figure 13. Outline of the experiment treating the biofilms 2x/day. 1) Enamel slabs were incubated with parotid saliva for 2 h to form the AEP. 2) Saliva-coated enamel slabs were inoculated with *S. mutans* in culture medium supplemented with 1% glucose and the bacteria were let to adhere for 8 h. 3) Enamel slabs were let to rest overnight in culture medium supplemented with 0.1 mM glucose. Cariogenic biofilms were formed by repeating the daily pH-cycling regime depicted in the diagram (steps 4 and 5), to which the culture medium was changed twice per day (blue lines and arrows): 4) Cariogenic challenge was done by feeding the bacteria with 1% sucrose for 8 h/day. 5) Bacteria fasted overnight in culture medium having 0.1 mM glucose. The corresponding treatments with the salivary peptides (red lines and arrows) were done twice per day before and after the cariogenic challenges.

4.2.6 Biofilm harvesting and analyses

In the morning of the last day of biofilm formation, when the experiment was completed at 144 h, biofilms were washed three times with 0.9% NaCl. The biofilm biomass and cell viability were determined in eight enamel slabs randomly selected from each group. The remaining four biofilms were used to extract the ECM and intracellular proteins.

For biofilm mass and number of viable bacteria analyses, the corresponding biofilms were individually transferred to microcentrifuge tubes containing 1 mL of 0.9% NaCl and sonicated at an amplitude of 10% (Sonic dismembrator, model 500, Fisher Scientific) for 30 s on ice to separate the bacteria from the enamel slabs. An aliquot of 200 µL of the cell suspension was transferred to a microcentrifuge tube to which 200 µL of 2 M NaOH was added. Alkali-soluble protein concentration (mg protein/biofilm) was determined (BCA, Thermo Scientific) in the supernatant obtained after incubating the suspension for 15 min at 100 °C and centrifuging it at 10,000 × *g* for 10 minutes at 4 °C. The determination of biofilm biomass by the analysis of total alkali-soluble protein concentration was selected because there is a correlation between these two variables,

validating their use (Cury et al. 1994). For the assessment of bacterial viability, we standardized the method of resazurin reduction using 50 μL of the cell suspension that were transferred in duplicate to a well of a 96-well plate, to which 50 μL of KCl buffer (0.05 M KCl, 1 mM $CaCl_2$, and 0.1 mM $MgCl_2$) and 100 μL of a solution containing 2% resazurin in KCl buffer and 0.5% glucose, was added. Fluorescence intensity was measured with a fluorescence spectrophotometer (excitation wavelength: 560 nm, emission wavelength: 590 nm, model 650-40, Hitachi, Tokyo, Japan) after a 90-minute incubation period at 37 °C. Bacterial viability was determined using a calibration curve of fluorescence intensity versus cell viability (CFU/biofilm) performed on the same day from serial dilutions of one of the biofilms.

For ECM and intracellular protein extraction, the corresponding biofilms were collected and transferred to microcentrifuge tubes containing 500 μL of 0.1 N NaOH and 1 mM EDTA (for each 10 mg of biofilm wet weight) (Cury et al. 2000; Paes Leme et al. 2008). Biofilms were incubated for 1 h at 4 °C under constant agitation and then centrifuged at 10,000 × *g* for 10 min at 4 °C. The supernatant having the ECM proteins was transferred to a microcentrifuge tube, and the proteins were precipitated by adding three volumes of ice-cold acetone (Cury et al. 2000; Paes Leme et al. 2008). The pellet containing the bacteria was processed to extract the intracellular proteins by adding 500 μL of 0.1 N NaOH and 1 mM EDTA. The tube was vortexed, incubated for 15 min at 100 °C and centrifuged at 10,000 × *g* for 10 min at 4 °C. The supernatant containing the intracellular proteins was transferred to a microcentrifuge tube, and the proteins were precipitated and concentrated with three volumes of ice-cold acetone. The total protein concentration was determined in duplicate by the bicinchoninic acid assay using a spectrophotometer at a wavelength of 562 nm. A protein equivalent of 10 μg was digested with trypsin (5% trypsin in 50 mM NH_4HCO_3, pH 7.8) for 16 h at 37 °C and purified with a C18 column for proteomic analysis.

4.2.7 Culture medium analyses

The acid production by the bacteria in the biofilm was analyzed 2x/day by determining the pH of the culture medium (after each cariogenic challenge and in the following morning, after 16 h of incubation). For this, a pH electrode connected to a pH meter with a pH measurement resolution of ±0.01, previously calibrated with pH 4.0 and 7.0 standards was used.

After the pH determination, 25 μL of the culture medium from each well was used to quantify the calcium concentration (mM) on it, using the Arzenazo III colorimetric method (Vogel et al. 1983), and solutions with known concentrations of calcium as standards (0 – 1.2 mM). The variation coefficient of the repeated analyses (duplicate) was 1.9%. Also, aliquots of the fresh culture medium were obtained every day to determine the basal calcium concentration on them. Absorbance readings were performed at 650 nm on a 96-well plate spectrophotometer reader. The cumulative concentration of calcium in the culture medium (μg Ca/cm^2) was determined by the sum of the concentrations found in the last three days of exposure to sucrose (time points: 80 h, 104 h, and 128 h).

4.2.8 Proteome analysis

The analysis of tandem mass spectrometry of the ECM and intracellular proteins was performed according to a previously described protocol (Siqueira and Oppenheim 2009) using a Velos LTQ (Thermo-Finnigan, San Jose, CA). The obtained MS/MS spectra were searched against *S. mutans* protein databases (Swiss Prot and TrEMBL, Swiss Institute of Bioinformatics, Geneva, Switzerland, http://ca.expasy.org/sprot/) using SEQUEST algorithm in Proteome Discoverer 1.3 software (Thermo Scientific, San Jose, CA, USA). Search results were filtered for a False Discovery Rate of 1% employing a decoy search strategy utilizing a reverse database. The following biological process were used to classify the identified proteins: adaptative responses to environmental changes; bacterial adherence and biofilm formation; carbohydrate metabolism and energy production; cell division, replication and cell wall synthesis; nucleoside/nucleotide metabolism and synthesis; transcription; translation and protein synthesis; transport; other metabolic processes; and uncharacterized/unknown proteins. The relative percentage of the proteins identified per biological function was calculated from the total proteins found in each treatment group. This variable was used to estimate those biological functions in which the proteins were down- or upregulated when the relative percentage was twice higher or lower than the negative control, respectively.

4.2.9 Statistical analysis

The normal distribution of the errors and the homogeneity of the variances were checked. Once these assumptions were fulfilled, analyses of variance (ANOVA) were performed to test the effect of the treatments on the response variables. Tukey tests were performed

when an effect was observed for each response variable. All statistical analyses were done at a significance level α of 5%, using SPSS (IBM SPSS Statistics for Windows, Version 21.0. Armonk, NY: IBM Corp.).

4.3 Results

The pIs were calculated for each peptide and protein at pH 6.8. Histatin 3 and statherin, as positively and negatively charged proteins, respectively, demonstrated pIs of 10.4 and 4.4. DR9-DR9 exhibited the lowest pI value (3.4) just below that of the natural statherin peptide DR9, whereas RR14 showed the highest value (11.0) and DR9-RR14 was intermediate (7.1) (Table 5).

Table 5. Constructed peptides derived from statherin and histatin and their calculated pIs.

Peptide/Protein Name	Peptide/Protein Sequence	pI
DR9	DSpSpEEKFLR	3.6
DR9-DR9	DSpSpEEKFLRDSpSpEEKFLR	3.4
DR9-RR14	DSpSpEEKFLRRKFHEKHHSHRGYR	7.1
RR14	RKFHEKHHSHRGYR	11.0
Statherin	DSpSpEEKFLRRIGRFGYGYGPYQPVPEQPLYPQPYQPQYQQYTF	4.4
Histatin 3	DSHAKRHHGYKRKFHEKHHSHRGYRSNYLYDN	10.4

Sp represents a phosphorylated serine

The results of the study in which the effect on enamel demineralization of the engineered salivary peptides present only in AEP, showed a decrease in the pH of the culture medium after the cariogenic challenges. These drops were detected on the third day of the experiment (56 h). At this time point, it was possible to observe statistical differences among the treatment groups (ANOVA and Tukey test, $p < 0.0001$). The group treated with the positive control (G) was the one with the lowest acidogenicity, and the group treated with NaCl (H), as the negative control, was the one with the highest production of acids. From the fourth day of the experiment, pH values were similar among groups, being below a value of 5.0 (Figure 14a). Comparable results were obtained when the biofilms were treated daily, but no statistical differences were observed at any time among groups (ANOVA and Tukey test, $p > 0.05$) (Figure 14b).

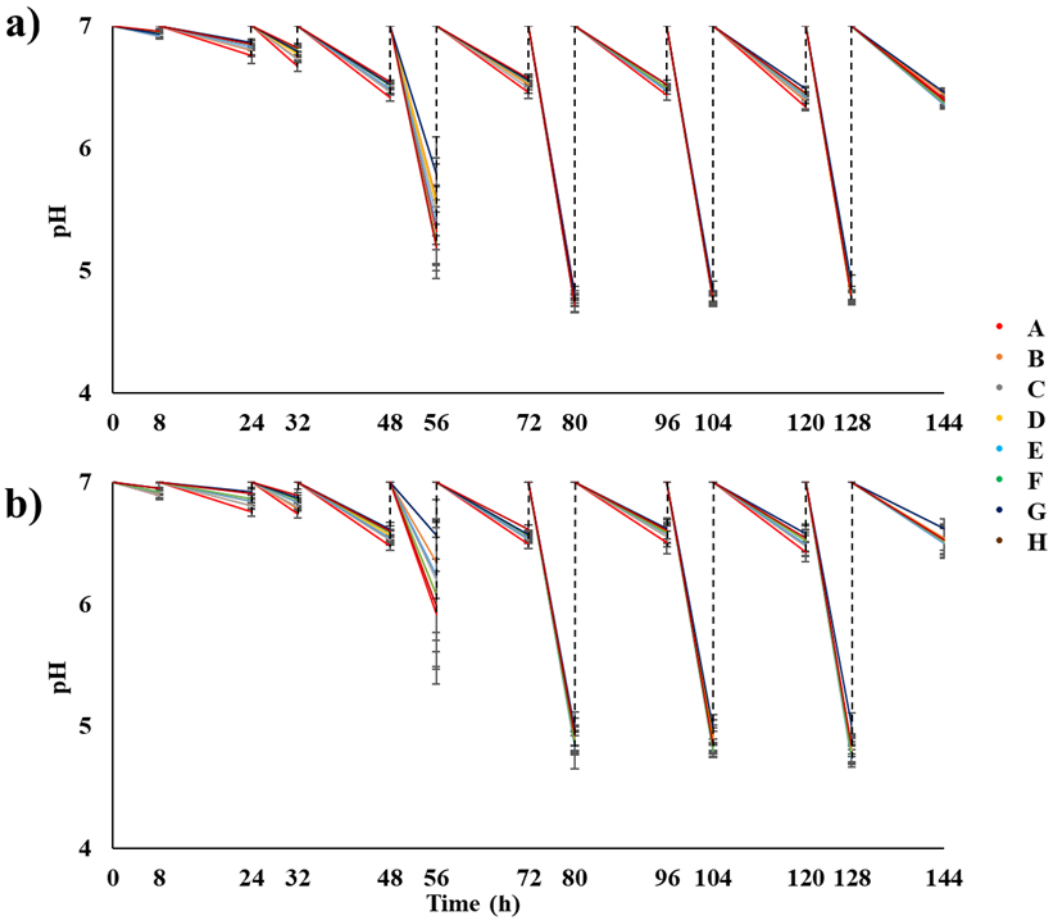

Figure 14. pH of the culture medium according to the treatments as a function of time. Statherin (A), histatin 3 (B), DR9 (C), DR9-DR9 (D), DR9-RR14 (E), RR14 (F), 12,300 µg F/mL (G), 50 mM NaCl, pH 6.8 (H). Each time the culture medium is changed, the pH returns to the basal pH (pH = 7.0, dashed lines). **a)** pH of the culture medium obtained when the peptides were present only in the AEP. **b)** pH of the culture medium found when the peptides were used both to form the AEP and to treat the biofilms. Mean ± S.D., n = 12.

The profile of the calcium concentration in the culture medium as a function of the time of biofilm formation showed for all treatment groups, an inverse relation with the pH. A lower pH and higher calcium concentrations indicate the demineralization of enamel due to the production of acids by the bacteria in the biofilm (Figure 15). However, the calcium released from the enamel was detectable only from the third day of the experiment (80 h) (Figure 15), being this the time point from which the pH of the culture medium was lower than 5.0 in all the treatment groups (Figure 14). In Figure 15 it was possible to observe that enamel demineralization was almost completely inhibited by fluoride (G), at every time evaluated. On the one hand, when the salivary proteins/peptides were used only to

form the AEP, there was a reduction in the demineralization only in the groups treated with statherin (A) and DR9-RR14 (E) at 80 h, being these values statistically different from the other groups (ANOVA and Tukey test, $p < 0.05$). Although the group treated with the peptide DR9-RR14 (E) showed a lower demineralization at 104 h and 128 h time points, there were no statistically significant differences among the groups treated with salivary proteins/peptides ($p > 0.05$) (Figure 15a). On the other hand, when the biofilms were additionally treated with the salivary proteins/peptides daily, there were no differences among groups at 80 h and 104 h. At 128 h, there was a significant reduction of enamel demineralization in the slabs treated with DR9-RR14 (E) compared to the negative control (H), but statistically similar to the groups treated with histatin 3 (B) and statherin (A) (ANOVA and Tukey test, $p < 0.05$) (Figure 15b).

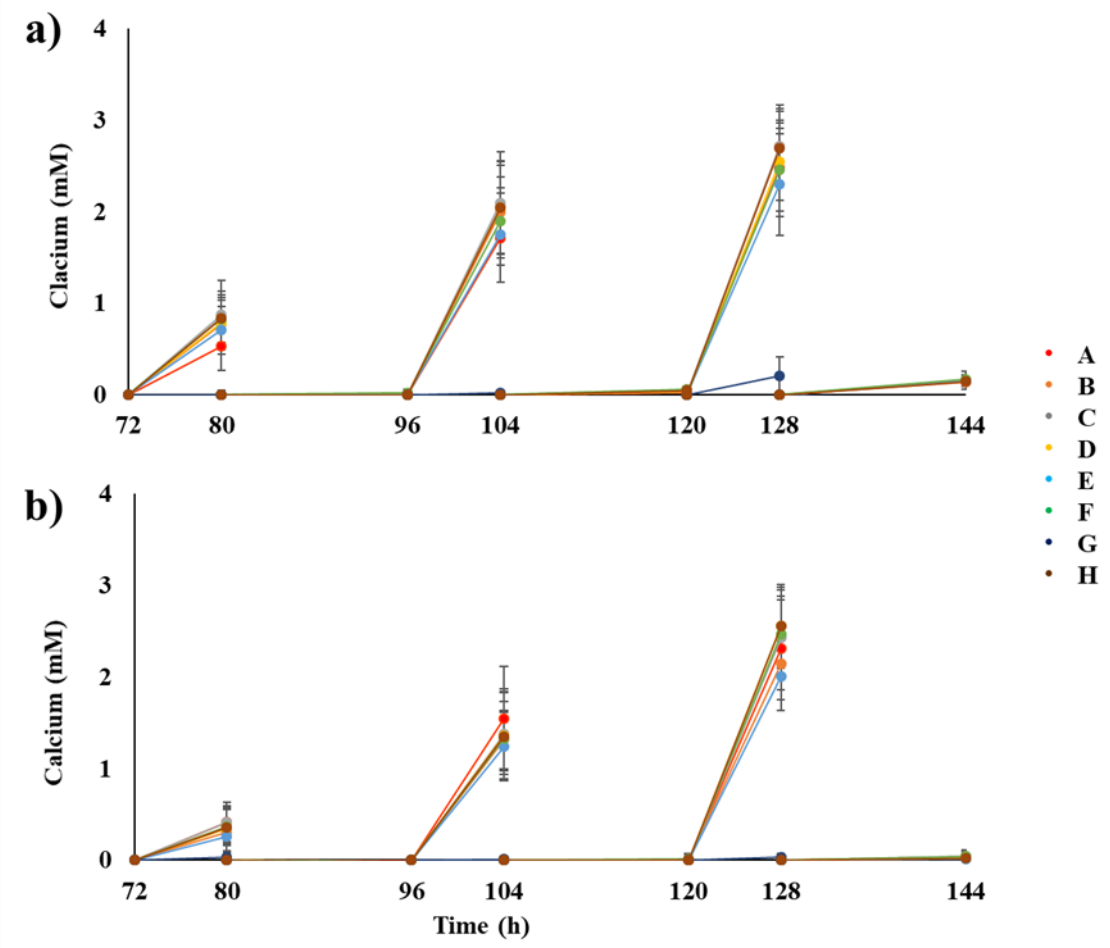

Figure 15. Calcium concentration in the culture medium according to the treatments. Concentration found after the cariogenic challenge done in the fourth (80 h), fifth (104 h) and sixth (128 h) day, and in the last three days after the overnight fasting

period (72 h, 96 h, 120 h, and 144 h). Statherin (A), histatin 3 (B), DR9 (C), DR9-DR9 (D), DR9-RR14 (E), RR14 (F), 12,300 µg F/mL (G), 50 mM NaCl, pH 6.8 (H). **a)** Calcium concentration in the culture medium obtained when the peptides were present only in the AEP. **b)** Calcium concentration in the culture medium found when the peptides were used both to form the AEP and to treat the biofilms. Mean ± S.D., n = 12.

Regarding the cumulative calcium concentration (µg Ca/cm²) in the culture medium, significant differences were found among all treatment groups. The least amount of demineralization was found in the enamel slabs treated with NaF, followed by the group treated with the hybrid peptide DR9-RR14 (E) (Figure 16). When the salivary proteins/peptides were used only to form the AEP, the demineralization obtained in the group treated with DR9-RR14 was similar to that of statherin (A), RR14 (F), DR9-DR9 (D) and Histatin 3 (B) groups; while the groups treated with NaCl (H) and DR9 (C), were those that had the highest demineralization values, being different from the two groups that demonstrated the highest protection against enamel demineralization (G and E) (ANOVA and Tukey test, $p < 0.0001$) (Figure 16a). After using the salivary proteins/peptides also to treat the biofilms daily, the calcium concentration found in the group treated with DR9-RR14 (E) was similar to that of the groups treated with histatin 3 (B), DR9-DR9 (D), and RR14 (F). Those groups treated with DR9 (C), statherin (A), and NaCl (H), were among those that showed the highest demineralization, being different from those that showed the highest protection against demineralization (G and E) (ANOVA and Tukey test, $p < 0.0001$) (Figure 16b).

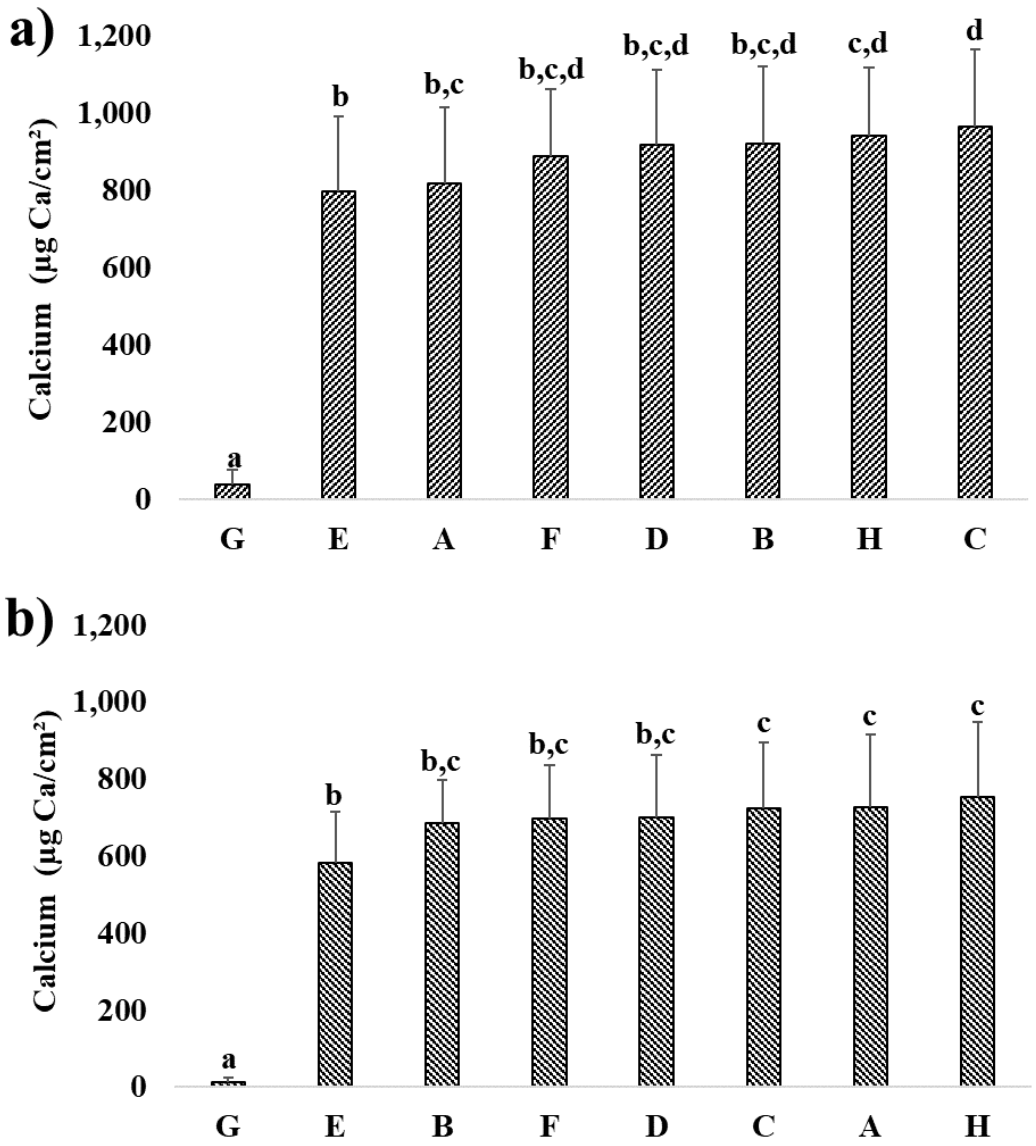

Figure 16. Cumulative calcium concentration in the culture medium according to the treatments. Statherin (A), histatin 3 (B), DR9 (C), DR9-DR9 (D), DR9-RR14 (E), RR14 (F), 12,300 µg F/mL (G), 50 mM NaCl, pH 6.8 (H). **a)** Cumulative calcium concentration in the culture medium obtained when the peptides were present only in the AEP. **b)** Cumulative calcium concentration in the culture medium found when the peptides were used both to form the AEP and to treat the biofilms. Means followed by distinct letters show statistical differences among groups (ANOVA and Tukey test, $p < 0.0001$; Mean ± S.D., n = 12).

Concerning the biomass analyses, the data showed a significant reduction of biofilm mass and bacterial viability in the positive control group treated with NaF (G) when compared to the other groups (Table 6 and Table 7, columns 3 and 4). Contrarily, the groups treated

with NaCl (H), RR14 (F) and DR9-RR14 (E) displayed the highest biofilm biomass when the peptides were used only to form the AEP (Table 6, column 3).

Table 6. Biomass (mg protein/biofilm) and bacterial viability (CFU/biofilm) according to the treatments done to form the AEP.

Treatment	Code	mg protein/biofilm	CFU/biofilm
		Mean (± S.D.)	Mean (± S.D.)
NaF	**G**	0.77 (0.07) [a]	4.97^10 (7.68^9) [a]
Histatin 3	**B**	0.96 (0.09) [b]	6.94^10 (9.62^9) [b]
Statherin	**A**	1.04 (0.14) [b.c]	6.96^10 (1.15^10) [b]
DR9-DR9	**D**	1.04 (0.10) [b.c.d]	6.99^10 (9.95^9) [b]
DR9	**C**	1.06 (0.11) [b.c.d]	7.02^10 (6.41^9) [b]
NaCl	**H**	1.10 (0.11) [c.d]	7.10^10 (9.89^9) [b]
RR14	**F**	1.11 (0.11) [c.d]	7.13^10 (5.33^9) [b]
DR9-RR14	**E**	1.16 (0.09) [d]	7.42^10 (5.77^9) [b]

Means followed by distinct letters show statistical differences among groups (ANOVA and Tukey test, $p < 0.001$).

Table 7. Biomass (mg protein/biofilm) and bacterial viability (CFU/biofilm) according to the treatments done to form the AEP and used daily.

Treatment	Code	mg protein/biofilm	CFU/biofilm
		Mean (± S.D.)	Mean (± S.D.)
NaF	**G**	1.08 (0.18) [a]	3.67^10 (1.42^10) [a]
NaCl	**H**	1.38 (0.19) [b]	7.45^10 (1.52^10) [b]
Histatin 3	**B**	1.40 (0.17) [b]	7.57^10 (1.19^10) [b]
Statherin	**A**	1.42 (0.16) [b]	7.44^10 (1.10^10) [b]
DR9	**C**	1.42 (0.19) [b]	7.23^10 (1.44^10) [b]
DR9-DR9	**D**	1.43 (0.17) [b]	7.64^10 (1.10^10) [b]
DR9-RR14	**E**	1.45 (0.20) [b]	7.72^10 (1.39^10) [b]
RR14	**F**	1.50 (0.18) [b]	7.34^10 (1.39^10) [b]

Means followed by distinct letters show statistical differences among groups (ANOVA and Tukey test, $p < 0.001$).

The proteome profiles obtained after generally classifying the identified intracellular and ECM proteins by the biological process in which each protein participates, showed that the proteins/peptides used both to form the AEP (Figure 17) and to daily treat the biofilms (Figure 18) modulate the expression of intracellular proteins, while the proteome profiles obtained from the ECM proteins were similar among groups. When the treatments were done only to form the AEP, group B did not express proteins participating in adaptative responses to environmental changes, while in the group C any protein participating in

nucleoside/nucleotide metabolism and synthesis was detected. Additionally, fluoride treatment (G) nullified protein expression in three biological functions: cell division, replication, and cell wall synthesis; nucleoside/nucleotide metabolism and synthesis; and transcription (Figure 17). The addition of daily treatments abolished the expression of proteins involved in nucleoside/nucleotide metabolism in the groups C, E, F, and G (Figure 18).

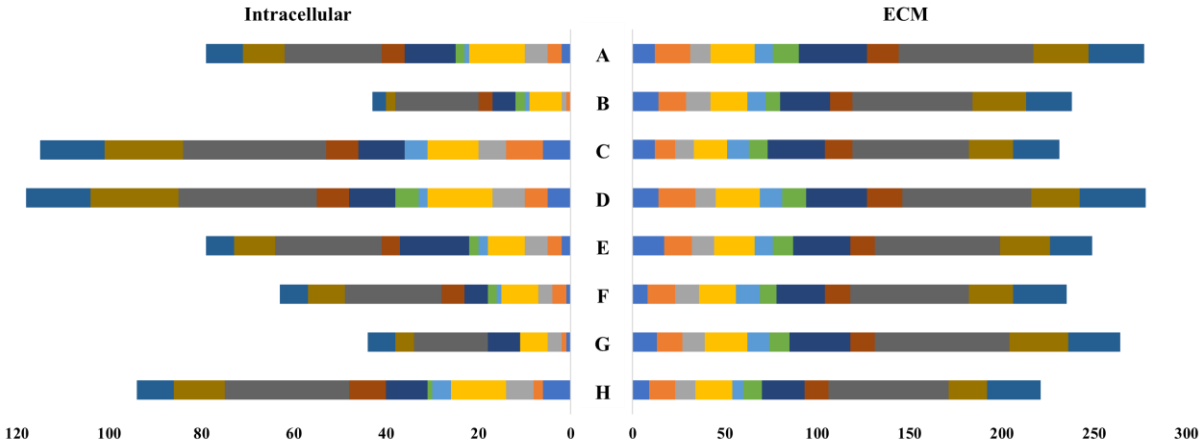

	A	B	C	D	E	F	G	H	A	B	C	D	E	F	G	H
Adaptative responses to environmental changes	2	0	6	5	2	1	1	6	12	14	12	14	17	8	13	9
Amino acid metabolism and biosynthesis	3	1	8	5	3	3	1	2	19	15	11	20	15	15	14	14
Bacterial adherence and biofilm formation	5	1	6	7	5	3	3	6	11	13	10	11	12	13	12	11
Carbohydrate metabolism and energy production	12	7	11	14	8	8	6	12	24	20	18	24	22	20	23	20
Cell division, replication and cell wall synthesis	1	1	5	2	2	1	0	4	10	10	12	12	10	13	12	6
Nucleoside/Nucleotide metabolism and biosynthesis	2	2	0	5	2	2	0	1	14	8	10	13	11	9	11	10
Other metabolic processes	11	5	10	10	15	5	7	9	37	27	31	33	31	26	33	23
Transcription	5	3	7	7	4	5	0	8	17	12	15	19	13	14	13	13
Translation and protein synthesis	21	18	31	30	23	21	16	27	73	65	63	70	68	64	73	65
Transport	9	2	17	19	9	8	4	11	30	29	24	26	27	24	32	21
Uncharacterized/Unknown	8	3	14	14	6	6	6	8	30	25	25	36	23	29	28	29

Figure 17. Distribution of *S. mutans* intracellular and ECM proteins into specific biological processes according to the treatments done to form the AEP. Statherin (A), histatin 3 (B), DR9 (C), DR9-DR9 (D), DR9-RR14 (E), RR14 (F), 12300 ppm F (G), 50 mM NaCl, pH 6.8 (H).

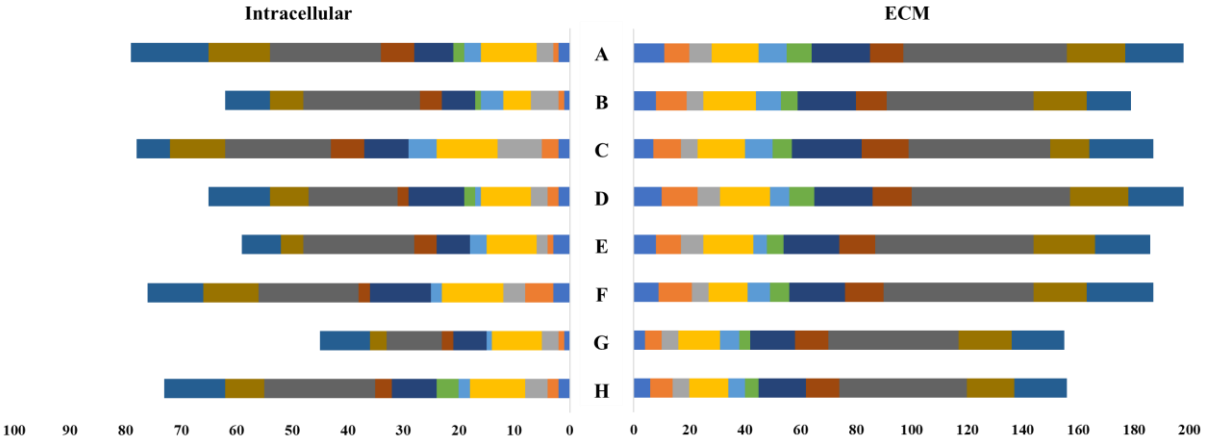

	A	B	C	D	E	F	G	H	A	B	C	D	E	F	G	H
Adaptative responses to environmental changes	2	1	2	2	3	3	1	2	11	8	7	10	8	9	4	6
Amino acid metabolism and biosynthesis	1	1	3	2	1	5	1	2	9	11	10	13	9	12	6	8
Bacterial adherence and biofilm formation	3	5	9	3	2	4	3	5	8	6	6	8	8	6	6	6
Carbohydrate metabolism and energy production	10	9	11	9	9	11	5	10	17	19	17	18	18	14	15	14
Cell division, replication and cell wall synthesis	3	4	5	1	3	2	1	2	10	9	10	7	5	8	7	6
Nucleoside/Nucleotide metabolism and biosynthesis	2	1	0	2	0	0	0	4	9	6	7	9	6	7	4	5
Other metabolic processes	7	6	8	10	6	11	6	8	21	21	25	21	20	20	16	17
Transcription	6	4	6	2	4	2	2	3	12	11	17	14	13	14	12	12
Translation and protein synthesis	20	21	19	16	20	18	10	20	59	53	51	57	57	54	47	46
Transport	11	6	10	7	4	10	3	7	21	19	14	21	22	19	19	17
Uncharacterized/Unknown	14	8	6	11	7	10	9	11	21	16	23	20	20	24	19	19

Figure 18. Distribution of *S. mutans* intracellular and ECM proteins into specific biological processes according to the treatments done to form the AEP and used daily. Statherin (A), histatin 3 (B), DR9 (C), DR9-DR9 (D), DR9-RR14 (E), RR14 (F), 12300 ppm F (G), 50 mM NaCl, pH 6.8 (H).

Despite the differences previously described, for both experiments, the relative percentage of the intracellular (Figure 17) and ECM (Figure 18) proteins classified per biological process were similar among groups. On the one hand, the most abundant intracellular proteins were those involved in translation and protein synthesis (28.9% ± 5.2%); carbohydrate metabolism and energy production (13.2% ± 1.8%); uncharacterized/unknown proteins (12.3% ± 4.1%); other metabolic processes (11.8% ± 3.3%); and transport (10.9% ± 3.1%). The less abundant proteins were those participating in nucleoside/nucleotide metabolism and synthesis (1.9% ± 1.9%); adaptative responses to environmental changes (3.0% ± 1.6%); cell division, replication and cell wall synthesis (3.0% ± 1.8%); amino acid metabolism and biosynthesis (3.3% ± 1.7%); transcription (5.6% ± 2.3%); and bacterial adherence and biofilm formation (5.9% ± 2.1%). On the other hand, the most abundant ECM proteins were those proteins participating in translation and protein synthesis (28.3% ± 1.5%); other metabolic processes (11.6% ± 1.1%); uncharacterized/unknown proteins (11.3% ± 1.3%); transport (10.6% ± 1.2%);

and carbohydrate metabolism and energy production (8.9% ± 0.7%) (Table 8). The less abundant proteins were those involved in nucleoside/nucleotide metabolism and synthesis (4.0% ± 0.7%); bacterial adherence and biofilm formation (4.2% ± 0.7%); cell division, replication and cell wall synthesis (4.3% ± 0.9%); adaptative responses to environmental changes (4.6% ± 1.0%); amino acid metabolism and biosynthesis (5.8% ± 0.9%); and transcription (6.5% ± 1.1%) (Table 8).

The expression of intracellular proteins participating in the following biological functions was found to be either down- or upregulated at least twice with respect to the negative control, especially when the treatments were done only to form the AEP: amino acid metabolism and biosynthesis; cell division, replication and cell wall synthesis; and nucleoside/nucleotide metabolism and synthesis (Table 8). Although the proteins that promote adaptative responses to environmental changes were downregulated, other bacterial proteins directly related to the cariogenicity of the biofilms like those participating in bacterial adherence and biofilm formation, and carbohydrate metabolism and energy production, were not modulated by the engineered peptides (Table 8).

The list of the proteins identified in each of the experiments is included as appendices (Appendix 3, Appendix 4, Appendix 5, Appendix 6).

Table 8. Relative percentage of *S. mutans* intracellular proteins classified by the biological function according to the experimental design.

Experimental design	AEP only								AEP and daily								Mean	S.D.
Biological function	Treatment								Treatment									
	A	B	C	D	E	F	G	H	A	B	C	D	E	F	G	H		
Adaptative responses to environmental changes	2.5	0.0	5.2	4.2	2.5	1.6	2.3	6.4	2.5	1.5	2.5	3.1	5.1	3.9	2.4	2.7	**3.0**	**1.6**
Amino acid metabolism and biosynthesis	3.8	2.3	7.0	4.2	3.8	4.8	2.3	2.1	1.3	1.5	3.8	3.1	1.7	6.6	2.4	2.7	**3.3**	**1.7**
Bacterial adherence and biofilm formation	6.3	2.3	5.2	5.9	6.3	4.8	6.8	6.4	3.8	7.6	11.4	4.6	3.4	5.3	7.3	6.8	**5.9**	**2.1**
Carbohydrate metabolism and energy production	15.2	16.3	9.6	11.9	10.1	12.7	13.6	12.8	12.7	13.6	13.9	13.8	15.3	14.5	12.2	13.5	**13.2**	**1.8**
Cell division, replication and cell wall synthesis	1.3	2.3	4.3	1.7	2.5	1.6	0.0	4.3	3.8	6.1	6.3	1.5	5.1	2.6	2.4	2.7	**3.0**	**1.8**
Nucleoside/Nucleotide metabolism and biosynthesis	2.5	4.7	0.0	4.2	2.5	3.2	0.0	1.1	2.5	1.5	0.0	3.1	0.0	0.0	0.0	5.4	**1.9**	**1.9**
Other metabolic processes	13.9	11.6	8.7	8.5	19.0	7.9	15.9	9.6	8.9	9.1	10.1	15.4	10.2	14.5	14.6	10.8	**11.8**	**3.3**
Transcription	6.3	7.0	6.1	5.9	5.1	7.9	0.0	8.5	7.6	6.1	7.6	3.1	6.8	2.6	4.9	4.1	**5.6**	**2.3**
Translation and protein synthesis	26.6	41.9	27.0	25.4	29.1	33.3	36.4	28.7	25.3	31.8	24.1	24.6	33.9	23.7	24.4	27.0	**28.9**	**5.2**
Transport	11.4	4.7	14.8	16.1	11.4	12.7	9.1	11.7	13.9	9.1	12.7	10.8	6.8	13.2	7.3	9.5	**10.9**	**3.1**
Uncharacterized/Unknown	10.1	7.0	12.2	11.9	7.6	9.5	13.6	8.5	17.7	12.1	7.6	16.9	11.9	13.2	22.0	14.9	**12.3**	**4.1**

Mean (± S.D) of the relative percentage per treatment found at both experimental designs. The percentage of proteins found to be down- or upregulated with respect to the negative control (H) are highlighted in red and blue, respectively.

4.4 Discussion

This is the first time that a cariogenic biofilm model was used to evaluate the effects of engineered salivary peptides on enamel demineralization. The model has the advantage of reduced biofilm manipulation during its development, limiting the removal of the salivary peptides from the enamel surface observed when cariogenic challenges were performed 8x/day with a 10% sucrose solution (Ccahuana-Vásquez and Cury 2010) (pilot studies, data not shown). As it is mandatory for a model to be validated, the biofilm model showed a dose-dependent effect of fluoride in the reduction of enamel demineralization, allowing us to use it to test the caries protective effect of the engineered salivary peptides, having a group treated with fluoride as a positive control. Additionally, to the best of our knowledge, this is the first study in which the intracellular and ECM proteome of *S. mutans* cariogenic biofilms are described, and the results obtained from the negative control (H) serve as a reference proteome profile.

Regarding the engineered peptides, the hybrid peptide DR9-RR14 (E) had a potential protective effect against enamel demineralization when adsorbed onto the enamel, forming the AEP, before the formation of cariogenic biofilms (Figure 16). The anticarious effect observed in the group treated with the peptide DR9-RR14 was similar to that obtained when the enamel was treated with statherin (A), the duplicated peptide DR9-DR9 (F), the peptide RR14 (F), and histatin 3 (B) (Figure 16). Although the total enamel demineralization reduction was similar among these groups (cumulative calcium concentration, Figure 16), the daily calcium concentration found during biofilm development (Figure 15) suggests that statherin (A), at 80 h and 104 h, and DR9-RR14 (E) at 104 h and 128 h, were able to reduce the demineralizing effect of the acids produced by the bacteria in the biofilm between 15% to 36%, respectively, in comparison to the negative control (H). The mechanism by which the DR9-RR14 peptide exerts the anticarious effect cannot be explained by the antibacterial effect observed in planktonic *S. mutans* (Basiri et al. 2017), since both the biomass and the bacterial viability were similar to those values found in the other groups, except for the positive control (G) (Table 6). However, the pH values obtained up to 56 h suggest a possible effect on bacterial metabolism (Figure 14) since the bacteria treated with histatin 3 (B), DR9 (C), and DR9-DR9 (D) produced less acid than the other groups. This possible effect was eliminated as soon as biofilm cariogenicity increased when the biofilms became mature, or by the

eventual release of adsorbed peptides onto the enamel surface during acid production or biofilm manipulation.

The DR9-RR14 peptide adsorbed onto the enamel may potentially be controlling the caries process by limiting the formation of enamel dissolution foci (Kosoric et al. 2007; Shah et al. 2011; Tang et al. 2003). By doing so, this peptide reduces the diffusion of acids from the biofilm to the enamel mineral, or limits the transport of the dissolved dental mineral ions into the culture medium, as previously observed when the AEP was formed from total saliva (Zahradnik et al. 1976). Thanks to the structural analysis of the interaction between statherin and HAp (Makrodimitris et al. 2007), we can predict that the two phosphoserines in the 2nd and 3rd positions of the DR9-RR14 peptide are responsible for stabilizing the protein/mineral interaction, while the positively charged amino acids in the sixth and ninth positions interact with phosphate through electrostatic interactions (Goobes et al. 2007). Additionally, these amino acids form a α-helix when in contact with the dental surface, facilitating the interaction of amino acid functional groups with the mineral ions. The aforementioned structure is considered a fundamental for the protein/mineral interaction (Long et al. 2001; Makrodimitris et al. 2007; Raj et al. 1992) and the promotion of tooth mineral homeostasis (Shah et al. 2011). Although the arginine (R) at the 10th position of the hybrid peptide corresponds to the RR14 fragment, the same amino acid is found at that position in statherin, interacting electrostatically and facilitating the adsorption of the protein onto HAp. Thus, it could be speculated, regardless of the pH of the solution, that the adsorption of the RR14 fragment of the hybrid peptide is stabilized by the interaction energy between the positively charged amino acids at position 10, as well as those at positions 11, 15, 20, and 23, with the tooth mineral. Besides, the secondary structure prediction of the DR9-RR14 peptide suggests an α-helix formation from the amino acids in the 3rd to the 15th positions (Heffernan et al. 2016), which could be limiting the enamel demineralization process occurring under this structure (Long et al. 2001; Makrodimitris et al. 2007; Raj et al. 1992). The same mechanism may explain the caries-protective effect observed in the groups treated with the duplicated peptide DR9-DR9, which contains 4 phosphorylated amino acids in positions 2, 3, 10 and 11 (Basiri et al. 2017), and forms two α-helixes from the amino acids in the positions 4th to the 9th, and 13th to 16th (Heffernan et al. 2016), justifying the potential anticarious effect also previously demonstrated in a static model using demineralizing solutions. This hypothesis that the caries-protective effect displayed by

DR9-RR14 and DR9-DR9 peptides is due to a physicochemical protection, and is supported by the fact that the expression of those intracellular and ECM proteins involved in critical processes related to the cariogenicity of the biofilms were not affected neither by the engineered peptides nor by any other protein/peptide used in this study (Table 8; Figure 17).

Contrary to what was expected, the anticarious effect of the engineered peptides did not increase when biofilms were treated daily with them (Figure 16). This simulates the daily use of mouthwash for the delivery of peptides to the oral cavity, replacing the peptides that might be released from the dental surface to the culture medium in the function of time. In this study we obtained the same trend in reduction of demineralization observed when the peptides were used only to form the AEP: the peptide DR9-RR14 (E) showed to have a potential anticarious effect, like that found in the groups treated with histatin 3 (B), DR9-DR9 (D), and RR14 (F) (Figure 16). Surprisingly, the group treated with statherin (A) was one of the groups displaying higher mineral loss, similar to that obtained in the negative control (H) (Figure 16). These results suggest that the peptides in aqueous suspension (50 mM NaCl, pH 6.8) were not able to penetrate through the biofilms. According to the reaction-diffusion theory, charged molecules such as the proteins/peptides used in this study may bind to the ECM components and bacteria on the external surface of the biofilms (Nichols et al. 1989), retaining them on the surface and limiting their diffusion through the biofilm. Due to the high growth rate of the bacteria in the biofilm during the exposure to sucrose, the bacteria-bound molecules could have acted as bridges among bacteria cells, favoring the growth of biofilms, explaining why the biofilms were thicker than those formed in the absence of the daily treatments (Table 7, column 3). In case these peptides/proteins displayed an antimicrobial effect on the bacteria in the external surface of the biofilms, it could have been neutralized by the fast bacterial growth favored by sucrose metabolism, justifying why both the biomass and cell viability did not differ among the groups treated with these molecules (Table 7). These findings are also supported by the fact that most of the intracellular and ECM proteins participating in each of the biological functions were similarly identified in all treatment groups (Appendix 5, Appendix 6), confirming that the bacteria were metabolically active and efficiently growing in the biofilms until the last day of the experiment, when biofilms were collected. As observed when the peptides were only in the AEP, there was a trend for the means of the pH values obtained until the third day of the experiment (72 h) to be

different among groups (Figure 14b). Although these differences were not statistically significant, there were fewer acids being produced by the bacteria in the biofilms when they were treated with histatin 3 (B) and its derived peptides RR14 (F) and DR9-RR14 (E), suggesting a possible antimicrobial effect exerted by these molecules only on young biofilms (Figure 14b). The encapsulation of the engineered peptides in nanoparticles may be a strategy to release them at the tooth/biofilm interface when the cariogenic biofilms become mature and carious lesions are likely to be developed, which should be further investigated.

In all the experiments, fluoride almost completely inhibited the enamel demineralization (Figure 16). This result was expected because a fluoridated solution containing 12,300 μg F/mL was used, simulating the topical application of acidified fluoride gel to form a layer of crystals similar to calcium fluoride (CaF_2-like) covering the enamel surface (ten Cate 1997), in the same way that the salivary proteins cover the teeth by forming a proteinaceous film onto dental surfaces (Siqueira et al. 2007a). The fact that this fluoride inhibited enamel demineralization is due to a considerable amount of these CaF_2-like crystals formed onto the enamel surface during the 24 h application period used in this study since the amount of CaF_2-like formed is directly proportional to the vehicle and time of fluoride application. In this study, the fluoridated solution was prepared from NaF, in which the fluoride is ionic and available to react immediately with the structural calcium of the enamel, as observed during the application of fluoride using aqueous vehicles such as gel or foam (Calvo et al. 2012; Villena et al. 2009). Thereby, with the 24-hour application time, often higher than the clinically recommended of four-minutes (Tenuta et al. 2008), the amount of these reservoirs formed onto the dental surface was of 188.2 μg F/cm^2 enamel (± 77.1) (data not shown), nine times higher than that obtained after four minutes (21.7 ± 15.1 μg F/cm^2 enamel) (Tenuta et al. 2008). A similar trend was observed when the fluoride varnish is maintained on the dental surface for up to 36 hours (Fernández et al. 2014). The fact that the CaF_2-like reservoirs are solubilized slowly, continuously releasing fluoride to the biofilm fluid (Paes Leme et al. 2004), making it available to interfere with the caries process (Cury and Tenuta 2009), explains the inhibition of demineralization observed in our experiments (Figure 16). Furthermore, fluoride delivered from the dissolution of the CaF_2-like crystals may have had an antimicrobial effect on *S. mutans*, since fluoride inhibits bacterial growth and metabolism when continuously kept at concentrations of 10 μg F/mL (526 μM) or higher (Bradshaw

et al. 2002; Marquis 1995), reducing biofilm biomass and bacterial viability (Loesche et al. 1975), as observed in this study (Table 6 and Table 7). To support this observation, we also determined fluoride concentration in the culture medium over the time of the experiment and in the biofilm collected at 144 h (data not shown). The results showed that during the adherence phase (first 24 h), 40 µg F/mL was found in the culture medium, indicating that this high concentration of fluoride had a bacteriostatic effect inhibiting bacterial adherence to the enamel (Zahradnik et al. 1978a). Then, biofilms started to form slowly during the upcoming days of the experiment, where the fluoride in the culture medium was approximately ~1 µg F/mL, which is expected not to exert a bacteriostatic effect on *S. mutans* (Cury et al. 2016). Although the fluoride concentration found in the biofilm fluid and in the biofilm solids was ~56 µM and 5 µM, respectively, the proteome analysis of the intracellular compartment from bacteria treated with fluoride (G) showed the depletion of three out of ten biological functions (cell division, replication and cell wall synthesis; nucleoside/nucleotide metabolism and biosynthesis; transcription) as well as the downregulation of the synthesis of proteins related to the adaptative responses to environmental changes (Table 8), suggesting that this fluoride concentration may have impaired biofilm formation and metabolism.

Concerning the methodological aspects, the use of a monospecies biofilm model was selected because *S. mutans* is considered the most cariogenic microorganism found in the dental biofilm (Hamada et al. 1984) due to its acidogenicity, aciduricity (Quivey et al. 2000) and ability to synthesize extracellular polysaccharides from sucrose metabolism (Klein et al. 2015; Koo et al. 2013; Paes Leme et al. 2006). For the same reasons, sucrose was selected because it is considered as the most cariogenic carbohydrate from the human diet (Paes Leme et al. 2006). Thus, the cariogenic biofilm model used appropriately simulates the de- and remineralization processes that occur at the tooth-biofilm interface when exposed to fermentable carbohydrates from the diet (Figure 12 and Figure 13) (Cury and Tenuta 2009). Regarding the treatments, the caries protective effect of the combination of the engineered peptides in the AEP with the daily use of fluoride was not evaluated in this study. These results would be highly relevant considering the effectiveness of fluoride in the control of the caries process (Marinho et al. 2003; Walsh et al. 2010). The use of single peptide solutions in the absence of saliva could be considered a limitation of this study since the possible interaction between the salivary components and our engineered peptides during the formation of the AEP was not

simulated (Yin et al. 2006), which could influence the observed caries-protective effect. However, the results of this study, using a single component approach of the AEP and a *S. mutans* cariogenic biofilm model, suggested for the first time that our engineered salivary peptides DR9-RR14 and DR9-DR9, when adsorbed to the enamel surface or used as a daily treatment, have a potential anticarious effect, constituting a new translational approach for the prevention/treatment of dental caries.

4.5 References

Amaechi BT, Tenuta LMA, Ricomini Filho AP, Cury JA. 2019. Protocols to study dental caries in vitro: Microbial caries models. Methods Mol Biol. 1922:357-368.

Azzopardi PV, O'Young J, Lajoie G, Karttunen M, Goldberg HA, Hunter GK. 2010. Roles of electrostatics and conformation in protein-crystal interactions. PLoS One. 5(2):e9330.

Basiri T, Johnson ND, Moffa EB, Mulyar Y, Serra Nunes PL, Machado MAAM, Siqueira WL. 2017. Duplicated or hybridized peptide functional domains promote oral homeostasis. J Dent Res.22034517708552.

Bowen WH, Tenuta LMA, Koo H, Cury JA. 2019. Dental caries: Etiology and pathogenesis. In: Lamont RJ, Hajishengallis GN, Koo H, Jenkinson HF, editors. Oral microbiology and immunology. Third ed. Washington, DC: ASM Press. p. 251-265.

Bradshaw DJ, Marsh PD, Hodgson RJ, Visser JM. 2002. Effects of glucose and fluoride on competition and metabolism within in vitro dental bacterial communities and biofilms. Caries Res. 36(2):81-86.

Calvo AF, Tabchoury CP, Del Bel Cury AA, Tenuta LM, da Silva WJ, Cury JA. 2012. Effect of acidulated phosphate fluoride gel application time on enamel demineralization of deciduous and permanent teeth. Caries Res. 46(1):31-37.

Ccahuana-Vásquez RA, Cury JA. 2010. S. Mutans biofilm model to evaluate antimicrobial substances and enamel demineralization. Braz Oral Res. 24(2):135-141.

Cury JA, de Oliveira BH, dos Santos AP, Tenuta LM. 2016. Are fluoride releasing dental materials clinically effective on caries control? Dent Mater. 32(3):323-333.

Cury JA, Mambrin S, Gazal W. 1994. In situ models to study dental plaque and/or calculus inhibition. . Journal of Dental Research. 73:424.

Cury JA, Rebelo MA, Del Bel Cury AA, Derbyshire MT, Tabchoury CP. 2000. Biochemical composition and cariogenicity of dental plaque formed in the presence of sucrose or glucose and fructose. Caries Res. 34(6):491-497.

Cury JA, Tenuta LM. 2009. Enamel remineralization: Controlling the caries disease or treating early caries lesions? Braz Oral Res. 23 Suppl 1:23-30.

Dawes C. 1963. The nomenclature of the integuments of the enamel surface of tooth. Brit Dent J. 115:65-68.

Duke SA, Forward GC. 1982. The conditions occurring in vivo when brushing with toothpastes. Br Dent J. 152(2):52-54.

Fernández CE, Tenuta LM, Zárate P, Cury JA. 2014. Insoluble naf in duraphat® may prolong fluoride reactivity of varnish retained on dental surfaces. Braz Dent J. 25(2):160-164.

Gauci S, van Breukelen B, Lemeer SM, Krijgsveld J, Heck AJ. 2008. A versatile peptide pi calculator for phosphorylated and n-terminal acetylated peptides experimentally tested using peptide isoelectric focusing. Proteomics. 8(23-24):4898-4906.

Goobes R, Goobes G, Shaw WJ, Drobny GP, Campbell CT, Stayton PS. 2007. Thermodynamic roles of basic amino acids in statherin recognition of hydroxyapatite. Biochemistry. 46(16):4725-4733.

Hamada S, Koga T, Ooshima T. 1984. Virulence factors of streptococcus mutans and dental caries prevention. J Dent Res. 63(3):407-411.

Heffernan R, Dehzangi A, Lyons J, Paliwal K, Sharma A, Wang J, Sattar A, Zhou Y, Yang Y. 2016. Highly accurate sequence-based prediction of half-sphere exposures of amino acid residues in proteins. Bioinformatics. 32(6):843-849.

Klein MI, Hwang G, Santos PH, Campanella OH, Koo H. 2015. Streptococcus mutans-derived extracellular matrix in cariogenic oral biofilms. Front Cell Infect Microbiol. 5:10.

Koo H, Falsetta ML, Klein MI. 2013. The exopolysaccharide matrix: A virulence determinant of cariogenic biofilm. J Dent Res. 92(12):1065-1073.

Kosoric J, Williams RAD, Hector MP, Anderson P. 2007. A synthetic peptide based on a natural salivary protein reduces demineralisation in model systems for dental caries and erosion. International Journal of Peptide Research and Therapeutics. 13(4):497-503.

Kummer KM, Taylor EN, Durmas NG, Tarquinio KM, Ercan B, Webster TJ. 2013. Effects of different sterilization techniques and varying anodized tio(2) nanotube dimensions on bacteria growth. J Biomed Mater Res B Appl Biomater. 101(5):677-688.

Loesche WJ, Syed SA, Murray RJ, Mellberg JR. 1975. Effect of topical acidulated phosphate fluoride on percentage of streptococcus mutans and streptococcus sanguis in plaque. Ii. Pooled occulusal and pooled approximal samples. Caries Res. 9(2):139-155.

Long JR, Shaw WJ, Stayton PS, Drobny GP. 2001. Structure and dynamics of hydrated statherin on hydroxyapatite as determined by solid-state nmr. Biochemistry. 40(51):15451-15455.

Makrodimitris K, Masica DL, Kim ET, Gray JJ. 2007. Structure prediction of protein-solid surface interactions reveals a molecular recognition motif of statherin for hydroxyapatite. J Am Chem Soc. 129(44):13713-13722.

Marinho VC, Higgins JP, Sheiham A, Logan S. 2003. Fluoride toothpastes for preventing dental caries in children and adolescents. Cochrane Database Syst Rev. (1):CD002278.

Marquis RE. 1995. Antimicrobial actions of fluoride for oral bacteria. Can J Microbiol. 41(11):955-964.

Martins C, Castro GF, Siqueira MF, Xiao Y, Yamaguti PM, Siqueira WL. 2013. Effect of dialyzed saliva on human enamel demineralization. Caries Res. 47(1):56-62.

Nancollas GH, Mohan MS. 1970. The growth of hydroxyapatite crystals. Arch Oral Biol. 15(8):731-745.

Nichols WW, Evans MJ, Slack MP, Walmsley HL. 1989. The penetration of antibiotics into aggregates of mucoid and non-mucoid pseudomonas aeruginosa. J Gen Microbiol. 135(5):1291-1303.

Paes Leme AF, Bellato CM, Bedi G, Cury AA, Koo H, Cury JA. 2008. Effects of sucrose on the extracellular matrix of plaque-like biofilm formed in vivo, studied by proteomic analysis. Caries Res. 42(6):435-443.

Paes Leme AF, Dalcico R, Tabchoury CP, Del Bel Cury AA, Rosalen PL, Cury JA. 2004. In situ effect of frequent sucrose exposure on enamel demineralization and on plaque composition after apf application and f dentifrice use. J Dent Res. 83(1):71-75.

Paes Leme AF, Koo H, Bellato CM, Bedi G, Cury JA. 2006. The role of sucrose in cariogenic dental biofilm formation--new insight. J Dent Res. 85(10):878-887.

Quivey RG, Jr., Kuhnert WL, Hahn K. 2000. Adaptation of oral streptococci to low ph. Adv Microb Physiol. 42:239-274.

Raj PA, Johnsson M, Levine MJ, Nancollas GH. 1992. Salivary statherin. Dependence on sequence, charge, hydrogen bonding potency, and helical conformation for adsorption to hydroxyapatite and inhibition of mineralization. J Biol Chem. 267(9):5968-5976.

Shah S, Kosoric J, Hector MP, Anderson P. 2011. An in vitro scanning microradiography study of the reduction in hydroxyapatite demineralization rate by statherin-like peptides as a function of increasing n-terminal length. Eur J Oral Sci. 119 Suppl 1:13-18.

Shimotoyodome A, Kobayashi H, Tokimitsu I, Matsukubo T, Takaesu Y. 2006. Statherin and histatin 1 reduce parotid saliva-promoted streptococcus mutans strain mt8148 adhesion to hydroxyapatite surfaces. Caries Res. 40(5):403-411.

Siqueira WL, Custodio W, McDonald EE. 2012. New insights into the composition and functions of the acquired enamel pellicle. J Dent Res. 91(12):1110-1118.

Siqueira WL, Helmerhorst EJ, Zhang W, Salih E, Oppenheim FG. 2007a. Acquired enamel pellicle and its potential role in oral diagnostics. Ann N Y Acad Sci. 1098:504-509.

Siqueira WL, Margolis HC, Helmerhorst EJ, Mendes FM, Oppenheim FG. 2010. Evidence of intact histatins in the in vivo acquired enamel pellicle. J Dent Res. 89(6):626-630.

Siqueira WL, Oppenheim FG. 2009. Small molecular weight proteins/peptides present in the in vivo formed human acquired enamel pellicle. Arch Oral Biol. 54(5):437-444.

Siqueira WL, Zhang W, Helmerhorst EJ, Gygi SP, Oppenheim FG. 2007b. Identification of protein components in in vivo human acquired enamel pellicle using lc-esi-ms/ms. J Proteome Res. 6(6):2152-2160.

Tang R, Hass M, Wu W, Gulde S, Nancollas GH. 2003. Constant composition dissolution of mixed phases. Ii. Selective dissolution of calcium phosphates. J Colloid Interface Sci. 260(2):379-384.

ten Cate JM. 1997. Review on fluoride, with special emphasis on calcium fluoride mechanisms in caries prevention. Eur J Oral Sci. 105(5 Pt 2):461-465.

Tenuta LM, Cerezetti RV, Del Bel Cury AA, Tabchoury CP, Cury JA. 2008. Fluoride release from caf2 and enamel demineralization. J Dent Res. 87(11):1032-1036.

Valente MT, Moffa EB, Crosara KTB, Xiao Y, de Oliveira TM, Machado M, Siqueira WL. 2018. Acquired enamel pellicle engineered peptides: Effects on hydroxyapatite crystal growth. Sci Rep. 8(1):3766.

Villena RS, Tenuta LM, Cury JA. 2009. Effect of apf gel application time on enamel demineralization and fluoride uptake in situ. Braz Dent J. 20(1):37-41.

Vitorino R, Calheiros-Lobo MJ, Williams J, Ferrer-Correia AJ, Tomer KB, Duarte JA, Domingues PM, Amado FM. 2007. Peptidomic analysis of human acquired enamel pellicle. Biomed Chromatogr. 21(11):1107-1117.

Vogel GL, Chow LC, Brown WE. 1983. A microanalytical procedure for the determination of calcium, phosphate and fluoride in enamel biopsy samples. Caries Res. 17(1):23-31.

Walsh T, Worthington HV, Glenny AM, Appelbe P, Marinho VC, Shi X. 2010. Fluoride toothpastes of different concentrations for preventing dental caries in children and adolescents. Cochrane Database Syst Rev. (1):CD007868.

Xiao Y, Karttunen M, Jalkanen J, Mussi MC, Liao Y, Grohe B, Lagugné-Labarthet F, Siqueira WL. 2015. Hydroxyapatite growth inhibition effect of pellicle statherin peptides. J Dent Res. 94(8):1106-1112.

Yao Y, Lamkin MS, Oppenheim FG. 1999. Pellicle precursor proteins: Acidic proline-rich proteins, statherin, and histatins, and their crosslinking reaction by oral transglutaminase. J Dent Res. 78(11):1696-1703.

Yin A, Margolis HC, Yao Y, Grogan J, Oppenheim FG. 2006. Multi-component adsorption model for pellicle formation: The influence of salivary proteins and non-salivary phospho proteins on the binding of histatin 5 onto hydroxyapatite. Arch Oral Biol. 51(2):102-110.

Zahradnik RT, Moreno EC, Burke EJ. 1976. Effect of salivary pellicle on enamel subsurface demineralization in vitro. J Dent Res. 55(4):664-670.

Zahradnik RT, Propas D, Moreno EC. 1977. In vitro enamel demineralization by streptococcus mutans in the presence of salivary pellicles. J Dent Res. 56(9):1107-1110.

Zahradnik RT, Propas D, Moreno EC. 1978a. Effect of fluoride topical solutions on enamel demineralization by lactate buffers and streptococcus mutans in vitro. J Dent Res. 57(9-10):940-946.

Zahradnik RT, Propas D, Moreno EC. 1978b. Effect of salivary pellicle formation time on in vitro attachment and demineralization by streptococcus mutans. J Dent Res. 57(11-12):1036-1042.

Chapter 5

5 General discussion, perspectives and conclusions

5.1 General discussion

Dental caries remains to be one of the most prevalent chronic diseases affecting people from all ages, even though the caries prevalence has been dramatically reduced over the last half century due to the widespread use of fluoride (Petersen et al. 2005). As the global burden of treating dental carious lesions is a matter of public health concern (Jin et al. 2016), new therapeutic strategies should be developed to help control the incidence of cavitated and non-cavitated white spot carious lesions, and to promote the arrest or even the reversal of existing lesions. Modification of the AEP composition may be useful to design strategies for caries control, since its proteinaceous components serve as receptors for bacterial ligands (adhesins), acting as a conditioning film that influence which bacteria will firstly adhere to dental surfaces (Li et al. 2004). Additionally, this proteinaceous film has the ability to keep the homeostasis of teeth mineral composition by forming a semipermeable barrier onto the tooth surface, reducing its demineralization (Martins et al. 2013; Zahradnik et al. 1976; Zahradnik et al. 1977; 1978). Recently, it was suggested the potential use of the statherin- and histatin-derived engineered salivary peptides DR9-DR9 and DR9-RR14 as a therapeutic strategy for the control of the dental caries development (Basiri et al. 2017). However, the anticaries effect of the engineered peptides was observed using a chemical caries model (Basiri et al. 2017) which does not mimic the full process of carious lesions development. Hence, it is not known whether the DR9-DR9 and DR9-RR14 peptides are capable of reduce *S. mutans* adherence to the dental surfaces, and to reduce the cariogenicity of *S. mutans* biofilms, controlling the development of carious lesions. To fulfil these gaps in knowledge, this thesis was done to evaluate the effect of the engineered peptides DR9-DR9 and DR9-RR14 on the adherence of *S. mutans* to the AEP formed onto HAp and on enamel demineralization using an *S. mutans* cariogenic biofilm development.

The assessment of the effect of the peptides on the adherence of *S. mutans* to the AEP formed onto hydroxyapatite is described in the first manuscript. In this study, HAp discs

were treated with the peptides to form a single-component AEP, and then *S. mutans* was allowed to adhere for 2 h, 4 h, and 8 h. The results of this study showed that the number of bacterial cells adhered increased over time, independently of the composition of the AEP (Table 2 and Figure 2). The comparison made among treatments at each time point showed that the composition of the AEP did affect the number of bacteria adhered to HAp, with the most significant differences found at 8 h (Figure 3). At this time point, bacteria attached to the surface treated with statherin (A) was significantly higher than that obtained with almost all the other groups, and similar to the engineered peptide DR9-RR14 (E). The great number of bacteria adhered observed in the group treated with statherin, suggests that this protein exposes receptor sites (cryptitopes), at the C-terminal region, for oral bacteria ligands upon adsorbed to the dental surfaces, facilitating the bacterial adhesion and subsequent proliferation on the dental surface, as previously observed with other oral microorganisms (Goobes et al. 2006). In fact, as the statherin-derived peptide DR9 belongs to the N-terminal region of the protein (Basiri et al. 2017; Xiao et al. 2015), the absence of receptors at the C-terminal region may be the first explanation to the lower number of bacteria found adhered to the AEP formed from the salivary peptides DR9 (C) and DR9-DR9 (D) (Figure 3). The second reason why fewer bacteria were found adhered to HAp discs treated with the statherin-derived peptides DR9 (C) and DR9-DR9 (D) is because of the acidic nature of this peptides at pH 7.0. Previous studies have shown that adsorbed acidic proteins reduce bacterial attachment by increasing the repulsive electrostatic forces between the anionic protein and the bacterial cell wall (Reynolds and Wong 1983; Simonson and Reiher 1981), or by competing with bacteria for HAp-binding sites (Rolla 1977). The finding that the DR9-RR14 peptide was the one that promoted the highest bacterial adherence at 8 h in comparison with the other groups (Figure 3), suggests that this peptide cannot exert antimicrobial activity against *S. mutans* once adsorbed onto HAp. Contrary to the reduction of bacterial attachment induced by acidic proteins previously discussed, basic proteins promote bacterial adherence (Reynolds and Wong 1983; Simonson and Reiher 1981), explaining why more bacteria was found attached to the HAp treated with RR14 than with histatin 3, since it was the molecule that exhibited the highest pI, and therefore, the highest cationic charge at the pH used during bacterial adherence (7.0) (Table 1). As the hybrid peptide has a pI of 7.1, its charge must be close to neutral during the adherence experiments, and no electrostatic forces mediated the attachment of *S. mutans* to HAp. Besides, the secondary structure prediction of the DR9-RR14 peptide suggests an α-helix formation from the

amino acids in the 3rd to the 15th positions (Heffernan et al. 2016), considered a fundamental structure for the protein/mineral interaction (Long et al. 2001; Makrodimitris et al. 2007; Raj et al. 1992). Thus, we speculate that the remaining 8 amino acids in the C-terminal region of the hybrid peptide may be forming a cryptitope that promotes specific bacterial adherence, however, the mechanism employed by DR9-RR14 to promote bacterial adherence remains to be further elucidated.

Overall, the results from the adherence study suggested the potential use of the engineered salivary peptide DR9-DR9 to control *S. mutans* biofilm development by reducing bacterial colonization of HAp surfaces, a hypothesis that was further tested.

Before assessing the effect of the peptides on the formation of cariogenic biofilms and subsequently on enamel demineralization, it was necessary to modify a cariogenic *S. mutans* biofilm model previously developed (Ccahuana-Vásquez and Cury 2010). The reason why this model was modified is because it is a micromodel that only allows the use of volumes in the millilitre scale, and there is a limitation in the volume of the peptide solutions to be used. The proposed model, described in the second manuscript, allowed the use of volumes up to 200 µL and It was validated in terms of the dose-response effect to fluoride on enamel demineralization (Figure 8) when the use 2x/day of a toothpaste having low, regular and high fluoride concentration was simulated. During the validation of the model, fluoridated solutions containing 125, 275, 1250 µg F/mL were used, which reflect the dilution 1:3 that occurs in the oral cavity by saliva while toothbrushing with toothpastes containing 500, 1100 and 5000 µg F/g, respectively (Duke and Forward 1982). Fluoride was selected because it is considered as the agent responsible for the reduction of caries prevalence observed worldwide since the last half century (Petersen et al. 2005), and there is strong evidence to recommend its use throughout the population, regardless of age (dos Santos et al. 2013; Marinho et al. 2003; Walsh et al. 2010). The results showed that this model is sensitive enough to detect the effect of low concentrations of fluoride on the reduction of enamel demineralization (i.e. 125 µg F/mL).

Our model can be classified as a cycling model, which better mimic the *in vivo* caries process (Maske et al. 2017). pH shifts during biofilm growth were observed, firstly, when biofilms were subjected to cariogenic challenges for 8 consecutive hours (time points 80 h, 104 h, 128 h) and the pH dropped due to the acids produced as end products of sucrose

metabolism by the bacteria in the biofilm (Figure 6) (Bowen et al. 1966). As a result, the mineral phase of enamel was dissolved (Bowen et al. 2019), leading to an increase in calcium concentration in the culture medium (Figure 7A). Secondly, in the absence of sucrose, when the biofilms were let to rest overnight in a culture medium supplemented with the physiological glucose concentration found in saliva (0.1 mM), no demineralization occurred (time points 96 h, 120 h, 144 h), and remineralization took place. Our *S. mutans* cariogenic biofilm model can be used to test the caries-protective effect of fluoridated solutions and other compounds which amount is limited to the microliter scale, being this model suitable to be used both as a macro- and a micromodel.

As the model was validated and showed to be sensitive enough to detect dose-response effect to fluoride on enamel demineralization, it was further used to evaluate the ability of the engineered peptides DR9-DR9 and DR-RR14 to control enamel demineralization and to modulate crucial steps of cariogenic biofilm formation (third manuscript). The carious-protective effect was evaluated when the peptides were adsorbed onto the enamel surface forming the AEP, and when the biofilms were additionally treated 2x/day with the peptide solutions. The results showed that the hybrid peptide DR9-RR14 (E) showed to have a potential protective effect against enamel demineralization when adsorbed onto the enamel, forming the AEP, before the formation of cariogenic biofilms (Figure 16). The anticarious effect observed in the group treated with the peptide DR9-RR14 was similar to that obtained when the enamel was treated with statherin (A), the duplicated peptide DR9-DR9 (F), the peptide RR14 (F), and histatin 3 (B) (Figure 16). Although the total enamel demineralization reduction was similar among these groups (cumulative calcium concentration, Figure 16), the daily calcium concentration found during biofilms development (Figure 15) suggests that statherin (A), at 80 h and 104 h, and DR9-RR14 (E) at 104 h and 128 h, were able to reduce the demineralizing effect of the acids produced by the bacteria in the biofilm between 15% to 36%, respectively, in comparison to the negative control (H). The mechanism by which the DR9-RR14 peptide exerts the anticarious effect cannot be explained by the antibacterial effect observed in planktonic *S. mutans* (Basiri et al. 2017), since both the biomass and the bacterial viability were similar to those values found in the other groups, except for the positive control (G) (Table 6). However, the pH values obtained up to 56 h suggest a possible effect on the reduction of bacterial metabolism (Figure 14) since the bacteria treated with histatin 3 (B), DR9 (C), and DR9-DR9 (D) produced fewer acids than the other groups. This possible effect

was eliminated as soon as biofilm cariogenicity increased when the biofilms became mature, or by the eventual release of adsorbed peptides onto the enamel surface during acid production or biofilm manipulation.

The DR9-RR14 peptide adsorbed onto the enamel may potentially be controlling the caries process by limiting the formation of enamel dissolution foci (Kosoric et al. 2007; Shah et al. 2011; Tang et al. 2003). By doing so, this peptide reduces the diffusion of acids from the biofilm to the enamel mineral, or limits the transport of the dissolved dental mineral ions into the culture medium, as previously observed when the AEP was formed from total saliva (Zahradnik et al. 1976). Thanks to the structural analysis of the interaction between statherin and HAp (Makrodimitris et al. 2007), we can predict that the two phosphoserines in the 2nd and 3rd positions of the DR9-RR14 peptide are responsible for stabilizing the protein/mineral interaction, while the positively charged amino acids in the sixth and ninth positions interact with phosphate through electrostatic interactions (Goobes et al. 2007). Additionally, these amino acids form a α-helix when in contact with the dental surface, facilitating the interaction of amino acid functional groups with the mineral ions. The aforementioned structure is considered a fundamental for the protein/mineral interaction (Long et al. 2001; Makrodimitris et al. 2007; Raj et al. 1992) and the promotion of tooth mineral homeostasis (Shah et al. 2011). Although the arginine (R) at the 10th position of the hybrid peptide corresponds to the RR14 fragment, the same amino acid is found at that position in statherin, interacting electrostatically and facilitating the adsorption of the protein onto HAp. Thus, it could be speculated, regardless of the pH of the solution, that the adsorption of the RR14 fragment of the hybrid peptide is stabilized by the interaction energy between the positively charged amino acids at position 10, as well as those at positions 11, 15, 20, and 23, with the tooth mineral. Besides, the secondary structure prediction of the DR9-RR14 peptide suggests an α-helix formation from the amino acids in the 3rd to the 15th positions (Heffernan et al. 2016), which could be limiting the enamel demineralization process occurring under this structure (Long et al. 2001; Makrodimitris et al. 2007; Raj et al. 1992). The same mechanism may explain the caries-protective effect observed in the groups treated with the duplicated peptide DR9-DR9, which contains 4 phosphorylated amino acids in positions 2, 3, 10 and 11 (Basiri et al. 2017), and forms two α-helixes from the amino acids in the positions 4th to the 9th, and 13th to 16th (Heffernan et al. 2016), justifying the potential anticarious effect also previously demonstrated in a static model using

demineralizing solutions. This hypothesis that the caries-protective effect displayed by DR9-RR14 and DR9-DR9 peptides is due to a physicochemical protection, and is supported by the fact that the expression of those intracellular and ECM proteins involved in critical processes related to the cariogenicity of the biofilms were affected neither by the engineered peptides nor by any other protein/peptide used in this study (Table 8; Figure 17).

Contrary to what was expected, the anticarious effect of the engineered peptides did not increase when biofilms were treated daily with them (Figure 16). This simulates the daily use of mouthwash for the delivery of peptides to the oral cavity, replacing the peptides that might be released from the dental surface to the culture medium in the function of time. In this study we obtained the same trend in reduction of demineralization observed when the peptides were used only to form the AEP: the peptide DR9-RR14 (E) showed to have a potential anticarious effect, like that found in the groups treated with histatin 3 (B), DR9-DR9 (D), and RR14 (F) (Figure 16). Surprisingly, the group treated with statherin (A) was one of the groups displaying higher mineral loss, similar to that obtained in the negative control (H) (Figure 16). These results suggest that the peptides in aqueous suspension (50 mM NaCl, pH 6.8) were not able to penetrate through the biofilms. According to the reaction-diffusion theory, charged molecules such as the proteins/peptides used in this study may bind to the ECM components and bacteria on the external surface of the biofilms (Nichols et al. 1989), retaining them on the surface and limiting their diffusion through the biofilm. Due to the high growth rate of the bacteria in the biofilm during the exposure to sucrose, the bacteria-bound molecules could have acted as bridges among bacteria cells, favoring the growth of biofilms, explaining why the biofilms were thicker than those formed in the absence of the daily treatments (Table 7, column 3). In case these peptides/proteins displayed an antimicrobial effect on the bacteria in the external surface of the biofilms, it could have been neutralized by the fast bacterial growth favored by sucrose metabolism, justifying t that both the biomass and cell viability did not differ among the groups treated with these molecules (Table 7). These findings are also supported by the fact that most of the intracellular and ECM proteins participating in each of the biological functions were similarly identified in all treatment groups (Appendix 5, Appendix 6), confirming that the bacteria were metabolically active and efficiently growing in the biofilms until the last day of the experiment, when biofilms were collected. As observed when the peptides were only in

the AEP, there was a trend for the means of the pH values obtained until the third day of the experiment (72 h) to be different among groups (Figure 14b). Although these differences were not statistically significant, there were fewer acids being produced by the bacteria in the biofilms when they were treated with histatin 3 (B) and its derived peptides RR14 (F) and DR9-RR14 (E), suggesting a possible antimicrobial effect exerted by these molecules only on young biofilms (Figure 14b). The encapsulation of the engineered peptides in nanoparticles may be a strategy to release them at the tooth/biofilm interface when the cariogenic biofilms become mature and carious lesions are likely to be developed, which should be further investigated.

Currently, there is a huge interest in determining the microbiome of the human organism in order to know the microorganisms that make up the normal microbiota, which could be related to the health-disease balance. However, regardless of the presence or absence of specific microorganisms in the human body, the proteins that are being expressed and/or secreted when the microorganisms adhere to the APE must be known because they may further contribute to the architecture and development of the dental biofilm. Additionally, it is important to know the bacterial proteome when the environmental conditions favor the development of biofilm-mediated diseases, like dental caries (Bowen et al. 2019). Then, to better explain the results obtained, we also evaluated if the DR9-DR9 and DR9-RR14 peptides modulate the proteome of *S. mutans*, controlling its adhesion to the AEP formed onto dental surfaces and the subsequent effect on the cariogenic biofilm. The results showed that the engineered peptides do not modulate bacterial proteome upon attachment (Table 4) nor regulate the expression of the intracellular and extracellular bacterial proteins involved in biofilm cariogenicity. The comprehensive proteome profiles here reported represents the first attempt to describe the *S. mutans* proteome once adhered to a mineral surface, and to differentiate between those bacterial intracellular and extracellular proteins expressed when cariogenic biofilms were developed (Figure 17 and Figure 18).

Taking together the results from the studies described in the first and third manuscripts, it can be suggested that, independently of the effect of the peptides on bacterial attachment, cariogenic biofilms are developed when the bacteria is exposed to a highly cariogenic environment, as in the case of the model here used. However, the AEP formed with the peptides helped to mitigate the deleterious effect of the acids produced by the bacteria in the biofilms once exposed to sucrose, protecting the enamel against

demineralization. These findings suggest that the engineered DR9-DR9 and DR9-RR14 peptides may modulate caries development mainly by a physicochemical mechanism.

5.2 Perspectives

Regarding the perspectives of this thesis, further studies should be done to evaluate the inhibitory effect of concentrations higher than 198 μM of our engineered peptides on the adhesion of *S. mutans* to HAp and on the reduction of enamel demineralization.

In all the experiments, a single-component peptide solution was used. However, the observed effect on the adherence of *S. mutans* and on the cariogenicity of the biofilms displayed by the engineered salivary peptides may differ if combined with saliva due to the possible interaction between the salivary components and our engineered peptides during the formation of the AEP (Yin et al. 2006), which was not simulated.

As the anticarious effect of the engineered peptides did not increase when the biofilms were treated daily with them, simulating the use of a mouthwash, the encapsulation of the engineered peptides in nanoparticles may be a strategy to deliver the peptides at the tooth/biofilm interface when the cariogenic biofilms become mature and carious lesions are likely to be developed, which should be further investigated.

Additionally, the carious protective effect of the combination of the engineered peptides in the AEP with the daily use of fluoride was not evaluated in this study. These results would be highly relevant considering the effectiveness of fluoride in the control of the caries process (Marinho et al. 2003; Walsh et al. 2010).

The slight protection against demineralization conferred by the peptides was observed when highly cariogenic conditions were simulated, suggesting that future work should be done to test its caries-protective effect when cariogenic biofilms are growth under low cariogenic conditions (i.e. exposure to sucrose 2 h or 4 h per day).

5.3 Conclusions

Considering the results of the studies done, it can be concluded the following:

- The statherin-derived DR9-DR9 engineered salivary peptide reduce *S. mutans* colonization of HAp surfaces.
- DR9-DR9 and DR9-RR14 peptides do not modulate the *S. mutans* proteome upon attachment to HAp, nor regulate the expression of the intracellular and extracellular bacterial proteins involved in biofilm cariogenicity.
- The modified cariogenic biofilm model constitutes a validated approach to assess the caries protective effect of treatment options whose quantity is limited to smaller volumes, as in the case of novel biotechnological strategies using salivary peptides.
- The engineered DR9-DR9 and DR9-RR14 peptides may modulate caries development mainly by a physicochemical mechanism.

5.4 References

Basiri T, Johnson ND, Moffa EB, Mulyar Y, Serra Nunes PL, Machado M, Siqueira WL. 2017. Duplicated or hybridized peptide functional domains promote oral homeostasis. J Dent Res. 96(10):1162-1167.

Bowen WH, Eastoe JE, Cock DJ. 1966. The effect of sugar solutions on the ph of plaque in caries-active monkeys (macaca irus). Arch Oral Biol. 11(8):833-838.

Bowen WH, Tenuta LMA, Koo H, Cury JA. 2019. Dental caries: Etiology and pathogenesis. In: Lamont RJ, Hajishengalis GM, Koo H, Jenkinson HF, editors. Oral microbiology and immunology. Third ed. Washington, DC: ASM Press. p. 251-265.

Ccahuana-Vásquez RA, Cury JA. 2010. S. Mutans biofilm model to evaluate antimicrobial substances and enamel demineralization. Braz Oral Res. 24(2):135-141.

dos Santos AP, Nadanovsky P, de Oliveira BH. 2013. A systematic review and meta-analysis of the effects of fluoride toothpastes on the prevention of dental caries in the primary dentition of preschool children. Community Dent Oral Epidemiol. 41(1):1-12.

Duke SA, Forward GC. 1982. The conditions occurring in vivo when brushing with toothpastes. Br Dent J. 152(2):52-54.

Goobes G, Goobes R, Schueler-Furman O, Baker D, Stayton PS, Drobny GP. 2006. Folding of the c-terminal bacterial binding domain in statherin upon adsorption onto hydroxyapatite crystals. Proc Natl Acad Sci U S A. 103(44):16083-16088.

Goobes R, Goobes G, Shaw WJ, Drobny GP, Campbell CT, Stayton PS. 2007. Thermodynamic roles of basic amino acids in statherin recognition of hydroxyapatite. Biochemistry. 46(16):4725-4733.

Heffernan R, Dehzangi A, Lyons J, Paliwal K, Sharma A, Wang J, Sattar A, Zhou Y, Yang Y. 2016. Highly accurate sequence-based prediction of half-sphere exposures of amino acid residues in proteins. Bioinformatics. 32(6):843-849.

Jin LJ, Lamster IB, Greenspan JS, Pitts NB, Scully C, Warnakulasuriya S. 2016. Global burden of oral diseases: Emerging concepts, management and interplay with systemic health. Oral Dis. 22(7):609-619.

Kosoric J, Williams RAD, Hector MP, Anderson P. 2007. A synthetic peptide based on a natural salivary protein reduces demineralisation in model systems for dental caries and erosion. International Journal of Peptide Research and Therapeutics. 13(4):497-503.

Li J, Helmerhorst EJ, Leone CW, Troxler RF, Yaskell T, Haffajee AD, Socransky SS, Oppenheim FG. 2004. Identification of early microbial colonizers in human dental biofilm. J Appl Microbiol. 97(6):1311-1318.

Long JR, Shaw WJ, Stayton PS, Drobny GP. 2001. Structure and dynamics of hydrated statherin on hydroxyapatite as determined by solid-state nmr. Biochemistry. 40(51):15451-15455.

Makrodimitris K, Masica DL, Kim ET, Gray JJ. 2007. Structure prediction of protein-solid surface interactions reveals a molecular recognition motif of statherin for hydroxyapatite. J Am Chem Soc. 129(44):13713-13722.

Marinho VC, Higgins JP, Sheiham A, Logan S. 2003. Fluoride toothpastes for preventing dental caries in children and adolescents. Cochrane Database Syst Rev. (1):CD002278.

Martins C, Castro GF, Siqueira MF, Xiao Y, Yamaguti PM, Siqueira WL. 2013. Effect of dialyzed saliva on human enamel demineralization. Caries Res. 47(1):56-62.

Maske TT, van de Sande FH, Arthur RA, Huysmans M, Cenci MS. 2017. In vitro biofilm models to study dental caries: A systematic review. Biofouling. 33(8):661-675.

Nichols WW, Evans MJ, Slack MP, Walmsley HL. 1989. The penetration of antibiotics into aggregates of mucoid and non-mucoid pseudomonas aeruginosa. J Gen Microbiol. 135(5):1291-1303.

Petersen PE, Bourgeois D, Ogawa H, Estupinan-Day S, Ndiaye C. 2005. The global burden of oral diseases and risks to oral health. Bull World Health Organ. 83(9):661-669.

Raj PA, Johnsson M, Levine MJ, Nancollas GH. 1992. Salivary statherin. Dependence on sequence, charge, hydrogen bonding potency, and helical conformation for adsorption to hydroxyapatite and inhibition of mineralization. J Biol Chem. 267(9):5968-5976.

Reynolds EC, Wong A. 1983. Effect of adsorbed protein on hydroxyapatite zeta potential and streptococcus mutans adherence. Infect Immun. 39(3):1285-1290.

Rolla G. 1977. Formation of dental integuments--some basic chemical considerations. Swed Dent J. 1(6):241-251.

Shah S, Kosoric J, Hector MP, Anderson P. 2011. An in vitro scanning microradiography study of the reduction in hydroxyapatite demineralization rate by statherin-like peptides as a function of increasing n-terminal length. Eur J Oral Sci. 119 Suppl 1:13-18.

Simonson LG, Reiher DA. 1981. Effect of human saliva and various compounds on the adsorption of the bacterium streptococcus mutans to hydroxyapatite. Arch Oral Biol. 26(2):143-146.

Tang R, Hass M, Wu W, Gulde S, Nancollas GH. 2003. Constant composition dissolution of mixed phases. Ii. Selective dissolution of calcium phosphates. J Colloid Interface Sci. 260(2):379-384.

Walsh T, Worthington HV, Glenny AM, Appelbe P, Marinho VC, Shi X. 2010. Fluoride toothpastes of different concentrations for preventing dental caries in children and adolescents. Cochrane Database Syst Rev. (1):CD007868.

Xiao Y, Karttunen M, Jalkanen J, Mussi MC, Liao Y, Grohe B, Lagugné-Labarthet F, Siqueira WL. 2015. Hydroxyapatite growth inhibition effect of pellicle statherin peptides. J Dent Res. 94(8):1106-1112.

Yin A, Margolis HC, Yao Y, Grogan J, Oppenheim FG. 2006. Multi-component adsorption model for pellicle formation: The influence of salivary proteins and non-salivary phospho proteins on the binding of histatin 5 onto hydroxyapatite. Arch Oral Biol. 51(2):102-110.

Zahradnik RT, Moreno EC, Burke EJ. 1976. Effect of salivary pellicle on enamel subsurface demineralization in vitro. J Dent Res. 55(4):664-670.

Zahradnik RT, Propas D, Moreno EC. 1977. In vitro enamel demineralization by streptococcus mutans in the presence of salivary pellicles. J Dent Res. 56(9):1107-1110.

Zahradnik RT, Propas D, Moreno EC. 1978. Effect of salivary pellicle formation time on in vitro attachment and demineralization by streptococcus mutans. J Dent Res. 57(11-12):1036-1042.

Appendices

Appendix 1. List of proteins identified in the planktonic bacteria according to the treatments and at each time point evaluated.

	Treatment																							
	A			B			C			D			E			F			G			H		
Time (h) / Gene Name	2	4	8	2	4	8	2	4	8	2	4	8	2	4	8	2	4	8	2	4	8	2	4	8
ackA						x									x			x			x			x
acp						x			x			x			x			x			x			x
aroA																		x			x			x
aroH						x																		
aspB						x			x			x			x			x			x			x
bacA1					x																			
clp	x	x			x		x			x									x	x				
clpC											x													
dapH						x									x			x			x			x
dnaK	x	x		x	x	x	x	x	x	x	x	x	x	x	x	x		x	x	x	x	x	x	x
eno	x	x		x	x	x	x	x	x	x	x	x	x	x	x	x		x	x	x	x	x	x	x
fabF						x									x			x			x			
fbaA						x									x			x						x
flaW									x						x			x						
frr						x			x			x						x			x			x
fusA		x			x	x	x	x	x			x	x		x			x			x	x		x
gapC	x	x		x	x	x	x	x	x	x	x	x	x	x	x	x		x	x	x	x	x	x	x
gapN						x												x			x			x

gatA														x									
gbpC					x			x					x					x				x	
glgP								x							x								
glk					x						x		x		x			x				x	
glnA					x			x					x		x			x				x	
glyA					x																		
gpmA	x	x			x	x		x	x		x	x			x			x	x		x			x	
greA													x								x			x	
groL	x	x		x	x	x	x	x	x	x	x	x	x	x	x	x		x	x	x	x	x	x	x	x
groS								x				x			x						x			x	
hsdM					x	x		x			x			x						x		x			
hup	x	x		x	x			x			x		x	x		x		x	x	x	x	x	x	x	x
ilvC	x	x			x	x		x	x	x	x	x	x	x				x	x		x	x	x	x	x
ilvE						x								x				x			x			x	
livK						x						x		x				x			x			x	
mleS						x			x												x				
mtlR			x										x			x									
nagB														x											
naoX						x			x					x											
oppA						x						x		x				x		x		x			x
pepN																					x				
pepO									x									x			x				
pfkA																		x			x			x	
pgi			x			x						x		x				x			x			x	
pgk	x	x		x	x	x	x	x	x	x	x	x	x	x	x	x		x	x	x	x	x	x	x	x
pgm						x			x					x										x	

ppaC																													x
proS																		x											
psaB													x						x										
ptsG																		x											
ptsI	x	x		x		x	x		x			x		x	x			x			x							x	
rmlB												x						x			x								
rpiA																		x											
rplA												x						x	x									x	
rplB																			x										
rplD																					x								
rplE	x	x			x	x	x			x		x	x		x			x	x		x	x			x			x	
rplF					x														x										
rplJ	x	x			x		x	x					x		x	x		x	x		x	x	x						
rplK				x	x					x					x													x	
rplL	x	x			x	x	x	x	x	x	x	x	x	x	x	x		x	x	x	x	x	x		x	x	x	x	x	
rplO					x					x			x						x										
rplU																													x	
rplV													x						x										
rplX																			x										
rpoC				x							x		x			x		x	x		x	x			x			x	
rpsB					x	x	x								x						x								
rpsC		x			x		x											x	x		x							x	
rpsD					x							x						x										x	
rpsE	x	x		x	x		x			x			x			x		x	x		x	x	x		x			x	
rpsG	x																		x										
rpsH																			x										

rpsJ	x	x		x	x		x		x	x		x	x		x		x					x
rpsL										x												
rpsM	x																					
rs1		x		x	x					x						x		x		x				x
secY															x							
serC					x	x								x								
SMU_1121c						x								x						x				x
SMU_1208c											x											
SMU_1377c	x				x	x			x			x			x			x			x			x
SMU_1641c	x	x		x	x	x	x	x	x	x	x	x	x	x	x		x	x	x	x	x	x	x	x
SMU_1960c									x															
SMU_2084c														x										
SMU_241c							x																	
SMU_491					x															x			
SMU_546																					x		
SMU_743		x																					
SMU_815														x									x
spaP	x	x		x	x	x		x	x	x	x	x		x	x	x		x	x	x	x	x	x	x
thrC																							x
tig						x											x			x			x
tkt												x											
tpiA		x			x	x	x	x	x		x	x			x	x		x			x			x
treA						x			x											x			
trxA								x															
tsf		x			x	x		x	x	x		x			x	x		x	x	x		x	x
tuf	x	x		x	x	x	x	x	x	x	x	x	x	x	x	x		x	x	x	x	x	x	x

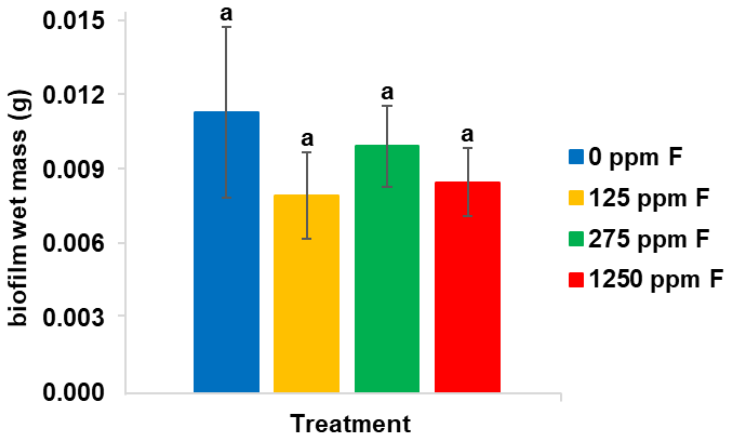

Appendix 2. Biofilm wet weight (g) according to the treatments. Means followed by different lower-case letters indicate statistically significant differences among the treatment groups (ANOVA and Tukey test, p >0.05).

Appendix 3. List of intracellular proteins identified when the proteins/peptides were used only to form the AEP.

Intracellular proteins												
Accession	**Gene name**	**Protein name**	**Protein function**	**Treatment**								
				A	**B**	**C**	**D**	**E**	**F**	**G**	**H**
Adaptative responses to environmental changes												
Q8DTJ8	bacD	Putative bacitracin synthetase	Antibiotic biosynthesis								x
Q8DWD4	adhD	Dihydrolipoyl dehydrogenase	Cell redox homeostasis	x							x
Q8DT76	addA	ATP-dependent helicase/nuclease subunit A	DNA repair				x	x			
Q8DRX0	mutL	DNA mismatch repair protein MutL	DNA repair								x
P27624	recA	Protein RecA	DNA repair	x			x		x		x
Q8DT81	SMU_1485c	Putative endonuclease	DNA repair			x					
Q8DRU4	SMU_2120c	Putative 3-methyladenine DNA glycosylase	DNA repair								x
Q8DWN4	trcF	Transcription-repair-coupling factor	DNA repair			x					
P72481	uvrA	UvrABC system protein A	DNA repair			x	x	x		x	
Q8CWX7	uvrB	UvrABC system protein B	DNA repair			x					
Q8DSP2	SMU_1733c	Putative SNF helicase	DNA replication, recombination and repair			x					
Q8DSU5	SMU_1664c	Putative acetoin utilization protein, acetoin dehydrogenase	Energy store								x
Q8DW04	SMU_287	Putative ComB, accessory factor for ComA	Quorum sensing			x	x				
Q8DSH1	scnK	Putative histidine kinase, ScnK-like protein	Signal transduction				x				
Amino acid metabolism and biosynthesis												
Q8DUV8	aroA	3-phosphoshikimate 1-carboxyvinyltransferase	Amino acid biosynthesis				x				
Q8DUV7	aroK	Shikimate kinase	Amino acid biosynthesis			x					
Q8DUP3	carB	Carbamoyl-phosphate synthase large chain	Amino acid biosynthesis	x		x					
Q8DVU9	glnA	Glutamine synthetase type 1 glutamate--ammonia ligase	Amino acid biosynthesis			x			x		x
Q8DW43	ilvC	Ketol-acid reductoisomerase (NADP(+))	Amino acid biosynthesis	x	x	x	x	x	x	x	x
Q8DTW7	ilvE	Branched-chain-amino-acid aminotransferase	Amino acid biosynthesis			x					
Q8DSV3	serC	Phosphoserine aminotransferase	Amino acid biosynthesis			x	x	x			
Q8DVY6	SMU_318	N-acetyldiaminopimelate deacetylase	Amino acid biosynthesis				x				
Q8DUR2	SMU_841	Putative aminotransferase	Amino acid biosynthesis	x		x					
Q8DUG5	SMU_965	Homoserine dehydrogenase	Amino acid biosynthesis			x					
Q8DVF8	trpE	Anthranilate synthase component 1	Amino acid biosynthesis				x		x		
Q8DUL2	SMU_913	Glutamate dehydrogenase	Amino acid metabolism					x			

Bacterial adherence and biofilm formation

Q54443	dexA	Dextranase	Adherence				x			x	
Q9KIJ3	sloC	Metal ABC transporter substrate-binding lipoprotein	Adherence					x			
P11000	wapA	Wall-associated protein	Adherence			x				x	x
Q8DU58	wapE	Uncharacterized protein	Adherence			x		x			x
Q8DVR0	brpA	Biofilm regulatory protein A	Biofilm formation			x		x			x
Q8DWM3	gbpB	Putative secreted antigen GbpB/SagA putative peptidoglycan hydrolase	Biofilm formation	x							
Q8DUW9	gbpD	Glucan-binding protein D with lipase activity BglB-like protein	Biofilm formation						x		
Q8CVC7	SMU_609	Putative 40K cell wall protein	Biofilm formation				x				
P23504	spaP	Cell surface antigen I/II	Cell wall antigen	x	x	x	x	x	x	x	x
P11701	ftf	Levansucrase	EPS biosynthesis	x			x				
P08987	gtfB	Glucosyltransferase-I	EPS biosynthesis			x					x
P13470	gtfC	Glucosyltransferase-SI	EPS biosynthesis	x		x	x	x			x
Q8DUS4	rgpA	Putative RgpAc glycosyltransferase	EPS biosynthesis	x			x		x		
Q8CVC4	SMU_1432c	Glucanase	EPS catabolism				x				

Carbohydrate metabolism and energy production

Q8DT55	phsG	Alpha-1,4 glucan phosphorylase	Carbohydrate metabolic process				x				
Q03174	fruA	Fructan beta-fructosidase	Carbohydrate metabolic process	x		x	x				x
Q8DWH3	fruB	Fructan hydrolase exo-beta-D-fructosidase FruB	Carbohydrate metabolic process			x					
Q8DWE8	fruP	Tagatose-6-phosphate kinase	Carbohydrate metabolic process				x				
Q8DVV3	gapC	Glyceraldehyde-3-phosphate dehydrogenase	Carbohydrate metabolic process	x	x	x	x	x	x	x	x
Q8DT31	glgP	Alpha-1,4 glucan phosphorylase	Carbohydrate metabolic process								x
Q59934	pfl	Formate acetyltransferase	Carbohydrate metabolic process	x	x	x	x	x	x		x
Q8CWY1	pfl2	Formate acetyltransferase (Pyruvate formate-lyase 2)	Carbohydrate metabolic process	x							
Q8DU72	pgm	Putative phosphoglucomutase	Carbohydrate metabolic process								x
P95780	rmlB	dTDP-glucose 4,6-dehydratase	Carbohydrate metabolic process	x			x	x			x
Q8DRZ0	SMU_2065	Putative UDP-glucose-4-epimerase	Carbohydrate metabolic process	x							
I6L8Z8	SMU_308	Sorbitol-6-phosphate 2-dehydrogenase	Carbohydrate metabolic process				x				
Q8DVN9	SMU_435	Putative N-acetylglucosamine-6-phosphate deacetylase	Carbohydrate metabolic process				x				
O68579	ppaC	Probable manganese-dependent inorganic pyrophosphatase	Energy metabolism	x	x	x	x	x	x	x	x
Q8DTS9	eno	Enolase	Glycolytic process	x	x	x	x	x	x	x	x

Q8DWG0	fbaA	Fructose-1,6-biphosphate aldolase	Glycolytic process	x	x	x	x	x	x	x	x
P26283	ldh	L-lactate dehydrogenase	Glycolytic process	x		x	x		x		x
Q8DVV2	pgk	Phosphoglycerate kinase	Glycolytic process	x	x	x	x	x	x	x	x
Q8DTX7	pykF	Pyruvate kinase	Glycolytic process	x	x	x	x	x	x	x	x
P72484	tpiA	Triosephosphate isomerase	Glycolytic process			x					
Cell division, replication and cell wall synthesis											
Q8DVD4	divIVA	Putative cell division protein DivIVA	Cell division	x		x	x	x			x
Q8DTL0	ftsE	Cell division ATP-binding protein FtsE	Cell division					x	x		x
Q8DVD9	ftsZ	Cell division protein FtsZ	Cell division			x					
Q8DSP6	mltG	Endolytic murein transglycosylase	Cell wall biosynthesis			x					
Q8DVM5	pbp2x	Putative penicillin-binding protein 2X	Cell wall biosynthesis		x	x					
Q8DUJ1	SMU_937	Putative mevalonate diphosphate decarboxylase	Peptidoglycan biosynthesis				x				
Q8DT49	ligA	DNA ligase	Replication								x
Q8DRY2	nrdD	Putative anaerobic ribonucleoside-triphosphate reductase	Replication			x					
Q8DU41	gyrA	DNA gyrase subunit A	Replication								x
Nucleoside/Nucleotide metabolism and biosynthesis											
Q8DRR2	guaB	Inosine-5'-monophosphate dehydrogenase	Nucleotide biosynthesis						x		
Q8DWJ5	purE	N5-carboxyaminoimidazole ribonucleotide mutase	Nucleotide biosynthesis		x			x			
Q8DWL3	purF	Amidophosphoribosyltransferase	Nucleotide biosynthesis				x		x		
Q8DWL5	purL	Phosphoribosylformylglycinamidine synthase	Nucleotide biosynthesis	x			x				
Q8DW83	SMU_187c	tRNA-dihydrouridine synthase	Nucleotide biosynthesis				x				
I6L8Y1	SMU_273	Putative hexulose-6-phosphate synthase	Nucleotide biosynthesis								
Q8DVL6	SMU_464	Nicotinate phosphoribosyltransferase	Nucleotide biosynthesis	x	x		x	x			x
Q8CVC5	SMU_1213c	Putative 5'-nucleotidase	Nucleotide catabolism				x				
Other metabolic processes											
Q8DWB9	adhE	Aldehyde-alcohol dehydrogenase	Alcohol metabolic process	x							
Q59925	fhs	Formate--tetrahydrofolate ligase	Biomolecules metabolism		x						
Q8DV28	SMU_689	Lysozyme	Cell wall catabolism	x							
Q9XB21	hup	DNA-binding protein HU	Chromosome condensation	x	x	x	x	x	x	x	x
Q7ZAL0	smc	Chromosome partition protein Smc	Chromosome condensation	x							

Q8DVB5	xseA	Exodeoxyribonuclease 7 large subunit	DNA catabolism				x			x	
Q8DVI3	SMU_505	Methyltransferase	DNA methylation	x							
Q8DSN3	acp	acyl carrier protein	Fatty acid biosynthesis							x	
Q8DSN6	fabF	3-oxoacyl-[acyl-carrier-protein] synthase 2	Fatty acid biosynthesis					x			
P34001	SMU_988	Uncharacterized protein	Lipid byosinthesis							x	
Q93D83	gpsA	Glycerol-3-phosphate dehydrogenase [NAD(P)+]	Lipid metabolism			x	x				
Q8DS57	ackA	acetate kinase	Metabolic processes					x			
Q8DTJ5	bacA1	Putative bacitracin synthetase 1 BacA	Metabolic processes		x	x	x			x	
Q8DTJ4	SMU_1343c	Putative polyketide synthase	Metabolic processes					x			
Q8DW46	SMU_229	Uncharacterized protein	Metabolic processes						x		
Q8DVN8	SMU_438c	Putative (R)-2-hydroxyglutaryl-CoA dehydratase activator-related protein	Metabolic processes								x
Q8DV33	SMU_683	Putative ATP-binding protein	Metabolic processes			x					
Q8DUJ0	SMU_938	Putative phosphomevalonate kinase	Metabolic processes					x			
Q8DVF0	dpr	Peroxide resistance protein Dpr	Oxidation-reduction process	x	x	x	x	x	x	x	x
Q8DTN9	flaW	Putative flavodoxin	Oxidation-reduction process								x
Q59931	gapN	NADP-dependent glyceraldehyde-3-phosphate dehydrogenase	Oxidation-reduction process	x	x	x	x	x	x	x	x
Q8DVU1	SMU_374	Putative oxidoreductase	Oxidation-reduction process					x			
Q8DWM7	ftsH	ATP-dependent zinc metalloprotease FtsH	Proteolysis			x	x	x	x		x
Q93D93	htpX	Protease HtpX homolog	Proteolysis								x
Q8DRQ6	htrA	Serine protease HtrA	Proteolysis				x	x			
Q8DS80	pbp2a	Putative membrane carboxypeptidase, penicillin-binding protein 2a	Proteolysis	x		x					
Q8DU26	pepN	aminopeptidase	Proteolysis					x			
Q8DSE4	pepP	Putative aminopeptidase P	Proteolysis			x					
Q8DVS2	pepX	Xaa-Pro dipeptidyl-peptidase	Proteolysis					x			
Q8DRR6	SMU_2153c	Putative peptidase	Proteolysis					x			
Q8DWB2	pnp	Polyribonucleotide nucleotidyltransferase	RNA degradation				x	x			x
Q8DUB2	SMU_1030	Putative polyribonucleotide nucleotidyltransferase Tn916 ORF8-like	RNA degradation	x							x
Q8DSQ0	SMU_1724c	Putative rRNA methylase	RNA methylation					x			
Q8DVG8	rlmN	Probable dual-specificity RNA methyltransferase RlmN	RNA methylation	x							
Q8DV10	ppc	Phosphoenolpyruvate carboxylase	Tricarboxylic acid cycle	x		x	x				
Transcription											
Q8DUH3	clp	Putative Clp-like ATP-dependent protease, ATP-binding subunit	Transcription	x	x	x	x	x	x		x

Q8DUN0	galR	Galactose operon repressor GalR	Transcription			x					x	
Q8DSP7	greA	Transcription elongation factor GreA	Transcription	x	x	x	x	x	x		x	
Q02425	mtlR	Putative transcriptional regulator MtlR	Transcription				x					
I6L8Z6	psaR	Putative transcriptional regulator	Transcription								x	
Q8DVV6	purR	Purine operon represso	Transcription			x						
Q8DS36	rpoA	DNA-directed RNA polymerase subunit alpha	Transcription				x					
Q8DS46	rpoB	DNA-directed RNA polymerase subunit beta(rpoB)	Transcription	x					x			
Q8DS47	rpoC	DNA-directed RNA polymerase subunit beta'	Transcription	x	x	x	x	x	x		x	
Q8DWE9	SMU_112c	Putative transcriptional regulator	Transcription			x						
Q8DWD9	SMU_124	Putative transcriptional regulator (MarR family)	Transcription			x		x			x	
Q8DSJ4	SMU_1789c	Probable transcriptional regulatory protein SMU_1789c	Transcription	x					x			
Q8DW49	SMU_226c	Putative transposase	Transcription				x					
Q8DV66	SMU_640c	Putative transcriptional regulator (GntR family)	Transcription								x	
Q8DUH6	SMU_953c	Putative transcriptional regulator/aminotransferase	Transcription								x	
Q8DVK3	sunL	Putative RNA-binding Sun protein possible rRNA methylase	Transcription				x					

Translation and protein synthesis

Q8CWY0	alaS	Alanine--tRNA ligase	Protein biosynthesis			x	x				x	
Q8DVD3	ileS	Isoleucine--tRNA ligase	Protein biosynthesis			x						
Q8CWX2	pheT	Phenylalanine--tRNA ligase beta subunit	Protein biosynthesis			x						
Q8DWH2	dnaJ	Chaperone protein DnaJ	Protein folding		x	x					x	
O06942	dnaK	Chaperone protein DnaK	Protein folding	x	x	x	x	x	x	x	x	
Q8CWW6	groL	60 kDa chaperonin	Protein folding	x	x	x	x	x	x	x	x	
Q8CWW5	groS	10 kDa chaperonin	Protein folding	x	x	x	x			x	x	
O06941	grpE	Protein GrpE	Protein folding			x	x		x		x	
Q8CWZ3	hslO	33 kDa chaperonin	Protein folding				x					
Q8CVC6	prsA	Foldase protein PrsA	Protein folding			x						
Q8CWZ6	tig	Trigger factor	Protein folding	x	x	x	x	x	x	x	x	
Q54431	ffh	Signal recognition particle protein	Protein targeting						x			
Q8DVV4	fusA	Elongation factor G	Translation	x	x	x	x	x	x		x	
Q8DSG5	gatA	Glutamyl-tRNA(Gln) amidotransferase subunit A	Translation				x					
Q8DSG6	gatB	Aspartyl/glutamyl-tRNA(Asn/Gln) amidotransferase subunit B	Translation	x		x	x		x		x	
Q8DVI8	hpf	Ribosome hibernation promoting factor	Translation	x		x		x			x	

Q8DVP9	infB	Translation initiation factor IF-2	Translation	x			x	x	x		x
Q8DTF3	lepA	Elongation factor 4	Translation				x				
Q8DRS4	mnmA	tRNA-specific 2-thiouridylase MnmA	Translation				x	x			
Q8DSY0	rplA	50S ribosomal protein L1	Translation								x
G1XVB9	rplB	50S ribosomal protein L2	Translation			x			x		
Q8DS17	rplD	50S ribosomal protein L4	Translation			x				x	x
Q8DUH2	rplJ	50S ribosomal protein L10	Translation			x		x			
Q8DUG9	rplL	50S ribosomal protein L7/L12	Translation	x	x	x	x	x	x	x	x
Q8DS23	rplN	50S ribosomal protein L14	Translation	x		x	x	x	x		x
Q8DS31	rplO	50S ribosomal protein L15	Translation				x				
Q8DS20	rplP	50S ribosomal protein L16	Translation				x	x			x
Q8DS37	rplQ	50S ribosomal protein L17	Translation		x	x		x	x	x	x
Q8DS29	rplR	50S ribosomal protein L18	Translation			x		x		x	
Q8DUQ6	rplU	50S ribosomal protein L21	Translation			x	x	x		x	
Q8DS19	rplV	50S ribosomal protein L22	Translation	x	x		x	x	x		x
Q8DS24	rplX	50S ribosomal protein L24	Translation	x	x	x	x	x		x	x
Q8DS11	rpsB	30S ribosomal protein S2	Translation	x	x	x	x	x	x		x
P59186	rpsC	30S ribosomal protein S3	Translation			x	x	x		x	
P59133	rpsD	30S ribosomal protein S4	Translation	x	x	x	x	x	x		x
P59125	rpsE	30S ribosomal protein S5	Translation		x		x	x	x	x	x
Q8DSD7	rpsF	30S ribosomal protein S6	Translation	x		x	x				x
Q8DVV5	rpsG	30S ribosomal protein S7	Translation	x							
Q8DW97	rpsI	30S ribosomal protein S9	Translation	x	x	x	x	x	x		x
Q8DS35	rpsM	30S ribosomal protein S13	Translation	x	x				x	x	
P66474	rpsR	30S ribosomal protein S18	Translation		x						
Q8DTW9	rs1	Putative ribosomal protein S1 sequence specific DNA-binding protein	Translation	x		x	x	x	x	x	x
Q8DTF9	SMU_1388	Putative RNA helicase	Translation			x					
Q8DWH1	truA	tRNA pseudouridine synthase A	Translation						x		
Q8DS12	tsf	Elongation factor Ts	Translation	x	x	x	x			x	x
P72483	tuf	Elongation factor Tu	Translation	x	x	x	x	x	x	x	x
Q8CWW9	vacB	Ribonuclease R	Translation				x				

Transport

Q8DW36	SMU_241c	Putative ABC transporter, ATP-binding protein amino acid transport system	Amino acid transport				x				
Q8DUY4	SMU_746c	Putative two-component membrane permease complex subunit	Amino acid transport			x					
Q8DUT1	SMU_815	Putative amino acid transporter, amino acid-binding protein	Amino acid transport				x			x	
Q8DW22	oppD	Putative oligopeptide ABC transporter, ATP-binding protein OppD	Peptide transport	x							
Q8DU24	pstB1	Phosphate import ATP-binding protein PstB 1	Phosphate transport								x
Q8DSF0	secA	Protein translocase subunit SecA	Protein transport	x							x
Q8DUN3	fruI	Inducible fructose permease	Sugar transport			x		x	x		x
Q8DT27	malF	Putative maltose/maltodextrin ABC transporter, permease protein MalF	Sugar transport				x				
Q8DS05	ptsG	Putative PTS system, glucose-specific IIABC component	Sugar transport			x		x			x
P45595	ptsI	Phosphoenolpyruvate-protein phosphotransferase	Sugar transport	x		x	x	x	x	x	x
Q8DU37	SMU_1120	Putative sugar ABC transporter, ATP-binding protein	Sugar transport				x				
Q8DSC2	SMU_1879	Putative PTS system, mannose-specific component IID	Sugar transport				x	x	x		x
Q8DS76	SMU_1957	Putative PTS system, mannose-specific IID component	Sugar transport					x			x
Q8DS75	SMU_1958c	Putative PTS system, mannose-specific IIC component	Sugar transport		x			x			
Q8DS74	SMU_1960c	Putative PTS system, mannose-specific IIB component	Sugar transport	x		x	x	x	x	x	x
Q8DS73	SMU_1961c	Putative PTS system, sugar-specific enzyme IIA component	Sugar transport						x	x	
P72477	abcX	Putative ABC transporter ATP-binding protein	Transport				x				
Q8DSU0	livK	Putative ABC transporter, branched chain amino acid-binding protein	Transport						x		
Q8DW25	oppA	Putative oligopeptide ABC transporter, substrate-binding protein OppA	Transport			x					
Q8DU85	opuAb	Putative ABC transporter, proline/glycine betaine permease protein	Transport	x							
Q8DRU6	opuCc	Putative ABC transporter osmoprotectant-binding protein, glycine betaine/carnitine/choline ABC transporter	Transport	x							
Q8DT32	pacL	Putative cation-transporting P-type ATPase PacL	Transport			x	x				
Q8DU70	SMU_1079c	Putative ABC transporter, ATP-binding protein	Transport			x					
Q8DU57	SMU_1093	Putative ABC transporter, permease protein	Transport	x			x		x		x
Q8DTZ3	SMU_1167c	Putative ABC transporter, ATP-binding protein	Transport			x	x				
Q8DTV6	SMU_1217c	Putative ABC transporter amino acid binding protein	Transport				x				
Q8DTP4	SMU_1289c	Putative permease, chloride channel	Transport				x				
Q8DTD8	SMU_1412c	Putative ABC transporter, membrane protein subunit and ATP-binding protein	Transport	x		x	x	x			
Q8DT43	SMU_1551c	Putative ABC transporter, ATP-binding protein	Transport			x					
Q8DSZ6	SMU_1605	Putative MDR permease possible transmembrane efflux protein	Transport			x					
Q8DSJ6	SMU_1787c	Putative secreted protein	Transport			x		x	x		
Q8DW35	SMU_242c	Putative amino acid ABC transporter, permease protein, glutamine transport system	Transport								x
Q8DW32	SMU_247	Putative ABC transporter ATP-binding protein	Transport	x	x	x					x

Q8DW31	SMU_248	Putative ABC transporter, membrane protein	Transport					x					
Q8DW05	SMU_286	Putative ABC transporter ATP-binding protein ComA	Transport				x						
Q8DVG6	SMU_524	Putative ABC transporter, ATP-binding protein	Transport				x						
Q8DUT7	SMU_806c	Putative glutamine ABC transporter, permease protein	Transport					x					
Q8DUL7	SMU_902	Putative ABC transporter, ATP-binding protein	Transport					x					
Q8DUK5	SMU_922	Putative ABC transporter, ATP-binding protein	Transport					x					
Q8DUK4	SMU_923	Putative ABC transporter, ATP-binding protein	Transport					x					
Q8DUJ3	SMU_935	Putative amino acid ABC transporter, permease protein	Transport				x						
Uncharacterized/Unknown													
Q8CWZ5	SMU_109	Uncharacterized protein	Uncharacterized						x				
Q8DU49	SMU_1104c	Uncharacterized protein	Uncharacterized				x						
Q8DWE4	SMU_117c	Uncharacterized protein	Uncharacterized					x					
Q8DWC3	SMU_141	Uncharacterized protein	Uncharacterized					x					
Q8DTC5	SMU_1427c	Uncharacterized protein	Uncharacterized										x
Q8DTB0	SMU_1447c	Uncharacterized protein	Uncharacterized					x				x	x
Q8DT86	SMU_1479	Uncharacterized protein	Uncharacterized	x	x	x	x	x	x				x
Q8DT20	SMU_1576c	Uncharacterized protein	Uncharacterized			x							
Q8DT19	SMU_1577c	Uncharacterized protein	Uncharacterized							x			
Q8DSS1	SMU_1700c	Uncharacterized protein	Uncharacterized										x
Q8DSM0	SMU_1760c	Uncharacterized protein	Uncharacterized	x		x	x						
Q8DSF8	SMU_1830c	Uncharacterized protein	Uncharacterized	x								x	
Q8DSA4	SMU_1904c	Uncharacterized protein	Uncharacterized			x	x						
Q8DRZ2	SMU_2061	Uncharacterized protein	Uncharacterized									x	
Q8DW41	SMU_235	Uncharacterized protein	Uncharacterized	x	x	x	x	x	x	x	x	x	x
Q8DVY0	SMU_329	Uncharacterized protein	Uncharacterized			x							
Q8DVX6	SMU_333	Uncharacterized protein	Uncharacterized	x									
Q8DVW2	SMU_350	Uncharacterized protein	Uncharacterized			x							
Q8DVJ1	SMU_497c	Uncharacterized protein	Uncharacterized				x						
Q8DVI6	SMU_502	Uncharacterized protein	Uncharacterized	x			x		x				
Q8DVH1	SMU_518	Uncharacterized protein	Uncharacterized				x						
Q8DV76	SMU_630	Uncharacterized protein	Uncharacterized			x							
Q8DWI5	SMU_63c	Uncharacterized protein	Uncharacterized	x		x	x	x	x				x

Q8DV34	SMU_682	Uncharacterized protein	Uncharacterized			x						
Q8DV27	SMU_690	Uncharacterized protein	Uncharacterized			x						
Q8DUY9	SMU_739c	Uncharacterized protein	Uncharacterized		x							
Q8DUR8	SMU_835	Uncharacterized protein	Uncharacterized				x					
Q8DUN2	SMU_874	Uncharacterized protein	Uncharacterized					x				
Q8DUH1	SMU_958	Uncharacterized protein	Uncharacterized						x			
Q8DTJ0	SMU_1347c	Uncharacterized protein	Unknown				x	x				
Q8DRT3	SMU_2133c	Putative membrane protein	Unknown	x		x	x			x	x	
Q8DUV9	SMU_782	UPF0342 protein	Unknown			x				x	x	

Appendix 4. List of ECM proteins identified when the proteins/peptides were used only to form the AEP.

ECM proteins

Accession	Gene name	Protein name	Protein function	Treatment							
				A	B	C	D	E	F	G	H
Adaptative responses to environmental changes											
Q8DW47	SMU_228	Putative alkaline-shock protein-like protein	Alkaline shock	x			x	x		x	
Q8DTJ8	bacD	Putative bacitracin synthetase	Antibiotic biosynthesis				x				x
Q8DWD4	adhD	Dihydrolipoyl dehydrogenase	Cell redox homeostasis	x		x	x	x		x	
I6L8Y0	ahpC	alkyl hydroperoxide reductase	Cell redox homeostasis					x			
I6L922	SMU_765	NADH oxidase/alkyl hydroperoxidase reductase peroxide-forming	Cell redox homeostasis		x						
Q8DUK3	tpx	Thiol peroxidase	Cell redox homeostasis	x	x	x	x	x	x	x	x
Q8DSD2	trxA	Thioredoxin	Cell redox homeostasis	x	x	x	x	x	x	x	x
P09738	sodA	Superoxide dismutase [Mn/Fe]	Cellular detoxification	x	x	x	x	x	x	x	x
Q03JI6	cas9-2	CRISPR-associated endonuclease Cas9 2	CRISP element metabolism		x						
Q8DUM6	hsdS	Putative type I restriction-modification system, specificity determinant	DNA modification				x		x		
Q8DVY2	radA	DNA repair protein RadA	DNA repair					x			
P27624	recA	Protein RecA	DNA repair	x	x	x	x	x	x	x	x
Q9AIV4	smnA	Nuclease SmnA	DNA repair		x						x
Q8DWN4	trcF	Transcription-repair-coupling factor	DNA repair		x	x		x			
Q8CWX7	uvrB	UvrABC system protein B	DNA repair					x			

Q8DSD8	ssb	Single-stranded DNA-binding protein	DNA replication, recombination and repair	x		x		x		x	
Q8DS68	ssb2	Single-stranded DNA-binding protein	DNA replication, recombination and repair							x	
Q8DUM2	SMU_897	Type I restriction enzyme R Protein	DNA restriction				x				
Q8DRX2	cinA	Putative competence-damage inducible protein	DNA transformation							x	
Q8DUD4	smf	Putative DNA processing Smf protein	DNA transformation							x	
Q8DSU5	SMU_1664c	Putative acetoin utilization protein, acetoin dehydrogenase	Energy store	x	x	x	x	x		x	
Q8DSJ5	SMU_1788c	Putative bacterocin transport accessory protein, Bta	Killing factor	x	x	x	x	x	x	x	x
Q8DW04	SMU_287	Putative ComB, accessory factor for ComA	Quorum sensing			x		x	x		
Q8DW76	SMU_198c	Putative conjugative transposon protein	Recombination	x	x	x				x	
Q8DVL4	pbp1a	Penicillin-binding protein 1a membrane carboxypeptidase	Response to antibiotics	x	x		x	x			
Q8DW95	SMU_173	Putative ppGpp-regulated growth inhibitor	Stress		x		x	x			x
Q8DSF9	SMU_1828	Universal stress protein	Stress	x	x	x	x	x	x		x

Amino acid metabolism and biosynthesis

Q8DSM8	akh	Aspartokinase	Amino acid biosynthesis					x			
P59311	argC	N-acetyl-gamma-glutamyl-phosphate reductase	Amino acid biosynthesis			x					
Q8DUV8	aroA	3-phosphoshikimate 1-carboxyvinyltransferase	Amino acid biosynthesis	x							
Q8DUW4	aroD	3-dehydroquinate dehydratase	Amino acid biosynthesis	x	x		x				
Q8DUW3	aroE	Shikimate dehydrogenase (NADP(+))	Amino acid biosynthesis	x	x	x	x	x	x	x	x
Q8DSF1	aroH	Phospho-2-dehydro-3-deoxyheptonate aldolase	Amino acid biosynthesis	x			x	x	x		x
Q8DUV7	aroK	Shikimate kinase	Amino acid biosynthesis				x	x	x	x	x
P10539	asd	aspartate-semialdehyde dehydrogenase	Amino acid biosynthesis		x			x		x	
Q8DTM1	aspB	Asparagine--oxo-acid transaminase	Amino acid biosynthesis				x			x	
Q8DUP3	carB	Carbamoyl-phosphate synthase large chain	Amino acid biosynthesis				x				x
Q8DVJ2	cysK	Cysteine synthase	Amino acid biosynthesis	x							x
Q8DUE5	dapA	4-hydroxy-tetrahydrodipicolinate synthase	Amino acid biosynthesis	x							
Q8DUL9	dapB	4-hydroxy-tetrahydrodipicolinate reductase	Amino acid biosynthesis	x	x		x		x	x	
Q8DVY7	dapH	2,3,4,5-tetrahydropyridine-2,6-dicarboxylate N-acetyltransferase	Amino acid biosynthesis	x		x	x	x			x
Q8DVU9	glnA	Glutamine synthetase type 1 glutamate--ammonia ligase	Amino acid biosynthesis	x	x	x	x	x	x	x	x
Q8DU67	glyA	Serine hydroxymethyltransferase	Amino acid biosynthesis	x			x	x		x	
Q8DTQ9	hisB	Imidazoleglycerol-phosphate dehydratase	Amino acid biosynthesis		x						
Q8DTQ6	hisG	ATP phosphoribosyltransferase	Amino acid biosynthesis				x				
Q8DW42	ilvA	L-threonine dehydratase	Amino acid biosynthesis	x	x		x		x	x	x

Q8DW45	ilvB	Acetolactate synthase	Amino acid biosynthesis	x	x	x	x		x	x	x
Q8DW43	ilvC	Ketol-acid reductoisomerase (NADP(+))	Amino acid biosynthesis	x	x	x	x	x	x	x	x
Q8DRT7	ilvD	Dihydroxy-acid dehydratase	Amino acid biosynthesis	x	x		x		x	x	
Q8DTW7	ilvE	Branched-chain-amino-acid aminotransferase	Amino acid biosynthesis	x	x	x	x	x	x	x	x
Q8DTG2	leuA	2-isopropylmalate synthase	Amino acid biosynthesis	x	x	x	x	x	x		x
Q8DVM9	proA	Gamma-glutamyl phosphate reductase	Amino acid biosynthesis	x							
Q8DSV3	serC	Phosphoserine aminotransferase	Amino acid biosynthesis	x	x	x	x	x	x	x	x
Q8DUG5	SMU_965	Homoserine dehydrogenase	Amino acid biosynthesis		x	x	x	x	x		
Q8DVF4	trpF	N-(5'-phosphoribosyl)anthranilate isomerase	Amino acid biosynthesis						x		
Q8DUL2	SMU_913	Glutamate dehydrogenase	Amino acid metabolism	x	x	x	x	x	x	x	x
Q8DVD8	ylmE	Pyridoxal phosphate homeostasis protein	Amino acid metabolism					x			
Bacterial adherence and biofilm formation											
Q54443	dexA	Dextranase	Adherence	x	x	x	x	x	x	x	x
Q8DRV2	gbpA	Glucan-binding protein A, GbpA	Adherence	x	x	x	x	x	x	x	x
Q9KIJ3	sloC	Metal ABC transporter substrate-binding lipoprotein	Adherence	x	x		x	x	x	x	x
P11000	wapA	Wall-associated protein	Adherence	x	x	x	x		x	x	x
Q8DVR0	brpA	Biofilm regulatory protein A	Biofilm formation	x							
Q8DWM3	gbpB	Putative secreted antigen GbpB/SagA putative peptidoglycan hydrolase	Biofilm formation	x	x	x	x	x	x	x	x
Q8DTF1	gbpC	Glucan-binding protein C, GbpC	Biofilm formation		x		x	x	x	x	
Q8DUW9	gbpD	Glucan-binding protein D with lipase activity BglB-like protein	Biofilm formation						x		
Q8CVC7	SMU_609	Putative 40K cell wall protein	Biofilm formation	x	x	x	x	x	x	x	x
P23504	spaP	Cell surface antigen I/II	Cell wall antigen	x	x	x	x	x	x	x	x
P11701	ftf	Levansucrase	EPS biosynthesis	x	x	x	x	x	x	x	x
P08987	gtfB	Glucosyltransferase-I	EPS biosynthesis		x	x	x	x	x	x	x
P13470	gtfC	Glucosyltransferase-SI	EPS biosynthesis	x	x	x		x	x	x	x
P49331	gtfD	Glucosyltransferase-S	EPS biosynthesis	x	x	x	x	x	x	x	x
Q8DT30	malQ	4-alpha-glucanotransferase	EPS biosynthesis		x			x			
Carbohydrate metabolism and energy production											
Q8DT55	phsG	Alpha-1,4 glucan phosphorylase	Carbohydrate metabolic process				x				
P95778	rmlA	Glucose-1-phosphate thymidylyltransferase	Carbohydrate biosynthesis	x			x	x	x		x
Q8DUS5	SMU_824	dTDP-4-dehydrorhamnose reductase	Carbohydrate biosynthesis	x	x		x	x	x	x	x

Q8DTT9	rpiA	Ribose-5-phosphate isomerase A	Carbohydrate degradation	x	x		x	x	x	x	
Q8DT00	bgl	Putative phospho-beta-glucosidase	Carbohydrate metabolic process							x	
Q03174	fruA	Fructan beta-fructosidase	Carbohydrate metabolic process	x	x	x	x	x	x	x	x
P96994	galT	Galactose-1-phosphate uridylyltransferase	Carbohydrate metabolic process								x
Q8DVV3	gapC	Glyceraldehyde-3-phosphate dehydrogenase	Carbohydrate metabolic process	x	x	x	x	x	x	x	x
Q8DT31	glgP	Alpha-1,4 glucan phosphorylase	Carbohydrate metabolic process	x	x	x	x	x	x	x	x
Q8DTC6	glmM	Phosphoglucosamine mutase	Carbohydrate metabolic process	x	x	x	x	x		x	
Q8DTY0	glmS	Glutamine--fructose-6-phosphate aminotransferase [isomerizing]	Carbohydrate metabolic process	x	x			x	x	x	
Q8DV70	nagB	Glucosamine-6-phosphate deaminase	Carbohydrate metabolic process	x			x		x	x	
Q59934	pfl	Formate acetyltransferase	Carbohydrate metabolic process	x	x	x	x	x	x	x	x
Q8CWY1	pfl2	Formate acetyltransferase (Pyruvate formate-lyase 2)	Carbohydrate metabolic process	x	x	x	x	x		x	x
Q8DU72	pgm	Putative phosphoglucomutase	Carbohydrate metabolic process	x	x	x	x	x	x	x	x
P95780	rmlB	dTDP-glucose 4,6-dehydratase	Carbohydrate metabolic process	x						x	x
Q07211	scrK	Fructokinase	Carbohydrate metabolic process			x					
I6L930	SMU_322c	UTP--glucose-1-phosphate uridylyltransferase	Carbohydrate metabolic process	x							
O68579	ppaC	Probable manganese-dependent inorganic pyrophosphatase	Energy metabolism	x	x	x	x	x	x	x	x
Q8CWX0	glgA	Glycogen synthase	Glycogen biosynthesis				x				
Q8DTS9	eno	Enolase	Glycolytic process	x	x	x	x	x	x	x	x
Q8DWG0	fbaA	Fructose-1,6-biphosphate aldolase	Glycolytic process	x	x	x	x	x	x	x	x
Q8DVE8	glk	Putative glucose kinase	Glycolytic process				x	x			
P59161	gpmA	2,3-bisphosphoglycerate-dependent phosphoglycerate mutase	Glycolytic process	x	x	x	x	x	x	x	x
P26283	ldh	L-lactate dehydrogenase	Glycolytic process	x	x	x	x	x	x	x	x
Q8DTX6	pfkA	ATP-dependent 6-phosphofructokinase	Glycolytic process	x	x	x	x	x	x	x	x
Q9X670	pgi	Glucose-6-phosphate isomerase	Glycolytic process	x	x	x	x	x	x	x	x
Q8DVV2	pgk	Phosphoglycerate kinase	Glycolytic process	x	x	x	x	x	x	x	x
Q8DTX7	pykF	Pyruvate kinase	Glycolytic process	x	x	x	x	x	x	x	x
P72484	tpiA	Triosephosphate isomerase	Glycolytic process	x	x	x	x	x	x	x	x

Cell division, replication and cell wall synthesis

Q8DVL1	gpsB	Cell cycle protein GpsB	Cell cycle	x	x		x				
Q8DUU2	obg	GTPase Obg	Cell cycle					x			x
Q8DVD4	divIVA	Putative cell division protein DivIVA	Cell division	x	x	x	x	x	x	x	x
Q8DTQ3	ezrA	Septation ring formation regulator EzrA	Cell division							x	

Q8DVE0	ftsA	Cell division protein FtsA O	Cell division	x	x	x	x	x	x	x	x
Q8DTL0	ftsE	Cell division ATP-binding protein FtsE	Cell division					x			
Q8DVD9	ftsZ	Cell division protein FtsZ	Cell division	x	x	x	x	x	x	x	x
Q8DVD7	sepF	Cell division protein SepF	Cell division				x				
Q8DUE4	SMU_991	Putative ribonucleotide reductase	Cell division	x		x	x	x	x		x
Q8DTM9	whiA	Probable cell division protein WhiA	Cell division	x		x			x		
Q8DWM4	mreC	Cell shape-determining protein MreC	Cell shape	x							
Q8DSP6	mltG	Endolytic murein transglycosylase	Cell wall biosynthesis		x	x				x	
O70055	dltC	D-alanyl carrier protein	Cell wall biosynthesis		x	x		x			
Q8DV08	murN	Putative peptidoglycan branched peptide synthesis protein alanine adding enzyme beta-lactam resistance factor MurN	Cell wall biosynthesis							x	
Q8DVM5	pbp2x	Putative penicillin-binding protein 2X	Cell wall biosynthesis			x	x				
Q8DSP4	murC	UDP-N-acetylmuramate--L-alanine ligase	Cell wall biosynthesis							x	
Q8DVA0	pbp2b	Penicillin-binding protein 2b	Cell wall biosynthesis			x				x	
Q8DUM9	pbpX	Putative penicillin-binding protein, class C fmt-like protein	Cell wall biosynthesis						x		
Q8DT57	murA1	UDP-N-acetylglucosamine 1-carboxyvinyltransferase 1	Peptidoglycan biosynthesis				x				
Q8DT24	murA2	UDP-N-acetylglucosamine 1-carboxyvinyltransferase 2	Peptidoglycan biosynthesis	x				x	x		
Q8DST2	murE	UDP-N-acetylmuramoyl-L-alanyl-D-glutamate--L-lysine ligase	Peptidoglycan biosynthesis			x	x				
Q8DSQ5	murI	Glutamate racemase	Peptidoglycan biosynthesis								
Q8DV07	murM	Putative peptidoglycan branched peptide synthesis protein MurM	Peptidoglycan biosynthesis		x		x		x	x	
Q8DTM0	dinG	3'-5' exonuclease DinG	Replication			x					
Q8DWN8	dnaN	Beta sliding clamp	Replication					x	x		
Q8DT49	ligA	DNA ligase	Replication								
Q8DSK4	nrdI	Putative ribonucleotide reductase protein, Nrd	Replication						x		
Q8DV42	SMU_668c	Ribonucleoside-diphosphate reductase	Replication								x
Q8DWN9	dnaA	Chromosomal replication initiator protein DnaA	Replication		x		x		x		
Q8DU41	gyrA	DNA gyrase subunit A	Replication	x	x	x	x	x	x	x	
Q8DTQ2	gyrB	DNA gyrase subunit B	Replication		x					x	
Q8DTW6	parC	DNA topoisomerase 4 subunit A	Replication	x					x	x	
Nucleoside/Nucleotide metabolism and biosynthesis											
Q8DS33	adk	adenylate kinase	Nucleotide biosynthesis	x		x	x	x	x	x	x
P95787	atpA	ATP synthase subunit alpha	Nucleotide biosynthesis	x	x	x	x	x	x	x	x
P95789	atpD	ATP synthase subunit beta	Nucleotide biosynthesis	x	x	x	x	x	x	x	x

Q8DU81	guaA	GMP synthase [glutamine-hydrolyzing]	Nucleotide biosynthesis							x	
Q8DRR2	guaB	Inosine-5'-monophosphate dehydrogenase	Nucleotide biosynthesis	x	x	x	x	x	x	x	x
Q8DU33	pdp	Putative pyrimidine-nucleoside phosphorylase	Nucleotide biosynthesis								x
Q8DWM2	prs1	Ribose-phosphate pyrophosphokinase 1	Nucleotide biosynthesis				x				
Q8DU94	prs2	Putative ribose-phosphate pyrophosphokinase 2	Nucleotide biosynthesis			x					
Q8DW14	purA	Adenylosuccinate synthetase	Nucleotide biosynthesis		x						
P72478	purB	adenylosuccinate lyase	Nucleotide biosynthesis	x	x	x	x	x	x	x	x
Q8DWJ7	purD	Phosphoribosylamine--glycine ligase	Nucleotide biosynthesis	x							
Q8DWJ5	purE	N5-carboxyaminoimidazole ribonucleotide mutase	Nucleotide biosynthesis	x		x	x	x		x	x
Q8DWK8	purH	Bifunctional purine biosynthesis protein PurH	Nucleotide biosynthesis				x				
Q8DTV2	pyrE	Orotate phosphoribosyltransferase	Nucleotide biosynthesis	x			x	x	x	x	x
Q8DWG1	pyrG	CTP synthase	Nucleotide biosynthesis	x	x			x			
Q8DSY1	pyrH	Uridylate kinase	Nucleotide biosynthesis				x				
Q8DS79	SMU_1950	Pseudouridine synthase	Nucleotide biosynthesis	x							
Q8DVL6	SMU_464	Nicotinate phosphoribosyltransferase	Nucleotide biosynthesis	x	x	x	x	x	x	x	x
Q8DST6	upp	Uracil phosphoribosyltransferase	Nucleotide biosynthesis	x		x	x	x	x	x	
Q8CVC5	SMU_1213c	Putative 5'-nucleotidase	Nucleotide catabolism	x	x	x	x	x	x	x	x
Q8DV23	cmk	Cytidylate kinase	Nucleotide metabolic process	x							

Other metabolic processes

Q8DTA7	aldB	Alpha-acetolactate decarboxylase	Acid metabolism	x							
Q8DWB9	adhE	Aldehyde-alcohol dehydrogenase	Alcohol metabolic process	x	x	x	x	x	x	x	x
Q8DV28	SMU_689	Lysozyme	Cell wall catabolism	x	x	x	x	x	x	x	x
Q9XB21	hup	DNA-binding protein HU	Chromosome condensation	x	x	x	x	x	x	x	x
Q8DVB5	xseA	Exodeoxyribonuclease 7 large subunit	DNA catabolism		x						
Q8DSP0	accD	Acetyl-coenzyme A carboxylase carboxyl transferase subunit beta	Fatty acid biosynthesis							x	
Q8DSN3	acp	acyl carrier protein	Fatty acid biosynthesis	x	x	x	x	x	x	x	x
Q8DSN6	fabF	3-oxoacyl-[acyl-carrier-protein] synthase 2	Fatty acid biosynthesis	x	x	x	x	x	x	x	x
Q8DSN5	fabG	Putative 3-oxoacyl-acyl-carrier-protein reductase / 3-ketoacyl-acyl carrier protein reductase	Fatty acid biosynthesis	x							
Q8DSN0	fabM	Trans-2-decenoyl-[acyl-carrier-protein] isomerase	Fatty acid biosynthesis	x	x					x	
Q8DSN8	fabZ	3-hydroxyacyl-[acyl-carrier-protein] dehydratase FabZ	Fatty acid biosynthesis	x						x	
Q93D83	gpsA	Glycerol-3-phosphate dehydrogenase [NAD(P)+]	Lipid metabolism			x					
Q8DTJ2	SMU_1345c	Putative peptide synthetase	Metabolic processes	x	x	x			x	x	

Q8DS57	ackA	acetate kinase	Metabolic processes			x	x	x		x		
Q8DWD5	adhC	Dihydrolipoamide acetyltransferase component of pyruvate dehydrogenase complex	Metabolic processes							x	x	
Q8DTJ5	bacA1	Putative bacitracin synthetase 1 BacA	Metabolic processes	x	x	x	x	x		x		
Q8DTJ7	bacA2	Putative surfactin synthetase	Metabolic processes			x	x					
Q8CVC3	cah	Putative carbonic anhydrase	Metabolic processes		x	x		x	x	x	x	
Q8CWW8	fabD	Malonyl CoA-acyl carrier protein transacylase	Metabolic processes	x		x	x	x	x	x		
Q8DVC3	feoB	Ferrous iron transport protein B	Metabolic processes			x						
Q8DVK1	pknB	Putative serine/threonine protein kinase	Metabolic processes		x							
Q8DUA0	SMU_1043c	Putative phosphotransacetylase	Metabolic processes	x	x	x	x	x	x	x	x	
Q8DTM7	SMU_1306c	Nucleotide-binding protein	Metabolic processes	x								
Q8DTK0	SMU_1337c	Putative alpha/beta superfamily hydrolase	Metabolic processes	x		x	x			x	x	
Q8DTJ4	SMU_1343c	Putative polyketide synthase	Metabolic processes					x				
Q8DSP9	SMU_1725	Acylphosphatase	Metabolic processes				x					
Q8DSI4	SMU_1801c	Putative GTP-binding protein	Metabolic processes	x								
Q8DW46	SMU_229	Uncharacterized protein	Metabolic processes	x	x					x		
Q8DWM1	SMU_24	aminotransferase	Metabolic processes	x	x	x	x	x		x	x	
Q8DW28	SMU_251	Uncharacterized protein	Metabolic processes					x		x		
Q8DVE5	SMU_546	Putative GTP-binding protein	Metabolic processes	x	x	x	x	x	x	x	x	
Q8DUW6	SMU_775c	Uncharacterized protein	Metabolic processes					x				
Q8DW01	tkt	Transketolase	Metabolic processes	x		x			x			
Q8DSG1	yfbQ	Putative aminotransferase	Metabolic processes							x		
Q8DWD7	adhA	Putative acetoin dehydrogenase (TPP-dependent), E1 component alpha subunit	Oxidation-reduction process			x						
Q8DWD6	adhB	Putative acetoin dehydrogenase (TPP-dependent), E1 component beta subunit	Oxidation-reduction process	x				x			x	
Q8DTL3	budC	Putative acetoin dehydrogenase	Oxidation-reduction process	x	x	x	x	x	x	x		
Q8DVF0	dpr	Peroxide resistance protein Dpr	Oxidation-reduction process	x	x	x	x	x	x	x	x	
Q8DTN9	flaW	Putative flavodoxin	Oxidation-reduction process	x	x	x	x	x	x	x	x	
Q59931	gapN	NADP-dependent glyceraldehyde-3-phosphate dehydrogenase	Oxidation-reduction process	x	x	x	x	x	x	x	x	
Q8CWY9	gltA	Glutamate synthase (Large subunit)	Oxidation-reduction process						x			
O68574	hlyX	Putative hemolysin	Oxidation-reduction process	x			x		x			
Q8DUA3	MU_1040c	Putative oxidoreductase, short-chain dehydrogenase/reductase	Oxidation-reduction process	x								
Q8DSV6	serA	Putative D-3-phosphoglycerate dehydrogenase	Oxidation-reduction process	x	x		x			x		
Q8DU52	SMU_1098c	Putative oxidoreductase	Oxidation-reduction process			x						
Q8DTT3	SMU_1240c	Putative nitroreductase	Oxidation-reduction process	x			x		x		x	

Q8DTM4	SMU_1309c	Putative glycerol dehydrogenase	Oxidation-reduction process					x			
Q8DSN4	SMU_1742c	Putative trans-2-enoyl-ACP reductase	Oxidation-reduction process	x	x	x	x	x	x	x	x
Q8DSD3	SMU_1867c	Putative alcohol dehydrogenase	Oxidation-reduction process				x				
Q8DRT8	SMU_2127	Putative succinate semialdehyde dehydrogenase	Oxidation-reduction process		x			x			
Q8DUN5	SMU_869	Ferredoxin--NADP reductase	Oxidation-reduction process			x					
Q8DST7	clpP	ATP-dependent Clp protease proteolytic subunit	Proteolysis	x			x	x	x	x	x
Q8DWM7	ftsH	ATP-dependent zinc metalloprotease FtsH	Proteolysis	x	x	x	x	x	x	x	x
Q8DRQ6	htrA	Serine protease HtrA	Proteolysis						x		
Q8DW33	mecA	Adapter protein MecA	Proteolysis				x				
Q8DS80	pbp2a	Putative membrane carboxypeptidase, penicillin-binding protein 2a	Proteolysis	x							
Q8DS62	pepA	Putative glutamyl-aminopeptidase endo-1,4-beta-glucanase	Proteolysis							x	
Q8DSE4	pepP	Putative aminopeptidase P	Proteolysis				x				
Q8DTB6	SMU_1438c	Putative Zn-dependent protease	Proteolysis		x	x		x			
Q8DVK2	SMU_483	Putative phosphoprotein phosphatase (PppL protein)	Protein metabolism	x			x	x			
Q8DV90	cshA	DEAD-box ATP-dependent RNA helicase CshA	RNA catabolic process	x	x	x	x	x	x	x	x
Q8DWB2	pnp	Polyribonucleotide nucleotidyltransferase	RNA degradation	x	x	x	x	x	x	x	x
Q59938	acn	Aconitate hydratase A	Tricarboxylic acid cycle				x	x	x		
Q8DV10	ppc	Phosphoenolpyruvate carboxylase	Tricarboxylic acid cycle	x	x	x	x	x	x	x	x
Transcription											
Q8DTB3	rnj	Ribonuclease J	RNA processing	x	x		x		x	x	x
Q8DT90	rnz	Ribonuclease Z	RNA processing								
Q8DSY7	ybeY	Endoribonuclease YbeY	RNA processing	x							
O07329	ccpA	Catabolite control protein A	Transcription	x	x	x	x	x	x	x	x
Q8DUH3	clp	Putative Clp-like ATP-dependent protease, ATP-binding subunit	Transcription	x	x	x	x	x	x	x	x
Q8DVD0	clpE	ATP-dependent protease ClpE	Transcription	x	x	x	x	x	x	x	x
Q8DUN0	galR	Galactose operon repressor GalR	Transcription	x			x				
I6L8Z3	gcrR	Response regulator GcrR for glucan-binding protein C	Transcription	x	x	x	x	x	x	x	x
Q8DSP7	greA	Transcription elongation factor GreA	Transcription	x	x	x	x	x	x	x	x
Q02425	mtlR	Putative transcriptional regulator MtlR	Transcription					x			
Q8DVQ2	nusA	Transcription termination/antitermination protein NusA	Transcription			x	x	x	x	x	
Q8DS82	nusG	Transcription termination/antitermination protein NusG	Transcription	x	x	x	x	x	x	x	x
I6L8Z6	psaR	Putative transcriptional regulator	Transcription				x				

P45596	ptsH	Phosphocarrier protein HPr	Transcription	x			x	x	x	x	x
Q8DVV6	purR	Purine operon represso	Transcription	x					x		
Q8DU91	rex	Redox-sensing transcriptional repressor Rex	Transcription				x				
Q8DS36	rpoA	DNA-directed RNA polymerase subunit alpha	Transcription	x	x	x	x	x	x	x	x
Q8DS46	rpoB	DNA-directed RNA polymerase subunit beta(rpoB)	Transcription	x	x	x	x	x	x	x	x
Q8DS47	rpoC	DNA-directed RNA polymerase subunit beta'	Transcription	x	x	x	x	x	x	x	x
Q8DWG2	rpoE	Probable DNA-directed RNA polymerase subunit delta	Transcription	x	x	x	x	x	x	x	x
O33662	sigA	RNA polymerase sigma factor SigA	Transcription	x		x	x				
Q8DU13	SMU_1146c	Putative response regulator	Transcription				x				
Q8DTP9	SMU_1282	Putative transcriptional regulator	Transcription			x					
Q8DTP6	SMU_1287	Putative transcriptional regulator	Transcription			x					
Q8DSJ4	SMU_1789c	Probable transcriptional regulatory protein SMU_1789c	Transcription								x
Q8DS71	SMU_1964c	Putative response regulator	Transcription	x			x				
Q8DS66	SMU_1969c	Putative transcriptional regulator	Transcription			x					
Q8DU17	spxA	Regulatory protein Spx	Transcription		x						

Translation and protein synthesis

Q8CWY0	alaS	Alanine--tRNA ligase	Protein biosynthesis	x	x		x	x		x	x
Q8DRW2	argS	Arginine--tRNA ligase	Protein biosynthesis	x	x	x	x	x	x	x	x
Q8DSG3	aspS1	Aspartate--tRNA(Asp/Asn) ligase	Protein biosynthesis					x	x		
Q8DRV9	aspS2	Aspartate--tRNA ligase 2	Protein biosynthesis		x					x	
Q8DS90	der	GTPase Der	Protein biosynthesis					x			
Q8DVX9	gltX	Glutamate--tRNA ligase	Protein biosynthesis	x			x				
Q8CWY5	glyS	Glycine--tRNA ligase beta subunit	Protein biosynthesis					x		x	
Q8DVD3	ileS	Isoleucine--tRNA ligase	Protein biosynthesis	x	x	x	x	x	x	x	x
Q8DS85	leuS	Leucine--tRNA ligase	Protein biosynthesis				x	x	x	x	
Q8CWX2	pheT	Phenylalanine--tRNA ligase beta subunit	Protein biosynthesis	x	x		x			x	x
Q8DSJ9	proS	Proline--tRNA ligase	Protein biosynthesis	x	x	x	x	x		x	x
Q8DTK9	rf2	Peptide chain release factor 2	Protein biosynthesis		x					x	
Q8DS21	rpmC	50S ribosomal protein L29	Protein biosynthesis	x	x	x	x				x
P59156	rsmA	Ribosomal RNA small subunit methyltransferase A	Protein biosynthesis					x			
Q8DS65	SMU_1970c	Phenylalanine--tRNA ligase beta subunit	Protein biosynthesis				x			x	
Q8DSL1	valS	Valine--tRNA ligase	Protein biosynthesis			x					

Q8DWN6	ychF	Ribosome-binding ATPase YchF	Protein biosynthesis							x	
Q8DS14	clpC	Class III stress response-related ATP-dependent Clp protease, ATP-binding subunit	Protein folding		x	x	x		x	x	x
Q8DUI0	clpX	ATP-dependent Clp protease ATP-binding subunit ClpX	Protein folding	x	x		x	x	x	x	
Q8DWH2	dnaJ	Chaperone protein DnaJ	Protein folding	x	x	x	x	x	x		x
O06942	dnaK	Chaperone protein DnaK	Protein folding	x	x	x	x	x	x	x	x
Q8CWW6	groL	60 kDa chaperonin	Protein folding	x	x	x	x	x	x	x	x
Q8CWW5	groS	10 kDa chaperonin	Protein folding	x	x	x	x	x	x	x	x
O06941	grpE	Protein GrpE	Protein folding	x	x	x	x	x	x	x	x
Q8CVC6	prsA	Foldase protein PrsA	Protein folding	x	x			x		x	x
Q8DVJ7	SMU_488	Putative hydrolase	Protein folding	x		x	x	x	x		x
Q8CWZ6	tig	Trigger factor	Protein folding	x	x	x	x	x	x	x	x
Q54431	ffh	Signal recognition particle protein	Protein targeting				x	x	x	x	x
Q8DTM5	aldR	Putative translation initiation inhibitor aldR regulator-like protein	Translation	x		x	x	x	x		x
Q8DVM2	cshB	DEAD-box ATP-dependent RNA helicase CshB	Translation		x				x		
Q8DWC2	def	Peptide deformylase	Translation	x	x	x	x	x	x		x
Q8DSE7	efp	Elongation factor P	Translation	x	x	x	x	x	x	x	x
Q8DSY2	frr	Ribosome-recycling factor	Translation	x	x	x	x	x	x	x	x
Q8DVV4	fusA	Elongation factor G	Translation	x	x	x	x	x	x	x	x
Q8DSG5	gatA	Glutamyl-tRNA(Gln) amidotransferase subunit A	Translation	x	x	x	x	x	x		x
Q8DSG6	gatB	Aspartyl/glutamyl-tRNA(Asn/Gln) amidotransferase subunit B	Translation	x	x		x	x	x	x	
Q8DSG4	gatC	Aspartyl/glutamyl-tRNA(Asn/Gln) amidotransferase subunit C	Translation	x	x	x	x	x	x	x	x
Q8DVI8	hpf	Ribosome hibernation promoting factor	Translation	x	x	x	x	x	x	x	x
Q8DS34	inf	Translation initiation factor IF-1	Translation	x		x			x		x
Q8DVP9	infB	Translation initiation factor IF-2	Translation	x	x	x	x	x	x	x	x
Q8DV22	infC	Translation initiation factor IF-3	Translation	x				x			
Q8DU64	prfA	Peptide chain release factor 1	Translation	x		x				x	x
Q8DVP8	rbfA	Ribosome-binding factor A	Translation	x							
Q8DSY0	rplA	50S ribosomal protein L1	Translation	x	x	x	x	x	x	x	x
G1XVB9	rplB	50S ribosomal protein L2	Translation	x	x	x	x	x	x	x	x
Q8DS16	rplC	50S ribosomal protein L3	Translation	x	x	x	x	x	x	x	x
Q8DS17	rplD	50S ribosomal protein L4	Translation	x	x	x	x	x	x	x	x
Q8DS25	rplE	50S ribosomal protein L5	Translation	x	x	x	x	x	x	x	x
Q8DS28	rplF	50S ribosomal protein L6	Translation	x	x	x	x	x	x	x	x

Q8DRS8	rplI	50S ribosomal protein L9	Translation	x	x	x	x	x	x	x	x
Q8DUH2	rplJ	50S ribosomal protein L10	Translation	x	x	x	x	x	x	x	x
Q8DSX9	rplK	50S ribosomal protein L11	Translation	x	x	x	x	x	x	x	x
Q8DUG9	rplL	50S ribosomal protein L7/L12	Translation	x	x	x	x	x	x	x	x
Q8DW98	rplM	50S ribosomal protein L13	Translation	x	x	x	x	x	x	x	x
Q8DS23	rplN	50S ribosomal protein L14	Translation	x	x	x	x	x	x	x	x
Q8DS31	rplO	50S ribosomal protein L15	Translation	x	x	x	x	x	x	x	x
Q8DS37	rplQ	50S ribosomal protein L17	Translation	x	x	x	x	x	x	x	x
Q8DS29	rplR	50S ribosomal protein L18	Translation	x	x	x	x	x	x	x	x
Q8DTP5	rplS	50S ribosomal protein L19	Translation				x			x	
Q8DV20	rplT	50S ribosomal protein L20	Translation	x			x			x	
Q8DUQ6	rplU	50S ribosomal protein L21	Translation	x	x	x	x	x	x	x	x
Q8DS19	rplV	50S ribosomal protein L22	Translation	x	x	x	x	x	x	x	x
G1XVC0	rplW	50S ribosomal protein L23	Translation	x	x	x	x	x	x	x	x
Q8DS24	rplX	50S ribosomal protein L24	Translation	x	x	x	x	x	x	x	x
Q8DUQ4	rpmA	50S ribosomal protein L27	Translation	x	x	x	x	x	x	x	x
Q8DS30	rpmD	50S ribosomal protein L30	Translation	x	x	x	x	x		x	
Q8DTN5	rpmE2	50S ribosomal protein L31 type B	Translation	x	x	x	x	x	x	x	x
Q8DRV7	rpmF	50S ribosomal protein L32	Translation							x	
Q8DS11	rpsB	30S ribosomal protein S2	Translation	x	x	x	x	x	x	x	x
P59186	rpsC	30S ribosomal protein S3	Translation	x	x	x	x	x	x	x	x
P59133	rpsD	30S ribosomal protein S4	Translation	x	x	x	x	x	x	x	x
P59125	rpsE	30S ribosomal protein S5	Translation	x	x	x	x	x	x	x	x
Q8DSD7	rpsF	30S ribosomal protein S6	Translation	x	x	x	x	x	x	x	x
Q8DVV5	rpsG	30S ribosomal protein S7	Translation	x	x	x	x	x	x	x	x
Q8DS27	rpsH	30S ribosomal protein S8(	Translation	x	x	x	x	x	x	x	x
Q8DW97	rpsI	30S ribosomal protein S9	Translation	x	x		x		x		x
P48853	rpsJ	30S ribosomal protein S10	Translation	x	x	x	x	x	x	x	x
P59378	rpsK	30S ribosomal protein S11	Translation	x	x	x	x	x	x	x	x
P59167	rpsL	30S ribosomal protein S12	Translation	x						x	
Q8DS35	rpsM	30S ribosomal protein S13	Translation	x	x	x	x	x	x	x	x
Q8DWB3	rpsO	30S ribosomal protein S15	Translation	x						x	
Q8DUN9	rpsP	30S ribosomal protein S16	Translation	x	x	x	x	x	x	x	x

Q8DS22	rpsQ	30S ribosomal protein S17	Translation	x		x			x	x	
P66474	rpsR	30S ribosomal protein S18	Translation				x			x	
Q8DS18	rpsS	30S ribosomal protein S19	Translation	x	x		x	x	x	x	x
Q8DU30	rpsT	30S ribosomal protein S20	Translation			x					
P66531	rpsU	30S ribosomal protein S21	Translation							x	
Q8DTW9	rs1	Putative ribosomal protein S1 sequence specific DNA-binding protein	Translation	x	x	x	x	x	x	x	x
Q8DTF9	SMU_1388	Putative RNA helicase	Translation					x			
Q8DUN8	SMU_866	UPF0109 protein	Translation			x					x
Q8DUE2	SMU_993	Ribosome biogenesis GTPase A	Translation	x							
Q8DS12	tsf	Elongation factor Ts	Translation	x	x	x	x	x	x	x	x
P72483	tuf	Elongation factor Tu	Translation	x	x	x	x	x	x	x	x
Transport											
Q8DT63	glnQ	Putative amino acid ABC transporter, ATP-binding protein	Amino acid transport	x	x	x	x	x		x	x
Q8DSU4	livF	Putative branched chain amino acid ABC transporter, ATP-binding protein	Amino acid transport							x	
Q8DSU3	livG	Putative branched chain amino acid ABC transporter, ATP-binding protein	Amino acid transport	x		x				x	
Q93DA2	metN	Methionine import ATP-binding protein MetN	Amino acid transport	x							
Q8DU84	opuAa	Putative ABC transporter, ATP-binding protein, proline/glycine betaine transport system	Amino acid transport	x			x			x	
Q8DRU8	opuCa	Putative osmoprotectant amino acid ABC transporter, ATP-binding protein	Amino acid transport				x				x
I6L912	SMU_1942c	Putative amino acid binding protein	Amino acid transport	x	x	x	x	x	x	x	
Q8DW36	SMU_241c	Putative ABC transporter, ATP-binding protein amino acid transport system	Amino acid transport	x							
Q8DUT8	SMU_805c	Putative amino acid ABC transporter, ATP-binding protein	Amino acid transport			x			x		
Q8DUT1	SMU_815	Putative amino acid transporter, amino acid-binding protein	Amino acid transport		x	x	x			x	
Q8DUS9	SMU_817	Putative amino acid transporter, amino acid-binding protein	Amino acid transport		x	x	x		x		
Q8DSZ8	lguL	Putative lactoylglutathione lyase	Metal ion binding	x	x	x	x	x	x	x	x
Q8DSF0	secA	Protein translocase subunit SecA	Protein transport	x	x					x	
Q8DUN3	fruI	Inducible fructose permease	Sugar transport								
Q8DT28	malX	Putative maltose/maltodextrin ABC transporter, sugar-binding protein MalX	Sugar transport	x	x	x	x	x	x		x
Q00749	msmE	Multiple sugar-binding protein	Sugar transport		x						
Q00752	msmK	Multiple sugar-binding transport ATP-binding protein MsmK	Sugar transport					x			
Q02420	mtlF	Mannitol-specific phosphotransferase enzyme IIA componen	Sugar transport	x							
Q8DT01	ptcB	Putative PTS system, cellobiose-specific IIB component	Sugar transport			x	x				
Q8DSC4	ptnA	Putative PTS system, mannose-specific component IIAB	Sugar transport	x	x		x	x	x	x	x

Q8DS05	ptsG	Putative PTS system, glucose-specific IIABC component	Sugar transport	x	x	x	x	x	x	x	x
P45595	ptsI	Phosphoenolpyruvate-protein phosphotransferase	Sugar transport	x	x	x	x	x	x	x	x
I6L910	ptxB	Putative PTS system, enzyme IIB component	Sugar transport		x						
P12655	scrA	PTS system sucrose-specific EIIBCA component	Sugar transport	x	x				x	x	
Q8DSC2	SMU_1879	Putative PTS system, mannose-specific component IID	Sugar transport							x	
Q8DS75	SMU_1958c	Putative PTS system, mannose-specific IIC component	Sugar transport	x				x		x	
Q8DS74	SMU_1960c	Putative PTS system, mannose-specific IIB component	Sugar transport	x	x	x	x	x	x	x	x
Q8DS73	SMU_1961c	Putative PTS system, sugar-specific enzyme IIA component	Sugar transport	x	x	x	x	x	x	x	x
P95788	atpG	ATP synthase gamma chain	Transport							x	
Q8DS49	comYA	Putative ABC transporter, ATP-binding protein ComYA late competence protein	Transport	x							
Q8DUA8	glrA	Putative ABC transporter, ATP-binding protein	Transport							x	
I6L926	lemA	Putative cytoplasmic membrane protein LemA-like protein	Transport		x				x		
Q8DSU0	livK	Putative ABC transporter, branched chain amino acid-binding protein	Transport	x	x	x	x	x	x	x	x
Q8DW25	oppA	Putative oligopeptide ABC transporter, substrate-binding protein OppA	Transport	x	x	x	x	x	x	x	x
Q8DU54	opuBa	Putative ABC transporter, ATP-binding protein, choline transporter	Transport	x						x	
I6L8X8	rgpD	Putative polysaccharide ABC transporter, ATP-binding protein	Transport							x	
Q8DSH4	scnF	Putative bacteriocin component ScnF-like protein, putative ABC transporter, ATP-binding protein	Transport			x	x				
Q8DW86	sloA	Putative ABC transporter, ATP-binding protein possible iron and/or manganese ABC transport system	Transport	x	x		x	x	x	x	x
Q8DUA2	SMU_1041	Putative ABC transporter, ATP-binding protein	Transport	x						x	
Q8DU71	SMU_1078c	Putative ABC transporter, ATP-binding protein	Transport		x						
Q8DU57	SMU_1093	Putative ABC transporter, permease protein	Transport		x						x
Q8DU36	SMU_1121c	Putative ABC transporter	Transport	x	x	x	x	x	x	x	x
Q8DTZ7	SMU_1163c	Putative ABC transporter, ATP-binding protein	Transport					x			
Q8DTZ4	SMU_1166c	Putative ABC transporter, permease protein	Transport					x	x		
Q8CM14	SMU_1348c	Putative ABC transporter ATP-binding protein	Transport		x	x	x		x	x	x
Q8DTD8	SMU_1412c	Putative ABC transporter, membrane protein subunit and ATP-binding protein	Transport						x		
Q8DT62	SMU_1520	Putative ABC transporter, glutamine binding protein	Transport	x	x	x	x	x	x	x	x
Q8DSZ6	SMU_1605	Putative MDR permease possible transmembrane efflux protein	Transport		x						
I6L8Y2	SMU_1927	Putative ABC transporter, ATP-binding protein	Transport			x					
Q8DRZ6	SMU_2057c	Putative cadmium-transporting ATPase P-type ATPase	Transport					x			
Q8DRY9	SMU_2066c	Putative transmembrane protein	Transport				x				
Q8DW32	SMU_247	Putative ABC transporter ATP-binding protein	Transport	x	x	x	x	x	x	x	x
Q8DW31	SMU_248	Putative ABC transporter, membrane protein	Transport	x	x			x		x	x

Q8DW05	SMU_286	Putative ABC transporter ATP-binding protein ComA	Transport				x	x			
Q8DVM1	SMU_459	Putative ABC transporter, amino acid binding protein	Transport						x	x	
Q8DUT7	SMU_806c	Putative glutamine ABC transporter, permease protein	Transport	x	x	x	x	x	x	x	x
Q8DUP0	SMU_864	Putative ABC transporter, permease component	Transport			x					x
Q8DUL7	SMU_902	Putative ABC transporter, ATP-binding protein	Transport	x							
Q8DUK5	SMU_922	Putative ABC transporter, ATP-binding protein	Transport					x			
Q8DUD7	SMU_998	Putative ABC transporter, periplasmic ferrichrome-binding protein	Transport	x	x	x	x	x	x	x	x
Q8DSR3	trkA	Putative potassium uptake system protein TrkA	Transport					x			
Q8DT34	trkB	Putative potassium uptake system protein TrkB	Transport					x			

Uncharacterized/Unknown

Q8DVN1	MU_448	Uncharacterized protein	Uncharacterized	x				x			
Q8DVH8	MU_510c	Uncharacterized protein	Uncharacterized	x	x	x	x	x	x		x
Q8DUC6	SMU_1014	Uncharacterized protein	Uncharacterized							x	
Q8DU92	SMU_1052	Uncharacterized protein	Uncharacterized								
Q8DU59	SMU_1090	Uncharacterized protein	Uncharacterized	x	x		x		x		x
Q8DU18	SMU_1140c	Uncharacterized protein	Uncharacterized						x		
Q8DTW8	SMU_1201c	Uncharacterized protein	Uncharacterized	x	x	x	x	x	x	x	x
Q8DTW2	SMU_1208c	Uncharacterized protein	Uncharacterized		x						
Q8DWD8	SMU_125	Uncharacterized protein	Uncharacterized				x				x
Q8DTL2	SMU_1323	Uncharacterized protein	Uncharacterized			x	x	x	x		x
Q8DTG7	SMU_1377c	Uncharacterized protein	Uncharacterized	x	x		x	x	x	x	x
Q8DTG6	SMU_1378	Uncharacterized protein	Uncharacterized		x						
Q8DTB5	SMU_1442c	Uncharacterized protein	Uncharacterized	x	x	x	x	x	x	x	x
Q8DTB0	SMU_1447c	Uncharacterized protein	Uncharacterized				x			x	
Q8DT86	SMU_1479	Uncharacterized protein	Uncharacterized	x			x				
Q8DSW7	SMU_1641c	Uncharacterized protein	Uncharacterized	x	x	x	x	x	x	x	x
Q8DWA2	SMU_165	Uncharacterized protein	Uncharacterized						x	x	
Q8DSS8	SMU_1681c	Uncharacterized protein	Uncharacterized	x			x	x		x	x
Q8DSM0	SMU_1760c	Uncharacterized protein	Uncharacterized	x	x	x	x	x	x	x	x
Q8DSL9	SMU_1761c	Uncharacterized protein	Uncharacterized				x			x	
Q8DSL6	SMU_1764c	Uncharacterized protein	Uncharacterized							x	
Q8DSE8	SMU_1846c	Uncharacterized protein	Uncharacterized	x	x	x	x	x	x	x	x

Q8DSC9	SMU_1872c	Uncharacterized protein	Uncharacterized	x			x				
Q8DSA4	SMU_1904c	Uncharacterized protein	Uncharacterized	x	x	x	x	x	x	x	x
I6L8Z9	SMU_1925c	Uncharacterized protein	Uncharacterized			x					
Q8DS83	SMU_1946	Uncharacterized protein	Uncharacterized			x					
Q8DW70	SMU_205c	Uncharacterized protein	Uncharacterized	x			x		x		
Q8DRZ2	SMU_2061	Uncharacterized protein	Uncharacterized			x			x		x
Q8DRX7	SMU_2079c	UPF0297 protein	Uncharacterized	x	x	x	x	x	x	x	x
Q8DW66	SMU_209c	Uncharacterized protein	Uncharacterized	x	x	x	x	x	x	x	x
Q8DW65	SMU_210c	Uncharacterized protein	Uncharacterized	x	x	x	x	x	x	x	x
Q8DRS2	SMU_2147c	Uncharacterized protein	Uncharacterized			x				x	
Q8DW41	SMU_235	Uncharacterized protein	Uncharacterized	x	x	x	x	x	x	x	x
Q8DVX7	SMU_332	Uncharacterized protein	Uncharacterized				x				
Q8DVX6	SMU_333	Uncharacterized protein	Uncharacterized			x		x			x
Q8DVU4	SMU_371	Uncharacterized protein	Uncharacterized								x
Q8DVS5	SMU_392c	Uncharacterized protein	Uncharacterized				x				
Q8DVS4	SMU_393	Uncharacterized protein	Uncharacterized		x	x	x	x			x
Q8DVQ5	SMU_415	Uncharacterized protein	Uncharacterized	x			x				
Q8DVP5	SMU_428	Uncharacterized protein	Uncharacterized						x		
Q8DVI6	SMU_502	Uncharacterized protein	Uncharacterized				x		x		
Q8DVG3	SMU_527	Uncharacterized protein	Uncharacterized		x						
Q8DVC8	SMU_564	Uncharacterized protein	Uncharacterized	x	x	x	x	x	x	x	x
Q8DVA9	SMU_586	Uncharacterized protein	Uncharacterized		x		x				
Q8DVA5	SMU_591c	Uncharacterized protein	Uncharacterized	x							
Q8DV71	SMU_635	Uncharacterized protein	Uncharacterized								x
Q8DWI5	SMU_63c	Uncharacterized protein	Uncharacterized				x		x	x	
Q8DV31	SMU_685	Uncharacterized protein	Uncharacterized	x					x	x	
Q8DV27	SMU_690	Uncharacterized protein	Uncharacterized		x						
Q8DUY0	SMU_751	Uncharacterized protein	Uncharacterized	x						x	x
Q8DUX7	SMU_757	Uncharacterized protein	Uncharacterized		x		x		x		
Q8DUX2	SMU_768	Uncharacterized protein	Uncharacterized	x		x	x		x	x	x
Q8DUP2	SMU_862	Uncharacterized protein	Uncharacterized								
Q8DUM1	SMU_898	Uncharacterized protein	Uncharacterized	x			x		x	x	x
Q8DTJ0	SMU_1347c	Uncharacterized protein	Unknown	x				x		x	

Q8DRT3	SMU_2133c	Putative membrane protein	Unknown				x						
Q8DVU6	SMU_369c	UPF0356 protein	Unknown	x	x	x	x	x		x	x		
Q8DVN2	SMU_447	UPF0291 protein	Unknown	x	x	x	x	x	x	x	x		
Q8DWH8	SMU_72	UPF0237 protein	Unknown	x	x	x	x	x	x	x	x		
Q8DUV9	SMU_782	UPF0342 protein	Unknown	x	x	x	x	x	x		x		

Appendix 5. List of intracellular proteins identified when the proteins/peptides were used to form the AEP and as daily treatments.

Intracellular proteins												
Accession	**Gene name**	**Protein name**	**Protein function**	**Treatment**								
				A	**B**	**C**	**D**	**E**	**F**	**G**	**H**
Adaptative responses to environmental changes												
Q8DTJ8	bacD	Putative bacitracin synthetase	Antibiotic biosynthesis				x	x			
Q8DWD4	adhD	Dihydrolipoyl dehydrogenase	Cell redox homeostasis			x		x			
Q8DTE3	cas9	CRISPR-associated endonuclease Cas9	CRISP element metabolism					x			
Q8DVY2	radA	DNA repair protein RadA	DNA repair	x							x
P27624	recA	Protein RecA	DNA repair			x	x				
Q8DSC6	recD2	ATP-dependent RecD-like DNA helicase	DNA repair		x						
Q8DT75	rexB	ATP-dependent helicase/deoxyribonuclease subunit B	DNA repair						x		
Q9AIV4	smnA	Nuclease SmnA	DNA repair						x		
P72481	uvrA	UvrABC system protein A	DNA repair								x
Q8DSP2	SMU_1733c	Putative SNF helicase	DNA replication, recombination and repair								
Q8DW67	SMU_208c	Putative transposon protein possible DNA segregation ATPase	Recombination	x							
Q8DU29	ciaH	Putative histidine kinase sensor CiaH	Signal transduction						x		
Q8DSH1	scnK	Putative histidine kinase, ScnK-like protein	Signal transduction								
Q8DV79	SMU_626	Putative competence protein	Transformation							x	
Amino acid metabolism and biosynthesis												
Q8DUW2	aroB	3-dehydroquinate synthase	Amino acid biosynthesis								x
P10539	asd	aspartate-semialdehyde dehydrogenase	Amino acid biosynthesis			x			x		
Q8DUP3	carB	Carbamoyl-phosphate synthase large chain	Amino acid biosynthesis						x		
Q8DW43	ilvC	Ketol-acid reductoisomerase (NADP(+))	Amino acid biosynthesis	x	x	x	x	x	x	x	x
Q8DTV5	nylA	Putative amidase	Amino acid biosynthesis						x		
Q8DSV3	serC	Phosphoserine aminotransferase	Amino acid biosynthesis			x					
Q8DUW0	SMU_781	Putative prephenate dehydrogenase	Amino acid biosynthesis				x				
Q8DUH7	SMU_952	Putative methyltransferase	Amino acid biosynthesis						x		
Bacterial adherence and biofilm formation												
Q8DU58	wapE	Uncharacterized protein	Adherence			x					
Q8DVR0	brpA	Biofilm regulatory protein A	Biofilm formation		x	x					x

Q8DTF1	gbpC	Glucan-binding protein C, GbpC	Biofilm formation			x				x		
Q8DUW9	gbpD	Glucan-binding protein D with lipase activity BglB-like protein	Biofilm formation			x						
P23504	spaP	Cell surface antigen I/II	Cell wall antigen	x	x	x	x	x	x	x	x	
P11701	ftf	Levansucrase	EPS biosynthesis		x							
P08987	gtfB	Glucosyltransferase-I	EPS biosynthesis	x	x	x	x		x		x	
P13470	gtfC	Glucosyltransferase-SI	EPS biosynthesis	x	x	x	x		x			
P49331	gtfD	Glucosyltransferase-S	EPS biosynthesis			x		x	x		x	
Q8DUS4	rgpA	Putative RgpAc glycosyltransferase	EPS biosynthesis							x		
Carbohydrate metabolism and energy production												
Q8DT55	phsG	Alpha-1,4 glucan phosphorylase	Carbohydrate metabolic process			x						
Q03174	fruA	Fructan beta-fructosidase	Carbohydrate metabolic process								x	
P96994	galT	Galactose-1-phosphate uridylyltransferase	Carbohydrate metabolic process						x			
Q8DVV3	gapC	Glyceraldehyde-3-phosphate dehydrogenase	Carbohydrate metabolic process	x	x	x	x	x	x	x	x	
Q8DT31	glgP	Alpha-1,4 glucan phosphorylase	Carbohydrate metabolic process	x	x				x		x	
Q8DTC6	glmM	Phosphoglucosamine mutase	Carbohydrate metabolic process								x	
P26424	lacB	Galactose-6-phosphate isomerase subunit LacB	Carbohydrate metabolic process	x					x			
Q59934	pfl	Formate acetyltransferase	Carbohydrate metabolic process			x	x		x			
Q8CWY1	pfl2	Formate acetyltransferase (Pyruvate formate-lyase 2)	Carbohydrate metabolic process	x		x	x	x				
Q8DU72	pgm	Putative phosphoglucomutase	Carbohydrate metabolic process		x							
P95780	rmlB	dTDP-glucose 4,6-dehydratase	Carbohydrate metabolic process			x		x				
Q8DWF5	SMU_104	Putative alpha-glucosidase glycosyl hydrolase	Carbohydrate metabolic process			x						
O68579	ppaC	Probable manganese-dependent inorganic pyrophosphatase	Energy metabolism	x	x	x	x	x	x		x	
Q8DTS9	eno	Enolase	Glycolytic process	x	x	x	x	x	x	x	x	
Q8DWG0	fbaA	Fructose-1,6-biphosphate aldolase	Glycolytic process	x	x	x	x	x	x	x	x	
P26283	ldh	L-lactate dehydrogenase	Glycolytic process	x	x		x	x	x		x	
Q8DVV2	pgk	Phosphoglycerate kinase	Glycolytic process	x	x	x	x	x	x	x	x	
Q8DTX7	pykF	Pyruvate kinase	Glycolytic process	x	x	x	x	x	x	x	x	
Cell division, replication and cell wall synthesis												
Q8DVD4	divIVA	Putative cell division protein DivIVA	Cell division			x		x				
Q8DSP6	mltG	Endolytic murein transglycosylase	Cell wall biosynthesis						x			
Q53526	dltA	D-alanine--D-alanyl carrier protein ligase	Cell wall biosynthesis		x							

Q8DSS4	dltD	Protein DltD	Cell wall biosynthesis		x						
Q8DVM5	pbp2x	Putative penicillin-binding protein 2X	Cell wall biosynthesis	x	x	x	x				
Q8DS45	pbp1b	Putative membrane carboxypeptidase, penicillin-binding protein 1b	Cell wall biosynthesis	x	x			x			
Q8DVA0	pbp2b	Penicillin-binding protein 2b	Cell wall biosynthesis			x					
Q8DVE2	murG	UDP-N-acetylglucosamine--N-acetylmuramyl-pyrophosphoryl-undecaprenol N-acetylglucosamine transferase	Peptidoglycan biosynthesis			x					
Q8DUJ1	SMU_937	Putative mevalonate diphosphate decarboxylase	Peptidoglycan biosynthesis								x
Q8DTX5	dnaE	DNA-directed DNA polymerase	Replication	x							
Q8DT49	ligA	DNA ligase	Replication					x	x	x	x
Q8DTY6	pcrA	ATP-dependent DNA helicase	Replication			x					

Nucleoside/Nucleotide metabolism and biosynthesis

P95785	atpF	ATP synthase subunit b	Nucleotide biosynthesis	x							
Q8DWM2	prs1	Ribose-phosphate pyrophosphokinase 1	Nucleotide biosynthesis	x			x				
Q8DWL5	purL	Phosphoribosylformylglycinamidine synthase	Nucleotide biosynthesis								x
I6L8Y1	SMU_273	Putative hexulose-6-phosphate synthase	Nucleotide biosynthesis								x
Q8DVL6	SMU_464	Nicotinate phosphoribosyltransferase	Nucleotide biosynthesis		x						x
Q8DU63	tdk	Thymidine kinase	Nucleotide biosynthesis								x
Q8DST6	upp	Uracil phosphoribosyltransferase	Nucleotide biosynthesis				x				

Other metabolic processes

Q8DWB9	adhE	Aldehyde-alcohol dehydrogenase	Alcohol metabolic process	x					x		x
Q8DTJ6	SMU_1341c	Putative gramicidin S synthetase	Catalytic activity				x				
Q9XB21	hup	DNA-binding protein HU	Chromosome condensation	x	x	x	x	x	x	x	x
Q7ZAL0	smc	Chromosome partition protein Smc	Chromosome condensation						x		x
Q8DSN3	acp	acyl carrier protein	Fatty acid biosynthesis		x				x		
Q8DUC1	cilA	Citrate lyase alpha chain	Fatty acid biosynthesis					x			
Q8DWD5	adhC	Dihydrolipoamide acetyltransferase component of pyruvate dehydrogenase complex	Metabolic processes				x				
Q8DTJ5	bacA1	Putative bacitracin synthetase 1 BacA	Metabolic processes				x			x	x
Q8CWW8	fabD	Malonyl CoA-acyl carrier protein transacylase	Metabolic processes						x		
Q8DT10	SMU_1588c	Putative hexosyltransferase	Metabolic processes			x					
Q8DSH9	SMU_1806	Putative glycosyltransferase	Metabolic processes	x							
Q8DRZ7	SMU_2056	Putative ATPase	Metabolic processes						x		
Q8DW46	SMU_229	Uncharacterized protein	Metabolic processes					x	x		

Q8DVN8	SMU_438c	Putative (R)-2-hydroxyglutaryl-CoA dehydratase activator-related protein	Metabolic processes				x				
Q8DVF0	dpr	Peroxide resistance protein Dpr	Oxidation-reduction process	x	x	x	x	x	x	x	x
Q59931	gapN	NADP-dependent glyceraldehyde-3-phosphate dehydrogenase	Oxidation-reduction process	x	x	x	x	x	x	x	x
Q8CWY9	gltA	Glutamate synthase (Large subunit)	Oxidation-reduction process			x				x	
Q8CZF1	pdhB	Putative pyruvate dehydrogenase E1 component beta subunit	Oxidation-reduction process			x				x	
Q8DW88	urdA	Urocanate reductase	Oxidation-reduction process		x		x				
Q8DST7	clpP	ATP-dependent Clp protease proteolytic subunit	Proteolysis					x			
Q8DWM7	ftsH	ATP-dependent zinc metalloprotease FtsH	Proteolysis				x				x
Q8DRQ6	htrA	Serine protease HtrA	Proteolysis		x						
Q8DS80	pbp2a	Putative membrane carboxypeptidase, penicillin-binding protein 2a	Proteolysis			x					
Q8DVS2	pepX	Xaa-Pro dipeptidyl-peptidase	Proteolysis				x		x		
Q8DRR6	SMU_2153c	Putative peptidase	Proteolysis						x		
Q8DWB2	pnp	Polyribonucleotide nucleotidyltransferase	RNA degradation								x
Q8DUB2	SMU_1030	Putative polyribonucleotide nucleotidyltransferase Tn916 ORF8-like	RNA degradation	x							
Q59938	acn	Aconitate hydratase A	Tricarboxylic acid cycle	x							
Q8DV10	ppc	Phosphoenolpyruvate carboxylase	Tricarboxylic acid cycle			x					
Transcription											
Q8DUH3	clp	Putative Clp-like ATP-dependent protease, ATP-binding subunit	Transcription	x	x	x	x	x	x	x	x
Q8DVD0	clpE	ATP-dependent protease ClpE	Transcription			x					
Q8DSP7	greA	Transcription elongation factor GreA	Transcription	x			x				
Q02425	mtlR	Putative transcriptional regulator MtlR	Transcription		x				x		
Q8DSE9	nusB	Transcription antitermination protein NusB	Transcription								x
Q8DS36	rpoA	DNA-directed RNA polymerase subunit alpha	Transcription			x		x			
Q8DS47	rpoC	DNA-directed RNA polymerase subunit beta'	Transcription	x	x						
O33662	sigA	RNA polymerase sigma factor SigA	Transcription					x			
Q8DUB7	SMU_1025	Putative transcriptional regulator	Transcription	x							
Q8DWE9	SMU_112c	Putative transcriptional regulator	Transcription			x					
Q8DWD9	SMU_124	Putative transcriptional regulator (MarR family)	Transcription		x	x					
Q8DTE1	SMU_1409c	Putative transcriptional regulator	Transcription							x	
Q8DSJ4	SMU_1789c	Probable transcriptional regulatory protein SMU_1789c	Transcription			x					
Q8DSH3	SMU_1812	Putative transposase, ISSmu2	Transcription								x
Q8DS71	SMU_1964c	Putative response regulator	Transcription	x							

I6L8Y6	SMU_309	Regulator of sorbitol operon	Transcription	x							
Q8DVJ5	SMU_491	Putative DeoR-type transcriptional regulator	Transcription					x			
Translation and protein synthesis											
Q8CWY0	alaS	Alanine--tRNA ligase	Protein biosynthesis	x							
Q8DRW2	argS	Arginine--tRNA ligase	Protein biosynthesis								x
Q8DRV9	aspS2	Aspartate--tRNA ligase 2	Protein biosynthesis								x
Q8CWY5	glyS	Glycine--tRNA ligase beta subunit	Protein biosynthesis		x						
Q8DVD3	ileS	Isoleucine--tRNA ligase	Protein biosynthesis		x						
Q8CWX2	pheT	Phenylalanine--tRNA ligase beta subunit	Protein biosynthesis	x							
Q8DWN6	ychF	Ribosome-binding ATPase YchF	Protein biosynthesis		x						
Q8DS14	clpC	Class III stress response-related ATP-dependent Clp protease, ATP-binding subunit	Protein folding		x						
Q8DWH2	dnaJ	Chaperone protein DnaJ	Protein folding				x				
O06942	dnaK	Chaperone protein DnaK	Protein folding	x	x	x	x	x	x	x	x
Q8CWW6	groL	60 kDa chaperonin	Protein folding	x	x	x	x	x	x	x	x
Q8CWW5	groS	10 kDa chaperonin	Protein folding		x	x			x		x
Q8CVC6	prsA	Foldase protein PrsA	Protein folding	x		x		x	x		x
Q8CWZ6	tig	Trigger factor	Protein folding	x	x	x	x	x	x	x	x
Q54431	ffh	Signal recognition particle protein	Protein targeting								x
Q8CWX8	ftsY	Signal recognition particle receptor FtsY	Protein targeting	x							
Q8DVV4	fusA	Elongation factor G	Translation	x	x	x	x	x	x	x	x
Q8DSG5	gatA	Glutamyl-tRNA(Gln) amidotransferase subunit A	Translation		x			x			
Q8DSG6	gatB	Aspartyl/glutamyl-tRNA(Asn/Gln) amidotransferase subunit B	Translation	x	x	x	x	x	x	x	x
Q8DVI8	hpf	Ribosome hibernation promoting factor	Translation		x	x	x	x	x		
Q8DVP9	infB	Translation initiation factor IF-2	Translation								x
Q8DTF3	lepA	Elongation factor 4	Translation	x							
Q8DTT8	mnmE	tRNA modification GTPase MnmE	Translation								x
Q8DSY0	rplA	50S ribosomal protein L1	Translation		x						
Q8DS17	rplD	50S ribosomal protein L4	Translation					x			x
Q8DUH2	rplJ	50S ribosomal protein L10	Translation						x		
Q8DUG9	rplL	50S ribosomal protein L7/L12	Translation	x	x	x	x	x	x	x	x
Q8DS20	rplP	50S ribosomal protein L16	Translation			x	x				
Q8DS37	rplQ	50S ribosomal protein L17	Translation	x		x		x			

Q8DS29	rplR	50S ribosomal protein L18	Translation						x		
Q8DUQ6	rplU	50S ribosomal protein L21	Translation	x		x					
Q8DS24	rplX	50S ribosomal protein L24	Translation	x	x	x	x	x	x	x	x
Q8DS11	rpsB	30S ribosomal protein S2	Translation	x	x	x	x	x	x	x	x
P59186	rpsC	30S ribosomal protein S3	Translation			x	x	x	x		
P59133	rpsD	30S ribosomal protein S4	Translation		x			x	x	x	x
Q8DSD7	rpsF	30S ribosomal protein S6	Translation		x			x			
Q8DVV5	rpsG	30S ribosomal protein S7	Translation								
Q8DW97	rpsI	30S ribosomal protein S9	Translation	x		x	x	x			
Q8DS18	rpsS	30S ribosomal protein S19	Translation					x			
Q8DTW9	rs1	Putative ribosomal protein S1 sequence specific DNA-binding protein	Translation	x	x	x	x	x	x		x
Q8DS12	tsf	Elongation factor Ts	Translation	x	x	x	x		x		x
P72483	tuf	Elongation factor Tu	Translation	x	x	x	x	x	x	x	x
Q8CWW9	vacB	Ribonuclease R	Translation	x							
Transport											
Q8DRU8	opuCa	Putative osmoprotectant amino acid ABC transporter, ATP-binding protein	Amino acid transport			x					
Q8DVC5	SMU_568	Putative amino acid ABC transporter, ATP-binding protein	Amino acid transport				x				
Q8DUT1	SMU_815	Putative amino acid transporter, amino acid-binding protein	Amino acid transport	x							
Q8DSZ8	lguL	Putative lactoylglutathione lyase	Metal ion binding			x					
Q8DU24	pstB1	Phosphate import ATP-binding protein PstB 1	Phosphate transport				x				
Q8DSF0	secA	Protein translocase subunit SecA	Protein transport				x				
Q8DUN3	fruI	Inducible fructose permease	Sugar transport	x				x		x	x
Q8DT27	malF	Putative maltose/maltodextrin ABC transporter, permease protein MalF	Sugar transport								
Q8DT28	malX	Putative maltose/maltodextrin ABC transporter, sugar-binding protein MalX	Sugar transport		x	x	x	x	x		
Q8DSC4	ptnA	Putative PTS system, mannose-specific component IIAB	Sugar transport			x		x			
P45595	ptsI	Phosphoenolpyruvate-protein phosphotransferase	Sugar transport	x							
Q8DS74	SMU_1960c	Putative PTS system, mannose-specific IIB component	Sugar transport	x	x	x	x	x	x	x	x
Q8DS69	SMU_1966c	Putative periplasmic sugar-binding protein	Sugar transport	x							
P95788	atpG	ATP synthase gamma chain	Transport						x		
Q8DSU0	livK	Putative ABC transporter, branched chain amino acid-binding protein	Transport			x					
Q8DU85	opuAb	Putative ABC transporter, proline/glycine betaine permease protein	Transport		x						
Q8DRU6	opuCc	Putative ABC transporter osmoprotectant-binding protein, glycine betaine/carnitine/choline ABC transporter	Transport								x

Q8DT32	pacL	Putative cation-transporting P-type ATPase PacL	Transport			x						
Q8DS87	psaB	Putative ABC transporter, permease protein	Transport		x							
Q8DSH4	scnF	Putative bacteriocin component ScnF-like protein, putative ABC transporter, ATP-binding protein	Transport				x					
Q8DSH6	scnG	Putative bacteroiocin operon protein ScnG-like protein	Transport	x								
Q8DU70	SMU_1079c	Putative ABC transporter, ATP-binding protein	Transport									
Q8DU57	SMU_1093	Putative ABC transporter, permease protein	Transport	x			x				x	
Q8DTZ7	SMU_1163c	Putative ABC transporter, ATP-binding protein	Transport						x			
Q8DTZ4	SMU_1166c	Putative ABC transporter, permease protein	Transport	x								
Q8DTD8	SMU_1412c	Putative ABC transporter, membrane protein subunit and ATP-binding protein	Transport						x		x	
Q8DTC1	SMU_1431c	Putative ABC transporter, ATP-binding protein	Transport	x								
Q8DSJ6	SMU_1787c	Putative secreted protein	Transport						x			
Q8DSA9	SMU_1898	Putative ABC transporter, ATP-binding and permease protein	Transport	x								
Q8DRZ6	SMU_2057c	Putative cadmium-transporting ATPase P-type ATPase	Transport	x								
I6L919	SMU_2109	Putative MDR permease possible multidrug efflux pump	Transport			x						
Q8DVR2	SMU_408	Putative permease	Transport		x				x			
Q8DVM1	SMU_459	Putative ABC transporter, amino acid binding protein	Transport			x						
Q8DVG6	SMU_524	Putative ABC transporter, ATP-binding protein	Transport						x			
Q8DV57	SMU_651c	Putative ABC transporter, substrate-binding protein	Transport		x				x			
Q8DUT7	SMU_806c	Putative glutamine ABC transporter, permease protein	Transport						x			
Q8DUL7	SMU_902	Putative ABC transporter, ATP-binding protein	Transport								x	
Q8DUK5	SMU_922	Putative ABC transporter, ATP-binding protein	Transport			x						
Q8DUK4	SMU_923	Putative ABC transporter, ATP-binding protein	Transport								x	
Q8DUD7	SMU_998	Putative ABC transporter, periplasmic ferrichrome-binding protein	Transport							x		
Uncharacterized/Unknown												
Q8DU93	SMU_1051	Putative iron-sulfur cofactor synthesis protein NifS family	Uncharacterized				x					
Q8CWZ5	SMU_109	Uncharacterized protein	Uncharacterized		x							
Q8DU49	SMU_1104c	Uncharacterized protein	Uncharacterized									
Q8DU40	SMU_1116c	Uncharacterized protein	Uncharacterized	x								
Q8DU32	SMU_1125c	Uncharacterized protein	Uncharacterized				x					
Q8DTE2	SMU_1406c	Uncharacterized protein	Uncharacterized						x			
Q8DTC5	SMU_1427c	Uncharacterized protein	Uncharacterized								x	
Q8DTB0	SMU_1447c	Uncharacterized protein	Uncharacterized					x	x			

Q8DT97	SMU_1465c	Uncharacterized protein	Uncharacterized	x							
Q8DT86	SMU_1479	Uncharacterized protein	Uncharacterized	x	x	x	x	x	x	x	x
Q8DT20	SMU_1576c	Uncharacterized protein	Uncharacterized								
Q8DT19	SMU_1577c	Uncharacterized protein	Uncharacterized				x			x	
Q8DWA2	SMU_165	Uncharacterized protein	Uncharacterized						x		
Q8DSP3	SMU_1732c	Uncharacterized protein	Uncharacterized								x
Q8DSM0	SMU_1760c	Uncharacterized protein	Uncharacterized	x	x	x	x			x	
Q8DW90	SMU_178	Uncharacterized protein	Uncharacterized				x				
Q8DSF8	SMU_1830c	Uncharacterized protein	Uncharacterized					x			
Q8DS78	SMU_1951c	Uncharacterized protein	Uncharacterized								x
Q8DW77	SMU_197c	Uncharacterized protein	Uncharacterized		x						
Q8DW70	SMU_205c	Uncharacterized protein	Uncharacterized								x
Q8DRX7	SMU_2079c	UPF0297 protein	Uncharacterized							x	
Q8DRV8	SMU_2104	Uncharacterized protein	Uncharacterized					x			
Q8DW41	SMU_235	Uncharacterized protein	Uncharacterized	x	x	x	x	x	x	x	x
Q8DW07	SMU_284	Uncharacterized protein	Uncharacterized						x		
Q8DVV8	SMU_354	Uncharacterized protein	Uncharacterized								x
Q8DWJ6	SMU_49	Uncharacterized protein	Uncharacterized	x							
Q8DVA9	SMU_586	Uncharacterized protein	Uncharacterized	x							x
Q8DVA7	SMU_588	Uncharacterized protein	Uncharacterized	x							
Q8DV71	SMU_635	Uncharacterized protein	Uncharacterized						x		
Q8DWI5	SMU_63c	Uncharacterized protein	Uncharacterized	x	x	x	x		x		
Q8DV34	SMU_682	Uncharacterized protein	Uncharacterized	x						x	
Q8DUY9	SMU_739c	Uncharacterized protein	Uncharacterized	x			x	x		x	
Q8DUU7	SMU_796	Uncharacterized protein	Uncharacterized		x						
Q8DUP2	SMU_862	Uncharacterized protein	Uncharacterized								x
Q8DTJ0	SMU_1347c	Uncharacterized protein	Unknown	x			x	x			
Q8DST3	SMU_1676c	Putative membrane protein	Unknown			x					
Q8DRT3	SMU_2133c	Putative membrane protein	Unknown	x			x		x	x	x
Q8DUV9	SMU_782	UPF0342 protein	Unknown	x	x	x			x	x	x

Appendix 6. List of ECM proteins identified when the proteins/peptides were used to form the AEP and as daily treatments.

ECM proteins												
Accession	**Gene name**	**Protein name**	**Protein function**	**Treatment**							
				A	**B**	**C**	**D**	**E**	**F**	**G**	**H**
Adaptative responses to environmental changes											
I6L8Y0	ahpC	alkyl hydroperoxide reductase	Cell redox homeostasis				x				
Q8DUK3	tpx	Thiol peroxidase	Cell redox homeostasis	x			x		x	x	x
Q8DSD2	trxA	Thioredoxin	Cell redox homeostasis	x	x	x	x	x	x	x	
P09738	sodA	Superoxide dismutase [Mn/Fe]	Cellular detoxification	x	x	x	x	x	x	x	x
Q8DTE3	cas9	CRISPR-associated endonuclease Cas9	CRISP element metabolism	x	x						
Q8DRW8	mutS	DNA mismatch repair protein MutS	DNA repair		x						
P27624	recA	Protein RecA	DNA repair	x	x	x	x	x	x	x	x
P72481	uvrA	UvrABC system protein A	DNA repair					x			
Q8DSD8	ssb	Single-stranded DNA-binding protein	DNA replication, recombination and repair	x	x	x	x	x	x		x
Q8DSU5	SMU_1664c	Putative acetoin utilization protein, acetoin dehydrogenase	Energy store	x			x	x	x		x
Q8DSJ5	SMU_1788c	Putative bacterocin transport accessory protein, Bta	Killing factor	x			x		x		
Q8DW76	SMU_198c	Putative conjugative transposon protein	Recombination		x	x					
Q8DU29	ciaH	Putative histidine kinase sensor CiaH	Signal transduction					x			
I6L903	SMU_1009	Putative histidine kinase	Signal transduction	x					x		
Q8DW95	SMU_173	Putative ppGpp-regulated growth inhibitor	Stress	x		x	x				
Q8DSF9	SMU_1828	Universal stress protein	Stress	x	x	x	x	x	x		x
Amino acid metabolism and biosynthesis											
Q8DUV8	aroA	3-phosphoshikimate 1-carboxyvinyltransferase	Amino acid biosynthesis		x	x	x	x			
Q8DUW4	aroD	3-dehydroquinate dehydratase	Amino acid biosynthesis				x				
Q8DUW3	aroE	Shikimate dehydrogenase (NADP(+))	Amino acid biosynthesis	x	x	x	x	x	x	x	x
P10539	asd	aspartate-semialdehyde dehydrogenase	Amino acid biosynthesis			x			x		
Q8DTM1	aspB	Asparagine--oxo-acid transaminase	Amino acid biosynthesis		x						x
Q8DUP3	carB	Carbamoyl-phosphate synthase large chain	Amino acid biosynthesis	x							
Q8DUL9	dapB	4-hydroxy-tetrahydrodipicolinate reductase	Amino acid biosynthesis				x				
Q8DVY7	dapH	2,3,4,5-tetrahydropyridine-2,6-dicarboxylate N-acetyltransferase	Amino acid biosynthesis	x			x	x			
Q8DVU9	glnA	Glutamine synthetase type 1 glutamate--ammonia ligase	Amino acid biosynthesis	x	x	x	x	x	x	x	x
Q8CWY8	gltB	NADPH-dependent glutamate synthase (Small subunit)	Amino acid biosynthesis		x						

Q8DU67	glyA	Serine hydroxymethyltransferase	Amino acid biosynthesis				x				
Q8DW42	ilvA	L-threonine dehydratase	Amino acid biosynthesis		x		x				
Q8DW45	ilvB	Acetolactate synthase	Amino acid biosynthesis								x
Q8DW43	ilvC	Ketol-acid reductoisomerase (NADP(+))	Amino acid biosynthesis	x	x	x	x	x	x	x	x
Q8DRT7	ilvD	Dihydroxy-acid dehydratase	Amino acid biosynthesis			x					
Q8DTW7	ilvE	Branched-chain-amino-acid aminotransferase	Amino acid biosynthesis	x	x	x	x	x	x	x	x
Q8DW44	ilvH	Acetolactate synthase, small subunit	Amino acid biosynthesis						x		
Q8DTG2	leuA	2-isopropylmalate synthase	Amino acid biosynthesis	x	x	x	x	x	x		
Q8DSV3	serC	Phosphoserine aminotransferase	Amino acid biosynthesis	x	x	x	x	x	x	x	x
Q8DTP2	SMU_1291c	Putative chorismate mutase	Amino acid biosynthesis						x		
Q8DUG5	SMU_965	Homoserine dehydrogenase	Amino acid biosynthesis						x		
Q8DWH9	thrC	Putative threonine synthase	Amino acid biosynthesis						x		
Q8DUL2	SMU_913	Glutamate dehydrogenase	Amino acid metabolism	x	x	x	x	x	x	x	x
Bacterial adherence and biofilm formation											
Q54443	dexA	Dextranase	Adherence					x			
Q8DRV2	gbpA	Glucan-binding protein A, GbpA	Adherence	x	x	x	x	x	x	x	x
Q9KIJ3	sloC	Metal ABC transporter substrate-binding lipoprotein	Adherence	x	x	x	x	x	x	x	x
Q8DWM3	gbpB	Putative secreted antigen GbpB/SagA putative peptidoglycan hydrolase	Biofilm formation	x	x	x	x	x	x	x	x
Q8DTF1	gbpC	Glucan-binding protein C, GbpC	Biofilm formation	x							
Q8CVC7	SMU_609	Putative 40K cell wall protein	Biofilm formation	x	x	x	x	x	x	x	x
P23504	spaP	Cell surface antigen I/II	Cell wall antigen	x	x	x	x	x	x	x	x
P11701	ftf	Levansucrase	EPS biosynthesis				x				
P08987	gtfB	Glucosyltransferase-I	EPS biosynthesis				x				x
P13470	gtfC	Glucosyltransferase-SI	EPS biosynthesis	x	x	x		x	x	x	
P49331	gtfD	Glucosyltransferase-S	EPS biosynthesis	x			x	x			
Carbohydrate metabolism and energy production											
Q8DUS5	SMU_824	dTDP-4-dehydrorhamnose reductase	Carbohydrate biosynthesis	x	x	x	x	x			
Q8DTT9	rpiA	Ribose-5-phosphate isomerase A	Carbohydrate degradation		x	x	x	x		x	
Q03174	fruA	Fructan beta-fructosidase	Carbohydrate metabolic process	x	x	x	x	x	x	x	x
Q8DVV3	gapC	Glyceraldehyde-3-phosphate dehydrogenase	Carbohydrate metabolic process	x	x	x	x	x	x	x	x
Q8DT31	glgP	Alpha-1,4 glucan phosphorylase	Carbohydrate metabolic process	x	x	x	x	x	x	x	x

Q8DTC6	glmM	Phosphoglucosamine mutase	Carbohydrate metabolic process							x	
Q8DV70	nagB	Glucosamine-6-phosphate deaminase	Carbohydrate metabolic process	x		x	x				
Q59934	pfl	Formate acetyltransferase	Carbohydrate metabolic process	x	x	x	x	x	x	x	x
Q8CWY1	pfl2	Formate acetyltransferase (Pyruvate formate-lyase 2)	Carbohydrate metabolic process		x						
Q8DU72	pgm	Putative phosphoglucomutase	Carbohydrate metabolic process	x	x		x	x			
P95780	rmlB	dTDP-glucose 4,6-dehydratase	Carbohydrate metabolic process					x		x	
O68579	ppaC	Probable manganese-dependent inorganic pyrophosphatase	Energy metabolism	x	x	x	x	x	x	x	x
Q8DT52	glgB	1,4-alpha-glucan branching enzyme GlgB	Glycogen biosynthesis		x						
Q8DTS9	eno	Enolase	Glycolytic process	x	x	x	x	x	x	x	x
Q8DWG0	fbaA	Fructose-1,6-biphosphate aldolase	Glycolytic process	x	x	x	x	x	x	x	x
P59161	gpmA	2,3-bisphosphoglycerate-dependent phosphoglycerate mutase	Glycolytic process	x	x	x	x	x	x	x	x
P26283	ldh	L-lactate dehydrogenase	Glycolytic process	x	x	x	x	x	x	x	x
Q8DTX6	pfkA	ATP-dependent 6-phosphofructokinase	Glycolytic process	x	x	x	x	x	x	x	x
Q9X670	pgi	Glucose-6-phosphate isomerase	Glycolytic process	x	x	x	x	x	x		x
Q8DVV2	pgk	Phosphoglycerate kinase	Glycolytic process	x	x	x	x	x	x	x	x
Q8DTX7	pykF	Pyruvate kinase	Glycolytic process	x	x	x	x	x	x	x	x
P72484	tpiA	Triosephosphate isomerase	Glycolytic process	x	x	x	x	x	x		x

Cell division, replication and cell wall synthesis

Q8DSX7	ftsK	DNA translocase FtsK	Cell cycle								x
Q8DVE1	ftsQ	Cell division protein DivIB	Cell cycle	x							
Q8DVL1	gpsB	Cell cycle protein GpsB	Cell cycle	x							
Q8DVQ8	SMU_412c	Putative Hit-like protein involved in cell-cycle regulation	Cell cycle			x					
Q8DVD4	divIVA	Putative cell division protein DivIVA	Cell division	x	x	x	x	x	x	x	x
Q8DVE0	ftsA	Cell division protein FtsA O	Cell division	x	x	x	x	x	x	x	x
Q8DVD9	ftsZ	Cell division protein FtsZ	Cell division	x	x	x	x		x	x	x
Q8DUE4	SMU_991	Putative ribonucleotide reductase	Cell division			x			x		
Q8DSP6	mltG	Endolytic murein transglycosylase	Cell wall biosynthesis		x						
O70055	dltC	D-alanyl carrier protein	Cell wall biosynthesis	x	x	x		x	x		x
Q8DVM5	pbp2x	Putative penicillin-binding protein 2X	Cell wall biosynthesis								
Q8DVA0	pbp2b	Penicillin-binding protein 2b	Cell wall biosynthesis			x					
Q8DT57	murA1	UDP-N-acetylglucosamine 1-carboxyvinyltransferase 1	Peptidoglycan biosynthesis	x							
Q8DST2	murE	UDP-N-acetylmuramoyl-L-alanyl-D-glutamate--L-lysine ligase	Peptidoglycan biosynthesis		x				x		

Q8DSQ5	murI	Glutamate racemase	Peptidoglycan biosynthesis			x	x		x		
Q8DV07	murM	Putative peptidoglycan branched peptide synthesis protein MurM	Peptidoglycan biosynthesis				x				
Q8DUJ1	SMU_937	Putative mevalonate diphosphate decarboxylase	Peptidoglycan biosynthesis		x						
Q8DWN8	dnaN	Beta sliding clamp	Replication			x					
Q8DT49	ligA	DNA ligase	Replication							x	
Q8DW68	SMU_207c	Putative transposon protein	Replication	x	x		x	x			
Q8DWN9	dnaA	Chromosomal replication initiator protein DnaA	Replication	x						x	
Q8DU41	gyrA	DNA gyrase subunit A	Replication	x	x	x	x	x	x	x	x
Q8DTW6	parC	DNA topoisomerase 4 subunit A	Replication							x	
Nucleoside/Nucleotide metabolism and biosynthesis											
P95787	atpA	ATP synthase subunit alpha	Nucleotide biosynthesis	x	x	x	x	x	x	x	x
P95789	atpD	ATP synthase subunit beta	Nucleotide biosynthesis	x	x	x	x	x	x	x	x
Q8DRR2	guaB	Inosine-5'-monophosphate dehydrogenase	Nucleotide biosynthesis	x	x	x	x	x	x	x	x
Q8DU98	nadK	NAD kinase	Nucleotide biosynthesis	x							
Q8DWM2	prs1	Ribose-phosphate pyrophosphokinase 1	Nucleotide biosynthesis			x					
P72478	purB	adenylosuccinate lyase	Nucleotide biosynthesis	x	x	x	x	x	x		x
Q8DWJ5	purE	N5-carboxyaminoimidazole ribonucleotide mutase	Nucleotide biosynthesis	x							
Q8DUP5	pyrB	Aspartate carbamoyltransferase	Nucleotide biosynthesis				x				
Q8DTV2	pyrE	Orotate phosphoribosyltransferase	Nucleotide biosynthesis		x	x	x	x	x		
Q8DSY1	pyrH	Uridylate kinase	Nucleotide biosynthesis	x					x		
Q8DVL6	SMU_464	Nicotinate phosphoribosyltransferase	Nucleotide biosynthesis	x	x	x	x	x	x	x	x
Q8DST6	upp	Uracil phosphoribosyltransferase	Nucleotide biosynthesis				x				
Q8CVC5	SMU_1213c	Putative 5'-nucleotidase	Nucleotide catabolism	x			x				
Other metabolic processes											
Q8DWB9	adhE	Aldehyde-alcohol dehydrogenase	Alcohol metabolic process	x	x	x	x	x	x	x	x
Q8DV28	SMU_689	Lysozyme	Cell wall catabolism	x	x	x	x	x	x	x	
Q9XB21	hup	DNA-binding protein HU	Chromosome condensation	x	x	x	x	x	x	x	x
Q8DWK2	SMU_43	Putative site-specific DNA-methyltransferase restriction-modification protein	DNA methylation	x							
Q8DSN3	acp	acyl carrier protein	Fatty acid biosynthesis	x	x	x	x	x	x	x	x
Q8DSN6	fabF	3-oxoacyl-[acyl-carrier-protein] synthase 2	Fatty acid biosynthesis	x		x	x				
Q8DSN0	fabM	Trans-2-decenoyl-[acyl-carrier-protein] isomerase	Fatty acid biosynthesis		x						

Q8DSN8	fabZ	3-hydroxyacyl-[acyl-carrier-protein] dehydratase FabZ	Fatty acid biosynthesis	x				x			
Q8DTJ2	SMU_1345c	Putative peptide synthetase	Metabolic processes		x						x
Q8DS57	ackA	acetate kinase	Metabolic processes		x	x		x	x		
Q8DWD5	adhC	Dihydrolipoamide acetyltransferase component of pyruvate dehydrogenase complex	Metabolic processes		x	x	x	x	x		
Q8DTJ5	bacA1	Putative bacitracin synthetase 1 BacA	Metabolic processes	x	x		x	x			
Q8DTJ7	bacA2	Putative surfactin synthetase	Metabolic processes	x				x			
Q8DVK1	pknB	Putative serine/threonine protein kinase	Metabolic processes			x					
Q8DUA0	SMU_1043c	Putative phosphotransacetylase	Metabolic processes		x	x	x		x		x
Q8DTM7	SMU_1306c	Nucleotide-binding protein	Metabolic processes	x	x	x	x		x		x
Q8DTK0	SMU_1337c	Putative alpha/beta superfamily hydrolase	Metabolic processes					x		x	
Q8DW46	SMU_229	Uncharacterized protein	Metabolic processes			x	x		x		
Q8DWM1	SMU_24	aminotransferase	Metabolic processes	x	x	x	x	x	x	x	x
Q8DW28	SMU_251	Uncharacterized protein	Metabolic processes				x				
Q8DVE5	SMU_546	Putative GTP-binding protein	Metabolic processes	x	x	x	x	x	x	x	x
Q8DW01	tkt	Transketolase	Metabolic processes	x							
Q8DTL3	budC	Putative acetoin dehydrogenase	Oxidation-reduction process	x	x	x	x	x	x	x	x
Q8DVF0	dpr	Peroxide resistance protein Dpr	Oxidation-reduction process	x	x	x	x	x	x	x	x
Q8DTN9	flaW	Putative flavodoxin	Oxidation-reduction process	x	x	x	x	x		x	x
Q59931	gapN	NADP-dependent glyceraldehyde-3-phosphate dehydrogenase	Oxidation-reduction process	x	x	x	x	x	x	x	x
O68574	hlyX	Putative hemolysin	Oxidation-reduction process	x		x					
Q8DUA3	MU_1040c	Putative oxidoreductase, short-chain dehydrogenase/reductase	Oxidation-reduction process								x
Q8DSZ9	SMU_1602	Putative NAD(P)H-flavin oxidoreductase	Oxidation-reduction process			x					
Q8DSN4	SMU_1742c	Putative trans-2-enoyl-ACP reductase	Oxidation-reduction process		x	x	x	x	x	x	
Q8DWM7	ftsH	ATP-dependent zinc metalloprotease FtsH	Proteolysis	x	x	x	x	x	x	x	x
Q8DRQ6	htrA	Serine protease HtrA	Proteolysis			x			x		
Q8DV90	cshA	DEAD-box ATP-dependent RNA helicase CshA	RNA catabolic process	x	x	x	x	x	x	x	x
Q8DWB2	pnp	Polyribonucleotide nucleotidyltransferase	RNA degradation	x	x	x	x	x	x	x	x
Q8DV10	ppc	Phosphoenolpyruvate carboxylase	Tricarboxylic acid cycle			x			x	x	x
Transcription											
Q8DTB3	rnj	Ribonuclease J	RNA processing	x	x	x	x	x	x	x	x
Q8DT90	rnz	Ribonuclease Z	RNA processing			x					
Q8DSY7	ybeY	Endoribonuclease YbeY	RNA processing			x					

O07329	ccpA	Catabolite control protein A	Transcription	x		x	x	x	x	x	x
Q8DUH3	clp	Putative Clp-like ATP-dependent protease, ATP-binding subunit	Transcription	x	x	x	x	x	x	x	x
Q8DVD0	clpE	ATP-dependent protease ClpE	Transcription	x	x	x		x	x	x	x
I6L8Z5	covR	Putative response regulator CovR VicR-like protein	Transcription				x				
I6L8Z3	gcrR	Response regulator GcrR for glucan-binding protein C	Transcription	x	x	x	x	x	x	x	x
Q8DSP7	greA	Transcription elongation factor GreA	Transcription	x	x	x	x	x	x	x	x
Q8DVQ2	nusA	Transcription termination/antitermination protein NusA	Transcription	x	x	x	x	x	x	x	x
Q8DS82	nusG	Transcription termination/antitermination protein NusG	Transcription	x	x	x	x	x	x	x	x
P45596	ptsH	Phosphocarrier protein HPr	Transcription		x	x	x	x			x
Q8DS36	rpoA	DNA-directed RNA polymerase subunit alpha	Transcription	x	x	x	x	x	x	x	x
Q8DS46	rpoB	DNA-directed RNA polymerase subunit beta(rpoB)	Transcription	x		x	x	x	x	x	
Q8DS47	rpoC	DNA-directed RNA polymerase subunit beta'	Transcription	x	x	x	x	x	x	x	x
Q8DWG2	rpoE	Probable DNA-directed RNA polymerase subunit delta	Transcription	x	x	x	x	x	x	x	x
I6L923	sloR	Putative metal-dependent transcriptional regulator	Transcription						x		
Q8DS71	SMU_1964c	Putative response regulator	Transcription			x					
Q8DW57	SMU_218	Putative transcriptional regulator	Transcription				x				
Q8DW40	SMU_236c	Putative transcriptional regulator	Transcription			x					
Q8DVK3	sunL	Putative RNA-binding Sun protein possible rRNA methylase	Transcription						x		
Translation and protein synthesis											
Q8CWY0	alaS	Alanine--tRNA ligase	Protein biosynthesis	x	x		x	x		x	
Q8DTM2	asnS	Asparagine--tRNA ligase	Protein biosynthesis					x	x		
Q8DRV9	aspS2	Aspartate--tRNA ligase 2	Protein biosynthesis	x			x				
Q8DVX9	gltX	Glutamate--tRNA ligase	Protein biosynthesis				x				
Q8DVD3	ileS	Isoleucine--tRNA ligase	Protein biosynthesis	x	x	x	x	x	x		x
Q8CWX2	pheT	Phenylalanine--tRNA ligase beta subunit	Protein biosynthesis	x							
Q8DSJ9	proS	Proline--tRNA ligase	Protein biosynthesis		x	x	x	x		x	
Q8DS21	rpmC	50S ribosomal protein L29	Protein biosynthesis	x		x	x	x	x		x
Q8DS44	tyrS	Tyrosine--tRNA ligase	Protein biosynthesis						x		
Q8DWN6	ychF	Ribosome-binding ATPase YchF	Protein biosynthesis	x							
Q8DUI0	clpX	ATP-dependent Clp protease ATP-binding subunit ClpX	Protein folding	x	x	x	x	x	x	x	
O06942	dnaK	Chaperone protein DnaK	Protein folding	x	x	x	x	x	x	x	x
Q8CWW6	groL	60 kDa chaperonin	Protein folding	x	x	x	x	x	x	x	x

Q8CWW5	groS	10 kDa chaperonin	Protein folding	x	x	x	x	x	x	x	x
O06941	grpE	Protein GrpE	Protein folding	x	x	x	x	x	x		x
Q8CVC6	prsA	Foldase protein PrsA	Protein folding			x					
Q8DVJ7	SMU_488	Putative hydrolase	Protein folding				x				
Q8CWZ6	tig	Trigger factor	Protein folding	x	x	x	x	x	x	x	x
Q54431	ffh	Signal recognition particle protein	Protein targeting	x				x	x		
Q8DTM5	aldR	Putative translation initiation inhibitor aldR regulator-like protein	Translation		x						
Q8DWC2	def	Peptide deformylase	Translation	x	x	x	x	x	x	x	x
Q8DSE7	efp	Elongation factor P	Translation	x							
Q8DSY2	frr	Ribosome-recycling factor	Translation	x	x	x	x	x	x		x
Q8DVV4	fusA	Elongation factor G	Translation	x	x	x	x	x	x	x	x
Q8DSG5	gatA	Glutamyl-tRNA(Gln) amidotransferase subunit A	Translation		x						
Q8DSG6	gatB	Aspartyl/glutamyl-tRNA(Asn/Gln) amidotransferase subunit B	Translation				x		x		
Q8DSG4	gatC	Aspartyl/glutamyl-tRNA(Asn/Gln) amidotransferase subunit C	Translation	x						x	
Q8DVI8	hpf	Ribosome hibernation promoting factor	Translation	x	x	x	x	x	x	x	x
Q8DS34	inf	Translation initiation factor IF-1	Translation				x				
Q8DVP9	infB	Translation initiation factor IF-2	Translation	x	x	x	x	x	x	x	x
Q8DV22	infC	Translation initiation factor IF-3	Translation				x			x	
Q8DU64	prfA	Peptide chain release factor 1	Translation				x				
Q8DSY0	rplA	50S ribosomal protein L1	Translation	x	x	x	x	x	x	x	x
G1XVB9	rplB	50S ribosomal protein L2	Translation	x	x	x	x	x	x	x	x
Q8DS16	rplC	50S ribosomal protein L3	Translation	x	x	x	x	x	x		x
Q8DS17	rplD	50S ribosomal protein L4	Translation	x	x	x	x	x	x	x	x
Q8DS25	rplE	50S ribosomal protein L5	Translation	x	x	x	x	x	x	x	x
Q8DS28	rplF	50S ribosomal protein L6	Translation	x	x	x	x	x	x	x	x
Q8DRS8	rplI	50S ribosomal protein L9	Translation	x	x	x	x	x	x	x	x
Q8DUH2	rplJ	50S ribosomal protein L10	Translation	x	x	x	x	x	x	x	x
Q8DSX9	rplK	50S ribosomal protein L11	Translation	x	x	x	x	x	x	x	x
Q8DUG9	rplL	50S ribosomal protein L7/L12	Translation	x	x	x	x	x	x	x	x
Q8DW98	rplM	50S ribosomal protein L13	Translation	x	x	x	x	x	x	x	x
Q8DS23	rplN	50S ribosomal protein L14	Translation	x	x	x	x	x	x	x	x
Q8DS31	rplO	50S ribosomal protein L15	Translation	x	x	x	x	x	x	x	x
Q8DS37	rplQ	50S ribosomal protein L17	Translation	x	x	x	x	x	x	x	x

Q8DS29	rplR	50S ribosomal protein L18	Translation	x	x	x	x	x	x	x	x
Q8DTP5	rplS	50S ribosomal protein L19	Translation					x			
Q8DUQ6	rplU	50S ribosomal protein L21	Translation	x	x	x	x	x	x	x	x
Q8DS19	rplV	50S ribosomal protein L22	Translation	x	x	x		x	x	x	x
G1XVC0	rplW	50S ribosomal protein L23	Translation	x	x		x	x	x	x	x
Q8DS24	rplX	50S ribosomal protein L24	Translation	x	x	x	x	x	x	x	x
Q8DUQ4	rpmA	50S ribosomal protein L27	Translation	x	x	x	x	x	x	x	x
Q8DWE1	rpmB	50S ribosomal protein L28	Translation	x							
Q8DS30	rpmD	50S ribosomal protein L30	Translation			x	x	x	x		
Q8DTN5	rpmE2	50S ribosomal protein L31 type B	Translation	x	x	x	x	x	x	x	x
Q8DS11	rpsB	30S ribosomal protein S2	Translation	x	x	x	x	x	x	x	x
P59186	rpsC	30S ribosomal protein S3	Translation	x	x	x	x	x	x	x	x
P59133	rpsD	30S ribosomal protein S4	Translation	x	x	x	x	x	x	x	x
P59125	rpsE	30S ribosomal protein S5	Translation	x	x	x	x	x	x	x	x
Q8DSD7	rpsF	30S ribosomal protein S6	Translation	x	x	x	x	x	x	x	x
Q8DVV5	rpsG	30S ribosomal protein S7	Translation	x	x			x	x		
Q8DS27	rpsH	30S ribosomal protein S8(	Translation	x	x	x	x	x	x	x	x
Q8DW97	rpsI	30S ribosomal protein S9	Translation					x			
P48853	rpsJ	30S ribosomal protein S10	Translation	x	x	x	x	x	x	x	x
P59378	rpsK	30S ribosomal protein S11	Translation	x	x	x	x	x	x	x	x
Q8DS35	rpsM	30S ribosomal protein S13	Translation	x	x	x	x	x	x	x	x
Q8DWB3	rpsO	30S ribosomal protein S15	Translation	x	x	x	x	x	x	x	x
Q8DUN9	rpsP	30S ribosomal protein S16	Translation	x				x			
Q8DS22	rpsQ	30S ribosomal protein S17	Translation	x	x	x					
Q8DS18	rpsS	30S ribosomal protein S19	Translation	x	x	x	x	x	x	x	
Q8DTW9	rs1	Putative ribosomal protein S1 sequence specific DNA-binding protein	Translation	x	x	x	x	x	x	x	x
Q8DS12	tsf	Elongation factor Ts	Translation	x	x	x	x	x	x	x	x
P72483	tuf	Elongation factor Tu	Translation	x	x	x	x	x	x	x	x
Transport											
Q8DT63	glnQ	Putative amino acid ABC transporter, ATP-binding protein	Amino acid transport	x	x		x	x	x	x	
Q8DU84	opuAa	Putative ABC transporter, ATP-binding protein, proline/glycine betaine transport system	Amino acid transport					x			
I6L912	SMU_1942c	Putative amino acid binding protein	Amino acid transport			x					

Q8DUT1	SMU_815	Putative amino acid transporter, amino acid-binding protein	Amino acid transport						x		
Q8DUS9	SMU_817	Putative amino acid transporter, amino acid-binding protein	Amino acid transport	x							
Q8DSZ8	lguL	Putative lactoylglutathione lyase	Metal ion binding	x	x	x	x	x	x	x	x
Q8DSF0	secA	Protein translocase subunit SecA	Protein transport				x			x	
Q8DUN3	fruI	Inducible fructose permease	Sugar transport		x				x	x	x
Q00752	msmK	Multiple sugar-binding transport ATP-binding protein MsmK	Sugar transport	x			x				
Q8DT01	ptcB	Putative PTS system, cellobiose-specific IIB component	Sugar transport			x					
Q8DSC4	ptnA	Putative PTS system, mannose-specific component IIAB	Sugar transport		x		x	x		x	x
Q8DS05	ptsG	Putative PTS system, glucose-specific IIABC component	Sugar transport	x	x		x	x	x	x	x
P45595	ptsI	Phosphoenolpyruvate-protein phosphotransferase	Sugar transport	x	x	x	x	x	x	x	x
I6L910	ptxB	Putative PTS system, enzyme IIB component	Sugar transport				x				
P12655	scrA	PTS system sucrose-specific EIIBCA component	Sugar transport	x					x		
Q8DWF9	SMU_100	Putative sorbose PTS system, IIB component	Sugar transport						x		
Q8DS75	SMU_1958c	Putative PTS system, mannose-specific IIC component	Sugar transport	x	x	x		x	x	x	
Q8DS74	SMU_1960c	Putative PTS system, mannose-specific IIB component	Sugar transport	x	x	x	x	x	x	x	x
Q8DS73	SMU_1961c	Putative PTS system, sugar-specific enzyme IIA component	Sugar transport	x	x	x	x	x	x	x	x
P95786	atpH	ATP synthase subunit delta	Transport	x			x	x	x	x	x
I6L926	lemA	Putative cytoplasmic membrane protein LemA-like protein	Transport		x						
Q8DSU0	livK	Putative ABC transporter, branched chain amino acid-binding protein	Transport	x	x	x	x	x	x	x	x
Q8DUY5	lmrB	Putative drug-export protein multidrug resistance protein	Transport		x						
Q8DW25	oppA	Putative oligopeptide ABC transporter, substrate-binding protein OppA	Transport	x	x	x	x	x	x	x	x
Q8DU85	opuAb	Putative ABC transporter, proline/glycine betaine permease protein	Transport								x
I6L8Z4	rgpC	Transport permease protein	Transport		x						
Q8DW86	sloA	Putative ABC transporter, ATP-binding protein possible iron and/or manganese ABC transport system	Transport			x				x	x
Q8DUA2	SMU_1041	Putative ABC transporter, ATP-binding protein	Transport					x		x	x
Q8DU57	SMU_1093	Putative ABC transporter, permease protein	Transport	x			x	x			
Q8DU36	SMU_1121c	Putative ABC transporter	Transport	x	x	x	x	x	x		x
Q8DTZ4	SMU_1166c	Putative ABC transporter, permease protein	Transport	x							
Q8CM14	SMU_1348c	Putative ABC transporter ATP-binding protein	Transport				x				
Q8DTD8	SMU_1412c	Putative ABC transporter, membrane protein subunit and ATP-binding protein	Transport	x							
Q8DT62	SMU_1520	Putative ABC transporter, glutamine binding protein	Transport	x	x	x	x	x	x	x	x
Q8DW32	SMU_247	Putative ABC transporter ATP-binding protein	Transport	x	x	x	x	x	x	x	x
Q8DW31	SMU_248	Putative ABC transporter, membrane protein	Transport				x	x		x	

Q8DW05	SMU_286	Putative ABC transporter ATP-binding protein ComA	Transport					x				
Q8DUT7	SMU_806c	Putative glutamine ABC transporter, permease protein	Transport	x	x		x	x	x			
Q8DUD7	SMU_998	Putative ABC transporter, periplasmic ferrichrome-binding protein	Transport	x	x	x	x	x	x	x	x	
Q8DT34	trkB	Putative potassium uptake system protein TrkB	Transport					x				
Uncharacterized/Unknown												
Q8DVH8	MU_510c	Uncharacterized protein	Uncharacterized				x					
Q8DU92	SMU_1052	Uncharacterized protein	Uncharacterized	x								
Q8DU59	SMU_1090	Uncharacterized protein	Uncharacterized			x						
Q8DU49	SMU_1104c	Uncharacterized protein	Uncharacterized			x						
Q8DU43	SMU_1111c	Uncharacterized protein	Uncharacterized						x			
Q8DTW8	SMU_1201c	Uncharacterized protein	Uncharacterized	x	x	x	x	x	x	x		
Q8DTG7	SMU_1377c	Uncharacterized protein	Uncharacterized	x	x	x	x		x		x	
Q8DTB5	SMU_1442c	Uncharacterized protein	Uncharacterized	x	x	x	x	x	x	x	x	
Q8DT86	SMU_1479	Uncharacterized protein	Uncharacterized	x		x	x	x	x	x	x	
Q8DSW7	SMU_1641c	Uncharacterized protein	Uncharacterized	x	x	x	x	x	x	x	x	
Q8DSS8	SMU_1681c	Uncharacterized protein	Uncharacterized					x				
Q8DSM0	SMU_1760c	Uncharacterized protein	Uncharacterized	x	x	x	x	x	x	x	x	
Q8DSI7	SMU_1798c	Uncharacterized protein	Uncharacterized						x			
Q8DSE8	SMU_1846c	Uncharacterized protein	Uncharacterized	x	x	x	x	x	x		x	
Q8DSA4	SMU_1904c	Uncharacterized protein	Uncharacterized	x		x	x	x	x		x	
I6L8Z9	SMU_1925c	Uncharacterized protein	Uncharacterized	x						x		
Q8DW70	SMU_205c	Uncharacterized protein	Uncharacterized				x					
Q8DRX7	SMU_2079c	UPF0297 protein	Uncharacterized	x	x	x	x	x	x	x	x	
Q8DW66	SMU_209c	Uncharacterized protein	Uncharacterized	x	x	x	x	x	x	x	x	
Q8DW65	SMU_210c	Uncharacterized protein	Uncharacterized	x	x	x	x	x	x		x	
Q8DRQ9	SMU_2160	Uncharacterized protein	Uncharacterized			x			x			
Q8DW41	SMU_235	Uncharacterized protein	Uncharacterized	x	x	x	x	x	x	x	x	
Q8DVS4	SMU_393	Uncharacterized protein	Uncharacterized	x		x	x	x	x	x	x	
Q8DVC8	SMU_564	Uncharacterized protein	Uncharacterized	x	x	x	x	x	x	x	x	
Q8DWI5	SMU_63c	Uncharacterized protein	Uncharacterized						x	x		
Q8DV31	SMU_685	Uncharacterized protein	Uncharacterized	x	x	x	x		x			
Q8DUY9	SMU_739c	Uncharacterized protein	Uncharacterized		x				x		x	

Q8DUY0	SMU_751	Uncharacterized protein	Uncharacterized	x				x	x	x		
Q8DUX2	SMU_768	Uncharacterized protein	Uncharacterized			x		x		x		
Q8DUP2	SMU_862	Uncharacterized protein	Uncharacterized							x		
Q8DTJ0	SMU_1347c	Uncharacterized protein	Unknown			x		x			x	
Q8DRT3	SMU_2133c	Putative membrane protein	Unknown			x						
Q8DVU6	SMU_369c	UPF0356 protein	Unknown							x		
Q8DVN2	SMU_447	UPF0291 protein	Unknown	x			x				x	
Q8DWH8	SMU_72	UPF0237 protein	Unknown	x	x	x	x	x	x	x	x	
Q8DWH7	SMU_73	UPF0210 protein	Unknown							x		
Q8DUV9	SMU_782	UPF0342 protein	Unknown	x	x	x	x	x	x	x	x	
Q8DUV0	SMU_793	Uncharacterized protein	Unknown		x			x	x		x	

Curriculum vitae

Lina María Marín, BDS, MSc

EDUCATION

2015 – present **Ph.D. candidate**
Biomedical Engineering – Biomaterials and Dentistry – Cariology
Cotutelle between The University of Western Ontario, London – Canada, and the University of Campinas, Piracicaba – Brazil
Thesis: Effect of histatin and statherin peptides on cariogenic biofilm and on enamel demineralization
Supervisors: Dr. Walter L. Siqueira, Dr. Jaime A. Cury
Expected defense: August 2019

2010 – 2013 **MSc**
Basic Biomedical Sciences
El Bosque University, Bogotá Colombia
Thesis: Caries susceptibility of fluorotic enamel: an in vitro pH-cycling model
Supervisor: Dr. Jaime E. Castellanos

2002 – 2007 **BDS**
National University of Colombia
Bogotá Colombia

RESEARCH EXPERIENCE

2014 **Associate Instructor/Researcher**
School of Dentistry, El Bosque University, Bogotá Colombia
Duties: Full-time researcher at the Caries Research Unit – UNICA
Supervisor: Dr. Stefania Martignon

2009 – 2013 **Assistant Instructor/Researcher**
School of Dentistry, El Bosque University, Bogotá Colombia
Duties: Full-time researcher at the Caries Research Unit – UNICA
Supervisor: Dr. Stefania Martignon

2011 – 2012 **Research Assistant**

School of Dentistry, National University of Colombia, Bogotá Colombia
Project: Evaluation of virus load in the saliva of patients from the Hematopoietic Precursors Transplant Unit, Misericordia Hospital, Bogotá Colombia.
Supervisor: Dr. Sonia Bohórquez

2010 – 2011 **Research Assistant**
Young Researcher Fellowship
COLCIENCIAS / School of Dentistry, National University of Colombia, Bogotá Colombia
Project: Correlation between the state of HSV-1 infection and inflammatory cells in human trigeminal ganglia.
Supervisor: Dr. Jaime E. Castellanos

2007 – 2008 **Research Assistant**
Colombian Mandatory Professional Social Services with an emphasis on research
School of Dentistry, National University of Colombia, Bogotá Colombia
Project: Evaluation of the OAS and PKR pathways in response to b-interferon during type 1 Herpes Virus trigeminal neurons infection.
Supervisor: Dr. Jaime E. Castellanos

HONORS/AWARDS and GRANTS

2019 **CADR-NCOHR Student Travel Award**
Senior Basic Sciences Category

2017 **São Paulo Research Foundation – FAPESP**
FAPESP Research Internship Abroad
International Fellowship
Amount: CAD $29,600

2015 **São Paulo Research Foundation – FAPESP**
Doctorate Fellowship
Amount: CAD $46,000

2015 **Coordination for the Improvement of Higher Education Personnel – CAPES**
Program for Partner Graduate Students (PEC-PG)
Doctorate Scholarship
(Rejected)

2015 **Colciencias - Department of Science, Technology and Innovation**

Educational Forgivable Credit/Scholarship for Doctoral Studies Abroad
Amount: up to CAD $160,000
(Rejected)

2013 **IADR/Unilever Hatton Competition and Award**
Winner, Senior – Basic Science Category, Colombian Division

2013 **Meritorious Master´s Thesis**
MSc in Basic Biomedical Sciences, Faculty of Sciences, El Bosque University, Bogotá Colombia.

2012 **Internal Research Grant**
El Bosque University, Bogotá Colombia
Project: Fluorotic enamel susceptibility to dental caries: an in vitro pH-cycling model.
Amount: CAD $20.000

2010 **ORCA Conference Travel Fellowship**
European Organization for Caries Research (ORCA)

2008 **Otto de Greiff National Competition, Best Undergraduate Thesis Award, XII version**
Third Place, Health Sciences

2008 **Best Undergraduate Thesis Award, XII version**
First Place – School of Dentistry, National University of Colombia, Bogotá Colombia.

PUBLICATIONS

A. Chapters in books

1. **Marin LM**, Tenuta LM, Tabchoury CPM, Cury JA. Chemical composition and properties of the teeth (in Portuguese). Bioquímica Oral. 3rd ed. São Paulo: Artes Médicas. 2017.

2. Cury JA, Tenuta LM, Tabchoury CPM, **Marin LM**. Composition, functions and properties of the saliva (in Portuguese). Bioquímica Oral. 3rd ed. São Paulo: Artes Médicas. 2017.

3. Tenuta LM, **Marin LM**, Cury JA. Mechanisms of action of fluoride (in Portuguese). Bioquímica Oral. 3rd ed. São Paulo: Artes Médicas. 2017.

B. Peer Reviewed Journal Manuscripts

1. Almeida LF, **Marín LM**, Martínez-Mier EA, Cury JA. Fluoride Dentifrice Overcomes the Lower Resistance of Fluorotic Enamel to Demineralization. Caries Res. 2019. doi: 10.1159/000499668.

2. Bastidas-Legarda LY, Beltrán EO, **Marín-Gallón LM**, Castellanos JE, Bohórquez SP. Description of an in vivo oral mucosa HSV-1 infection model in mice. Acta Odontol Latinoam 2017;30(3):109-112.

3. **Marin LM**, Vieira, W, Tenuta LMA, Tabchoury CP, Cury JA. Concentração de fluoreto nos dentifrícios vendidos localmente no Brasil. Rev Assoc Paul Cir Dent 2016;70(3):317-322.

4. **Marin LM**, Cury JA, Tenuta LMA, Castellanos J, Martignon S. Higher fluorosis severity makes enamel less resistant to demineralization. Caries Res 2016;50(4):407-413.

5. **Marin LM**, Castellanos J, Tenuta LMA, Martignon S, Cury JA. Estandarización de la técnica de biopsia para determinación de fluoruro en esmalte dental. Revista Salud Bosque 2015;3(2):9-16.

6. Martignon S, Castiblanco GA, Cortés A, **Marin LM**, Gómez SI, Gómez OL, Abad DC, Carrillo GA, Lozano ML, Naranjo MC. Reporte de una metodología de calibración de examinadores en el uso del Sistema Internacional de Detección y Valoración de Caries (ICDAS). Univ Odontol 2015; 34(73):21-33.

7. Martignon S, **Marin LM**, Pitts N, Jácome-Liévano S. Consensus on domains, formation objectives and contents in cariology for undergraduate dental students in Colombia. Eur J of Dent Educ 2014;18:222-233.

8. Castellanos JE, **Marin LM**, Usuga-Vacca MV, Castiblanco GA, Martignon S. La remineralización del esmalte bajo el entendimiento actual de la caries dental. Univ Odontol 2013;32(69):49-59.

9. Martignon S, **Marin LM**, Tellez M, Ruiz JA, Gomez J, Rangel MC. Cariology Teaching Aspects in Spanish-Speaking Latin American Countries. J Dent Educ 2013;77(10):1330-1337.

10. Bernal LJ, Ávila LV, **Marin LM**, Casas JA, Bohórquez S del P, Barrientos S, Castellanos JE. Detección de la presencia de antígeno y ADN de virus Herpes Simplex tipo 1 en ganglios trigeminales humanos. Univ Odontol 2012;31(66):115-123.

11. Martignon S, Tellez M, Ruiz JA, Padilla A, Lopez S, Gomez J, **Marin LM**. Desempeño clínico de tres técnicas operatorias en preescolares de Bogotá: estudio clínico aleatorizado. Revista Colombiana de Investigación en Odontología 2010;1(2):202-212.

C. Refereed Abstracts and Conference Presentations

1. **Marin LM**, Xiao Y, Cury JA, Siqueira WL. Effect of engineered salivary peptides on *Streptococcus mutans* adherence to the enamel. 97th IADR General Session & Exhibition. Vancouver – Canada, 2019. J Dent Res, 98(special issue):958.

2. Almeida LF, **Marin LM**, Martinez-Mier EA, Cury JA. F-Dentifrice Overcomes the Lower Resistance of Fluorotic Enamel to Caries. 97th IADR General Session & Exhibition. Vancouver – Canada, 2019. J Dent Res 2018;98(special issue):2995.

3. **Marin LM**, Xiao Y, Cury JA, Siqueira WL. Bioengineered salivary peptides protection of enamel in *S. mutans* biofilm. 96th IADR General Session & Exhibition. London – United Kingdom, 2018. J Dent Res, 97(special issue A):2347.

4. Almeida LF, **Marin LM**, Martinez-Mier EA, Cury JA. Fluoride Formed on Fluorotic-Enamel Subjected to a pH-Cycling-Regimen Under F-Dentifrice. 47th Annual Meeting & Exhibition of the AADR. Fort Lauderdale – USA, 2018. J Dent Res 2018;97(special issue A):908.

5. **Marin LM**, Almeida LF, Cury JA. Reatividade do esmalte fluorótico com o F-gel acidulado. 34° Reunião Anual da Sociedade Brasileira de Pesquisa Odontológica. Braz Oral Res 2017;31(Supp2):AO0102.

6. **Marin LM**, Vieira-Filho W, Tenuta LM, Tabchoury CPM, Cury JA. Precisão e validade da determinação de fluoreto em dentifrícios com eletrodo íon específico pela técnica direta. 33° Reunião Anual da Sociedade Brasileira de Pesquisa Odontológica. Braz Oral Res 2016;30(Supp1):AO0090.

7. **Marin LM**, Tenuta LM, Tabchoury CPM, Cury JA. Available Fluoride Concentration in Local Toothpastes from Brazilian Regions. 63th ORCA Congress. Athens – Greece. 2016. Caries Res 2016;50:173.

8. Cury JA, **Marin LM**, Barijaona E, Tenuta LM, Tabchoury CPM, Decroix B, Holmgren CJ. Evaluation of Total and Total Soluble Fluoride of Toothpastes from Madagascar. 63th ORCA Congress. Athens – Greece. 2016. Caries Res 2016;50:174.

9. Tenuta LM, Dall-Agnol MA, Maia CB, **Marin LM**, Cury JA. In vivo prolonged retention of fluoride varnish increases reactivity with enamel. 63th ORCA Congress. Athens – Greece. 2016. Caries Res 2016;50:179.

10. **Marin LM**, Tenuta LM, Castellanos JE, Martignon S, Cury JA. Concentração do fluoreto no esmalte e na dentina pulpar de dentes com fluorose. 32° Reunião Anual da Sociedade Brasileira de Pesquisa Odontológica. Braz Oral Res 2015;29(Supp1):AO0083.

11. **Marin LM**, Castiblanco GA, Usuga-Vacca M, Cury JA, Martignon S. Fluoride Concentration of the Six Most Sold Toothpaste Brands in Colombia. 62nd ORCA Congress. Brussels – Belgium, 2015. Caries Res 2015;49(4):321-322.

12. **Marin LM**, Tenuta LM, Castellanos JE, Martignon S, Cury JA. Relationship between degree of fluorosis and enamel hypomineralization. XIX ABOPREV Meeting. Piracicaba – SP, Brazil. Braz J Oral Sci 2015;14(1):001.

13. **Marin LM**, Tenuta LM, Castellanos JE, Martignon S, Cury JA. Composition, mechanical properties and demineralization of fluorosed teeth. 92th IADR General Session & Exhibition. Cape Town – South Africa, 2014. J Dent Res 2014;93(special issue B):869.

14. Martignon S, Jácome-Liévano S, **Marin LM**. Current caries paradigm adoption in Colombian dental schools: Follow-up survey. 92th IADR General Session & Exhibition. Cape Town – South Africa, 2014. J Dent Res 2014;93(special issue B):189.

15. **Marin LM**, Tenuta LM, Castellanos JE, Martignon S, Cury JA. Evaluación de concentración de fluoruro en esmalte y dentina con diferentes severidades de fluorosis dental. XXIV Encuentro Nacional de Investigación Odontológica ACFO. San Juan de Pasto, 2013.

16. **Marin LM**, Millán LV, Martignon S, Lafaurie G. Evaluación del potencial erosivo del ácido hipocloroso sobre el esmalte dental. XXIV Encuentro Nacional de Investigación Odontológica ACFO. San Juan de Pasto, 2013.

17. **Marin LM**, Tenuta LM, Castellanos JE, Martignon S, Cury JA. Fluoride Distribution Pattern Throughout Enamel and Dentine of Fluorotic Teeth. 91th IADR General Session & Exhibition. Seattle – United States, 2013. J Dent Res 2013;92(special issue A):2039.

18. Martignon S, **Marin LM**, Lara JS, Douglas GVA, Gamboa LF. A Successful Experience with ICDAS-Training Courses in Colombia (2005-2011). 91th IADR General Session & Exhibition. Seattle – United States, 2013. J Dent Res 2013;92(special issue A):2903.

19. Nóbrega DF, Vieira-Dantas ED, Romão DA, Velo MMAC, **Marin LM**, Zura-Almuna MJ, Tabchoury CPM, Tenuta LM, Cury JA. "CaF" Formed on Enamel and Root Dentin by APF-gel Application. 91th IADR General Session & Exhibition. Seattle – United States, 2013. J Dent Res 2013;92(special issue A):3269.

20. Ochoa EM, Jácome-Liévano S, Otalvaro-Castro GJ, Ruiz JA, **Marin LM**, Martignon S. Curricular-perspective analysis of opportunities and problematics around the new-caries paradigm in Colombian dental schools. 59th Congress of the European Organisation for Caries Research. Cabo Frio - Brazil, 2012. Caries Res 2012;46:3-3.

21. Martignon S, Otalvaro-Castro GJ, Ochoa EM, **Marin LM**, Ruiz JA, Garcia LM, Franco AM, Jacome-Lievano S. Embracing the new caries paradigm among Colombian dental schools. 90th IADR General Session & Exhibition. Iguazu Falls – Brazil, 2012. J Dent Res 2012;91(special issue B):1141.

22. Jacome-Lievano S, **Marin LM**, Ochoa EM, Otalvaro-Castro GJ, Ruiz JA, Martignon S. Cariology-teaching in Colombia: Contrast of a workshop and a questionnaire. 90th IADR General Session & Exhibition. Iguazu Falls – Brazil, 2012. J Dent Res 2012;91(special issue B):1140.

23. Martignon S, Ruiz JA, Rangel MC, Tellez M, Gomez J, Falla S, **Marin LM**. Current Concepts in Cariology Teaching in Latin America. 58th Congress of the European Organisation for Caries Research. Kaunas - Lithuania, 2011. Caries Res 2011;45:207-208.

24. Martignon S, Tellez M, **Marin LM**, Ruiz JA, Padilla A, Qvist V. Operative Treatment Performance and Acceptance by Preschoolers with Early Childhood Caries in Bogotá, Colombia. 57th Congress of the European Organisation for Caries Research. Montpellier – France, 2010. Caries Res 2010; 44:193-194.

25. Beltran EO, Bastidas LY, **Marin LM**, Bohorquez SP, Castellanos JE. Experimental in-vivo Herpes infection of Trigeminal Ganglia through oral mucosa. 88th IADR General Session & Exhibition. Barcelona – Spain, 2010. J Dent Res 2010;89 (special issue B):428.

26. Bernal LJ, Avila LV, **Marin LM**, Casas A, Bohorquez SP, Castellanos JE, Barrientos, S. HSV-1 antigen, DNA and Latency-Associated-Transcripts in human Trigeminal Ganglia. 88th IADR General Session & Exhibition. Barcelona – Spain, 2010. J Dent Res 2010; 89 (special issue B):4286.

27. Beltran EO, Bastidas LY, **Marin LM**, Bohorquez SP, Castellanos JE. Establecimiento de un modelo murino de infección in-vivo por HSV-1 a través de la mucosa oral. XX Encuentro Nacional de Investigación Odontológica ACFO. Montería, 2009.

28. **Marin LM**, Prada-Arismendy J, Castellanos JE. Cambios en la expresión de Oligoadenilato Sintetasa 1a y 1b en neuronas trigeminales infectadas con Herpes Simplex tipo 1. XVIII Encuentro Nacional de Investigación Odontológica ACFO. Manizales, 2007.

29. **Marin LM**, Prada-Arismendy J, Bohorquez SP, Castellanos JE. Changes in Oligoadenylate Synthetase, Protein Kinase R and RNase-L mRNA in Trigeminal Ganglia cultures infected by Herpes Simplex. 2° IADR Latinoamerican Division Meeting. Atibaia – Brazil, 2007. Braz Oral Res 2007;21:348-348.

30. **Marin LM**, Prada-Arismendy J, Castellanos JE. Changes in Transcripts of Oligoadenylate Synthetase, Protein Kinase R, and RNasa-L in trigeminal ganglia cultures infected by Herpes Simplex Virus. 45° Annual Meeting of Infectous Diseases Society of America IDSA. San Diego – United States, 2007. 45° Annual Meeting of IDSA, Final Program and Abstracts. Arlington, VA: Infectious Diseases Society of America 2007:168-168.

D. Non-refereed Contributions

1. **Marin LM**. Risk Assessment for Early Childhood Caries. Oral Health Dialogue; 2(1):4-7.

2. Martignon S, Jácome-Liévano S, **Marin LM**. Consensus on domains, training objectives and contents in cariology for the undergraduate course in dentistry (in Spanish). Global Alliance for a Cavity-Free Future – Colombian Chapter. April 2013.

TEACHING and PROFESSIONAL EXPERIENCE

2018 – 2019 **Graduate Teaching Assistant**
Biomedical Engineering, The University of Western Ontario, London Canada
Course: Topics in Physiology / Seminar
Supervisor: Dr. Walter L. Siqueira

2017 **Graduate Teaching Assistant**
Biomedical Engineering, The University of Western Ontario, London Canada
Course: Core Biology
Supervisor: Dr. Walter L. Siqueira

2013 – 2014 **Coordinator**
Graduate Program in Dental Science (MSc), School of Dentistry, El Bosque University, Bogotá Colombia
Supervisor: Dr. Stefania Martignon

2013 – 2014 **Associate Instructor**
School of Dentistry, El Bosque University, Bogotá Colombia
Lecturer of the Graduate course Cariology.
Supervisor: Dr. Stefania Martignon

2010 – 2013 **Instructor**
Continuing Education Course: Training in the visual diagnosis of dental caries using the ICDAS criteria
El Bosque University, Bogotá Colombia

2009 – 2013 **Assistant Instructor**
School of Dentistry, El Bosque University, Bogotá Colombia
Lecturer of the undergraduate course Cariology and Restorative Dentistry.
Supervisor: Dr. Stefania Martignon

RESEARCH SUPERVISION

A. Co-op Students

1. Alyssa Bruinink (2018 – 2019)
   Enamel demineralization of bovine enamel treated with histatin- and statherin-derived engineered peptides.
   The University of Western Ontario. London ON, Canada.

2. Yuxin Duan (2018)
   Enamel demineralization of bovine enamel treated with histatin- and statherin-derived engineered peptides
   The University of Western Ontario. London ON, Canada.

3. Milena Petrica Mello (2016 – 2017)
   Preparation of bovine enamel slabs for use in cariogenic biofilm model
   University of Campinas. Piracicaba SP, Brazil.

B. Undergraduate Projects

1. Vanessa Paola Herrera Díaz, Amy Natalia Barrantes Hernández, Sthephanie Lorena Bello Cristancho (2013 – 2014)
   Effect of hypochlorous acid on dental tissues (in Spanish)
   Co-supervisors: Dr. Gloria I. Lafaurie, Dr. Luis F. Gamboa
   School of Dentistry, El Bosque University, Bogotá Colombia

2. Laura Viviana Arenas Wilches, Sara del Pilar Quintero Bahamón, Ana Karina Velasco González (2012 – 2013)
   Update of a workshop for visual diagnosis of dental caries directed at students of undergraduate, graduate and dentists of El Bosque University (in Spanish)
   Co-supervisors: Dr. Stefania Martignon, Dr. Luis F. Gamboa
   School of Dentistry, El Bosque University, Bogotá Colombia

C. Paediatric Dentistry Specialization Projects

1. Andreina Valerio (2013 – 2014)
   Determination of the fluoride content in some toothpastes marketed for children in Colombia (in Spanish)
   Co-supervisors: Dr. Luis F. Gamboa
   School of Dentistry, El Bosque University, Bogotá Colombia

LECTURER EXPERIENCE

2017	**Guest lecture** Saliva and its role in dental caries; Iberoamericana University, Dominican Republic
2015	**Guest lecture** Current concepts in dental caries management; Santa Cruz de la Sierra/La Paz, Bolivia
2014	**Guest lecture** Dental caries diagnosis and management: Current concepts; Panama City, Panama
2014 – 2018	**Colgate-Palmolive Company** National & International Lecturer / Key Opinion Leader

JOURNAL REVIEWER

2017 – present Clinical Oral Investigations

LANGUAGES

Spanish	Mother tongue
English	Substantial speaking/writing/reading
Portuguese	Substantial speaking/writing/reading